Electric Vehicle Design, Racing and Distance to Empty Algorithms

by

Lennon Patrick Rodgers

B.S. Mechanical Engineering
University of Illinois Urbana Champaign (2003)

M.S. Mechanical Engineering
Massachusetts Institute of Technology (2006)

Submitted to the Department of Mechanical Engineering
in Partial Fulfillment of the Requirements for the Degree of

Doctor of Philosophy in Mechanical Engineering

at the

MASSACHUSETTS INSTITUTE OF TECHNOLOGY

June 2013

Author.....
Department of Mechanical Engineering
May 14th, 2013

Certified by.....
Daniel D. Frey
Professor of Mechanical Engineering
Thesis Supervisor and Chair

Accepted by.....
David E. Hardt
Professor of Mechanical Engineering
Chairman, Committee on Graduate Students

Electric Vehicle Design, Racing and Distance to Empty Algorithms

by

Lennon Patrick Rodgers

Submitted to the Department of Mechanical Engineering
on May 14th, 2013 in Partial Fulfillment of the
Requirements for the Degree of Doctor of Philosophy in
Mechanical Engineering

Abstract

This research began with the goal of designing and building an electric motorcycle to compete in the Isle of Man TT Zero race. A set of parametric physics-based models was derived to size the batteries and motors, predict vehicle speeds and predict the time required to finish the race. In June 2011 the motorcycle design and simulations were tested in three races on the Isle of Man. Post-race analysis showed that the predictions had less than 10% error.

The energy estimation methods that were developed for the motorcycle were subsequently modified and applied to non-racing electric vehicles. Instead of predicting the energy required to travel a known route, it is more useful for non-racing applications to consider the reverse scenario, which is the distance the vehicle can travel before charging is required. This is referred to as the Distance to Empty (D_{TE}). Recent studies have shown that current D_{TE} algorithms are inadequate and cause "range anxiety" among users. This is because conventional approaches only use past driving data to estimate D_{TE} and thus are unable to accurately predict changes in driving conditions. However, the algorithm developed in this thesis uses measurements from the past along with knowledge of the future route. A multivariate linear regression model is used to adjust a historical average of energy consumption based on estimated changes in speed, traffic and temperature.

Finally, the new D_{TE} algorithm was compared to conventional methods by simulating a large number of full battery discharges under realistic driving conditions. A Markov-based stochastic speed profile generator was used as input to the models. Example simulations show that including future driving conditions in the D_{TE} algorithm can significantly reduce error.

Thesis Supervisor: Daniel D. Frey
Title: Professor of Mechanical Engineering

Acknowledgments

This work would not have been possible without the support of my committee members Dan Frey, Sanjay Sarma and Warren Seering. I am deeply appreciative of their guidance and friendship. I would also like to thank the following members of the Electric Vehicle Team who spent many late nights working on the motorcycle: Will Pritchett, Radu Gogoana, Mark Jeunnette, Randall Briggs, Paul Karplus, Erick Fuentes, Manyu Belani, Dan Kelly, Richard Yoon and Romi Kadri. Shane Colton was also a key team member, patient teacher and friend. Our professional motorcycle rider Allan Brew risked his life for the sake of engineering while also being a true gentleman. His wife Jan warmly hosted us on the Isle of Man with an unlimited amount of English tea. Mark Gardiner and Bill Dube were important advisors to the team and I am grateful for their help. Tom German shared his racing insights, which were captured in this thesis. Yet-Ming Chiang's unwavering support kick-started the motorcycle project and inspired us in many ways. The following organizations supported this research financially or with equipment: Singapore University of Technology and Design (SUTD), MIT-SUTD International Design Center (IDC), A123 Systems, BMW, MIT Energy Initiative (MITEI), MIT Transportation, MIT Department of Mechanical Engineering, MIT School of Engineering, MIT Edgerton Center, the Isle of Man government, Rahn's Motorcycling Engineering and Boston Moto. The following colleagues were a major help in my Distance to Empty algorithm work: Erik Wilhelm, Stephen Zoepf, Don MacKenzie, John Heywood and Sriram Krishnan. It was a great honor to work with these talented friends.

And last but not least – a special thanks to my wife Jenn and other family members for their enduring support.

Table of Contents

PART I: DESIGNING AN ELECTRIC MOTORCYCLE FOR THE ISLE OF MAN TT ZERO RACE 11

1. INTRODUCTION TO PART I 13

1.1 MOTIVATION 13

1.2 OVERVIEW 13

1.3 RELATED WORK 14

2. MOTORCYCLE SYSTEMS ENGINEERING 15

2.1 SUBSYSTEM MODELS 16

2.1.1 Backward-looking Simulations 16

2.1.2 Forward-looking Simulations 21

2.2 FULL-THROTTLE SIMULATIONS 24

2.3 CONSTANT VEHICLE SPEED SIMULATIONS 26

2.3.1 Proof that Constant Speed Minimizes Energy Consumption 26

2.4 CONSTANT POWER SIMULATIONS 29

2.5 BRAKING LOSSES 30

2.6 ESTIMATING THE REQUIRED MOTOR POWER AND BATTERY CAPACITY 31

3. MOTORCYCLE DESIGN AND TESTING 33

3.1 ELECTRICAL DESIGN 34

3.2 MECHANICAL DESIGN 36

3.3 TESTING 38

4. MOTORCYCLE RACE RESULTS AND ANALYSIS 43

4.1 ANALYZING THE MOTORCYCLE PERFORMANCE 43

4.2 MODEL VALIDATION 45

4.3 FRAMEWORK FOR SPURRING INNOVATION THROUGH RACING 47

4.3.1 Consider the Historical Context 48

4.3.2 Utilize the Power of Regulation 48

4.3.3 Drive Technology 48

4.3.4 Provide Valued Entertainment 48

4.3.5 Inspire Consumer Demand 49

PART II: ESTIMATING AN ELECTRIC VEHICLE'S DISTANCE TO EMPTY 51

5. INTRODUCTION TO PART II 53

5.1 MOTIVATION 54

5.2 OVERVIEW 54

5.3 RELATED WORK 55

6. STOCHASTIC VEHICLE SIMULATIONS FOR EVALUATING D_{TE} ALGORITHMS 57

6.1 SIMULATION ARCHITECTURE 57

6.2 STOCHASTIC SPEED PROFILE GENERATOR 58

6.2.1 Raw Driving Data 59

6.2.2 Categorizing and Grouping Data 59

6.2.3 Markov Model 62

6.2.4 Simulating Highway, City and Aggressive Driving Conditions 63

6.2.5 Creating a Stochastic Speed Profile 64

6.3 SUBSYSTEM MODELS 65

6.3.1 Vehicle Model 65

6.3.2 Transmission Model 66

6.3.3 Motor Model 66

6.3.4 Battery Model 67

6.3.5 Auxiliary Model 67

6.4 GENERATING STOCHASTIC VEHICLE SIMULATIONS 68

7. FUNDAMENTAL D_{TE} CONCEPTS 71

7.1 KEY D_{TE} EQUATIONS 71

7.2 MEASURING THE REMAINING BATTERY ENERGY 74

7.3 OTHER APPLICATIONS WITH A SIMILAR FORMULATION 75

7.4 CONVENTIONAL D_{TE} ALGORITHMS 75

7.5 USING ESTIMATES OF FUTURE CONDITIONS AND MODELS TO IMPROVE D_{TE} PREDICTIONS 79

8. A REGRESSION-BASED D_{TE} ALGORITHM 83

8.1 MULTIVARIATE LINEAR REGRESSION MODEL 84

8.2 EXPLANATORY VARIABLES 85

8.3 CREATING A TRAINING DATASET 86

8.4 ALGORITHM SIMULATION 87

8.5 VALIDATING THE ASSUMPTIONS AND FIT OF THE REGRESSION MODEL 88

9. COMPARING D_{TE} ALGORITHMS 91

9.1 MEASURING THE PERFORMANCE OF D_{TE} ALGORITHMS 91
9.2 RESULTS 92

PART III: SUMMARY AND CONTRIBUTIONS 97

10. CONCLUSIONS 99
10.1 SUMMARY OF THESIS 99
10.2 SUMMARY OF CONTRIBUTIONS 101
10.3 ONGOING WORK 102
10.3.1 Increasing Average Speeds at the Isle of Man TT Zero 103
10.3.2 Advancing D_{TE} Algorithms 104
10.3.3 Comparing D_{TE} Algorithms 104

REFERENCES 105

Part I: Designing an Electric Motorcycle for the Isle of Man TT Zero Race

1. Introduction to Part I

Part I describes the process of designing, building, testing and racing a high performance electric motorcycle for the 2011 Isle of Man Tourist Trophy (TT) Zero race. Systems engineering was used to size the batteries and motors, predict vehicle speeds and predict the time required to finish the race. Forward- and backward-looking vehicle simulations were used to predict the motorcycle performance under full-throttle conditions and estimate the total battery energy required to traverse the entire course. The mechanical and electrical designs are described along with the critical process of incremental testing. In June 2011 the motorcycle design and simulations were tested in three races on the Isle of Man. Post-race analysis showed that the predictions had less than 10% error.

1.1 Motivation

The Isle of Man Tourist Trophy (TT) race is the oldest existing motorcycle race and for over 100 years has served as a proving ground for both riders and engineers to advance motorcycle technology. Soichiro Honda, founder and then president of Honda Motor Corporation, once declared that the innovation required to win the Isle of Man race would "rank at the world's highest levels of engineering" [1]. The desire to create innovation through racing continues today and in 2009 an electric class was added to the TT with the aim of advancing zero emission vehicle technology. The Isle of Man TT Zero is an example of a new breed of "zero emission" races, which aim to spur innovation that will reduce the environmental impact of consumer vehicles. Racing has historically been a catalyst for innovation, particularly in the early years of motorcycles and automobiles [2]. New concepts were tested on the track and the desire to win drove companies to produce superior technology. Consumer demand for better performance motivated companies to transfer the technology from the racetrack to the mass market.

1.2 Overview

Systems engineering is used to ensure feasibility early in the design process, select the proper motor and battery size, and predict the motorcycle performance in Chapter 2. Both the

electrical and mechanical subsystem designs and testing methods are described in Chapter 3. Finally, the race data is used to evaluate the motorcycle performance and validate the integrated models in Chapter 4. The final chapter also outlines a set of guidelines for designing zero emission races with the aim of promoting innovation.

1.3 Related Work

The Isle of Man TT Zero race in 2009 served as the first ever large-scale electric motorcycle race. Since the field is still in infancy, there is very little engineering literature on the topic of designing electric motorcycles for racing. There is no literature on predicting energy requirements for the Isle of Man race since the gasoline motorcycles have never been energy limited. A university in Germany built an electric motorcycle for the TTXGP in 2012 and published a paper on their design, but they did not describe the methods used to size the motor and battery [3]. Two recent studies describe a motor controller [4] and motor [5] specifically designed for electric motorcycle racing.

Though there are few publications related to electric motorcycle racing, there is an extensive amount of literature for solar vehicle racing. Solar vehicle racing started in the mid 1980s and includes teams from international corporations and universities. Similar to electric motorcycle racing on the Isle of Man, one of the central challenges in solar racing is to predict the required battery energy and maximize vehicle performance. The problem of optimally controlling the vehicle to minimize energy has been studied for solar cars [6][7] and more generally for electric vehicles [8][9]. These methods could be applied to the TT Zero race, though extensions would be required to include corning (braking). Also, it is questionable that optimal control would yield large energy savings. More recent work describes designs for the hybrid-electric and all-electric Formula Society of Automotive Engineers (FSAE) competitions [10]. The most common approach is to simulate the vehicle using commercially available software along with custom models as needed. For example, commercially available software has been used to optimize a hybrid vehicle drivetrain [11][12]. Finally, there has been a large amount of work on general vehicle and subsystem (motors, etc.) modeling [13][14].

2. Motorcycle Systems Engineering

This section describes how system-level engineering was used in designing the electric motorcycle. More specifically it explains the methods used to explore how changes in the *design parameters* affect *performance metrics* (Table 2.1). Systems engineering was used to size the batteries and motors, predict vehicle speeds and predict the time required to finish the race. The process involved deriving a set of subsystem models (Section 2.1) and then simulating various scenarios based on specific inputs. Two types of simulations were considered. The first estimated the motor and battery power, and vehicle speed of the motorcycle when full-throttle is applied (Section 2.2). The second simulation estimated the battery energy required to traverse the entire course. The conventional approach to estimating a vehicle's energy consumption is to simulate the vehicle using an estimated speed profile as input (e.g. EPA "driving cycle" [15]). But the speed profiles are difficult to predict in this case because the TT course is complex with over 200 turns, varying elevation and is traversed at fluctuating high speeds. Thus a new approach was derived, which assumed that the required battery energy was in between estimates of lower and upper bounds. The lower bound, or best case, was determined by assuming the motorcycle maintained a constant vehicle speed throughout the course, which was shown to be the most energy efficient way to drive. The upper bound, or worst case, was determined by assuming the motorcycle maintained a constant motor power throughout the course, which would yield large speed fluctuations and is thus inefficient. The lower and upper bounds are derived in Sections 2.3 and 2.4, respectively. Section 2.5 adds braking to the speed, time and energy estimates. Finally, Section 2.6 explains how the methods described were used in practice to estimate the required motor power and battery energy.

Table 2.1: Design parameters and performance metrics.

Design Parameters	Performance Metrics
• Mass • Aerodynamics • Rolling resistance • Sprocket ratio • Finishing time • Battery specifications • Motor specifications • Motor controller specifications and settings • Drivetrain efficiencies	• Acceleration • Maximum and average speed • Battery energy consumed • Power (vehicle, batteries, motors)

2.1 Subsystem Models

The subsystem models derived here are used in later subsections to explore the motorcycle performance based on design parameters (Table 2.1). When the speed profile is specified as input, the simulation is referred to as backward-looking and when the throttle profile is specified the simulation is referred to as a forward-looking. The following subsections describe each of these approaches.

2.1.1 Backward-looking Simulations

A backward-looking simulation is shown in Figure 2.1. The speed is specified as a function of time, $\dot{x}(t)$, and is the input to the vehicle model. Environmental Protection Agency (EPA) "Driving Cycles" are commonly used to specify the speed [15], though this approach is not applicable to racing since the speeds and general driving conditions are different from those represented by the standard EPA specifications. A vehicle model determines the wheel force, F_w, required to follow the prescribed speed profile based on a set of design parameters. Similarly, the transmission and motor models determine how much electric power is needed by the motor, P_b. The battery model translates the total electrical need to an estimated amount of battery energy (E_b), which includes internal losses. These models are derived in the following subsections.

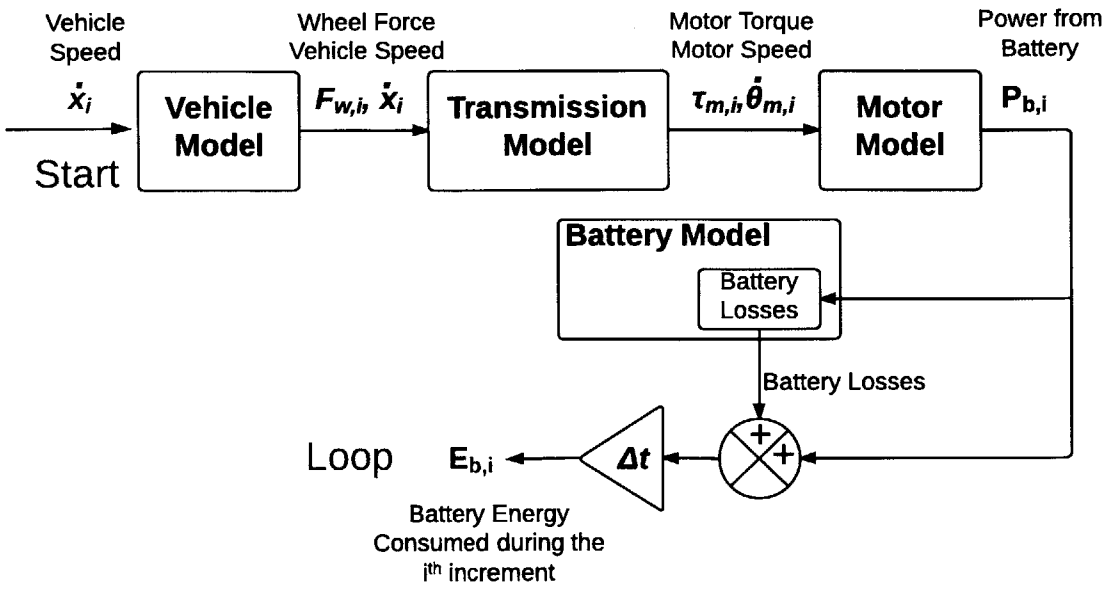

Figure 2.1: A backward-looking vehicle simulation.

Vehicle Model

The electric motorcycle can be modeled as a mass on an incline with externally applied forces (Figure 2.2). It is propelled forward by an electric motor acting through the rear wheel with a force, F_w, but slowed down by the aerodynamic drag, F_{aero}, the rolling resistance from the two wheels, $F_{rolling}$, and the horizontal component of weight, $F_{gravity}$. Newton's second law states:

$$\sum F = m\ddot{x} = F_w - F_{aero} - F_{rolling} - F_{gravity} \quad \textbf{2.1}$$

Which can be written as [30]:

$$m\ddot{x} = F_w - {}^1/_2\,\rho C_d A(\dot{x} + w)^2 - mgC_{rr}Cos\beta - mgSin\beta \quad \textbf{2.2}$$

Where m is the total mass of the vehicle and rider, w is the wind speed, C_{rr} is the rolling resistance coefficient, ρ is the density of air, C_dA is the aerodynamic coefficient, g is gravity, and β is the angle of the road. Solving for F_w:

$$F_w = m\ddot{x} + {}^1/_2\,\rho C_d A(\dot{x} + w)^2 + mgC_{rr}Cos\beta + mgSin\beta \quad \textbf{2.3}$$

The unknown parameters C_dA and C_{rr} can be found experimentally through wind tunnel and road testing. The acceleration, $\ddot{x}$, is determined by differentiating the known (specified) speed profile.

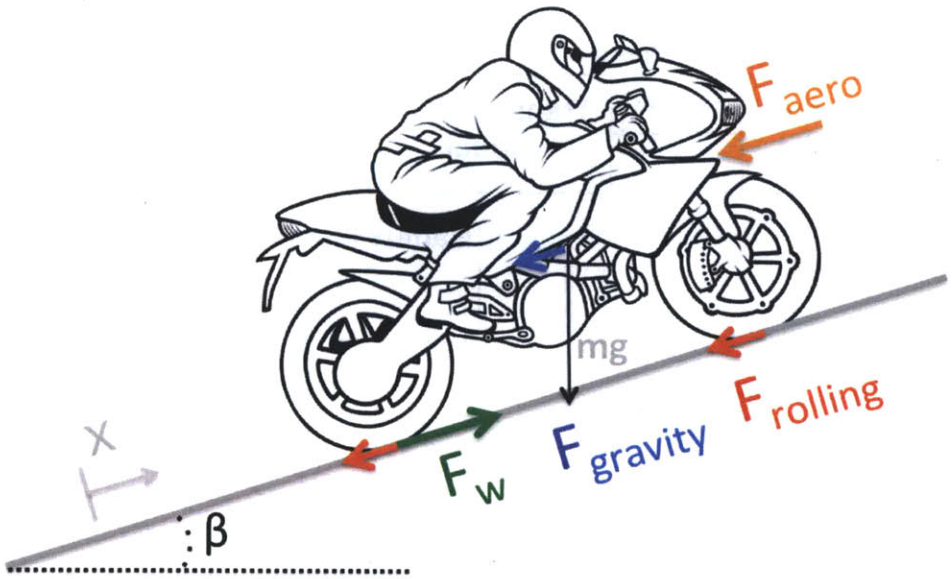

Figure 2.2: The motorcycle can be modeled as a mass on an incline with externally applied forces.

Transmission Model

The force on the rear wheel, F_w, originates from a motor acting through a chain and two sprockets. Summing the torques around the wheel yields (Figure 2.3):

$$\sum \tau = I_w \ddot{\theta}_w = \tau_w - F_w r_w \qquad \textbf{2.4}$$

Where τ_w is the torque on the rear wheel, I_w is the mass moment of inertia and $\ddot{\theta}_w$ is the rotational acceleration of the wheel(s). Assuming the wheel is the only rotating mass and is a uniformly distributed cylinder of radius r_w:

$$I_w = \frac{m_w r_w^2}{2} \qquad \textbf{2.5}$$

Where m_w is the total mass of all the wheels. The following relationship can be determined through geometry:

$$\dot{\theta}_w = \frac{\dot{x}}{r_w} \qquad \textbf{2.6}$$

Taking the derivative of Equation 2.6 yields:

$$\ddot{\theta}_w = \frac{\ddot{x}}{r_w} \qquad \textbf{2.7}$$

Combining Equations 2.4, 2.7 and 2.8:

$$\tau_w = \left(\frac{\ddot{x} m_w}{2} + F_w\right) r_w \qquad \textbf{2.8}$$

Conservation of energy can be used to relate the wheel torque to the motor torque (Figure 2.3):

$$\tau_w \dot{\theta}_w = \eta_d \tau_m \dot{\theta}_m \quad \textbf{2.9}$$

Where η_d is the transmission efficiency, which can be estimated or determined experimentally. Solving for the motor torque:

$$\tau_m = \tau_w \frac{\dot{\theta}_w}{\dot{\theta}_m} \frac{1}{\eta_d} \quad \textbf{2.10}$$

Defining the "sprocket ratio", z, as:

$$z \equiv \frac{\dot{\theta}_m}{\dot{\theta}_w} \quad \textbf{2.11}$$

Combining Equations 2.8, 2.10 and 2.11:

$$\tau_m = \left(\frac{m_w}{2}\ddot{x} + F_w\right) \frac{r_w}{z\eta_d} \quad \textbf{2.12}$$

And the motor speed can be determined by combining Equations 2.6 and 2.11:

$$\dot{\theta}_m = \frac{z\dot{x}}{r_w} \quad \textbf{2.13}$$

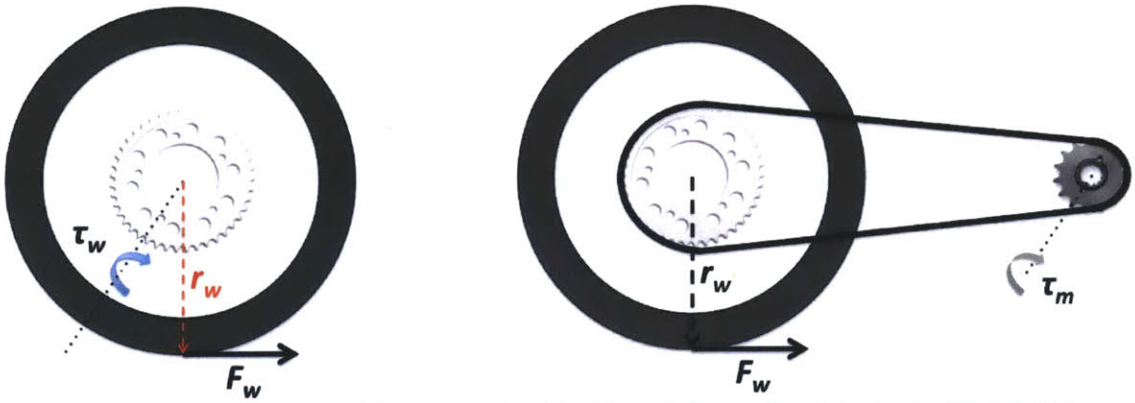

Figure 2.3: A free body diagram of the rear wheel (left) and the entire drivetrain (right). The torque on the motor results in a force on the wheel.

Motor Model

Conservation of power yields a relationship for the power going to the motor from the battery, P_b (Figure 2.4):

$$P_b = \frac{\tau_m \dot{\theta}_m}{\eta_{mc}\eta_m} \quad \textbf{2.14}$$

Where η_{mc} is the efficiency of the motor controller, which is typically assumed to be constant and ~90 to 95%. The efficiency of the motor, η_m, can vary greatly based on the motor torque and speed. A motor efficiency map relates the motor efficiency to torque and speed and is typically obtained experimentally using a dynamometer [17]. Combining Equations 2.12, 2.13 and 2.14:

$$P_b = \frac{\left(\frac{\ddot{x}m_w}{2} + F_w\right)\dot{x}}{\eta_{mc}\eta_m\eta_d} \quad \textbf{2.15}$$

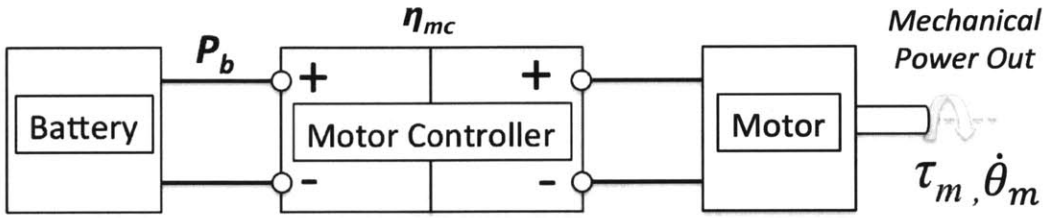

Figure 2.4: Energy flows from the Battery -> Motor Controller -> Motor -> Motor Torque.

Battery Model

A battery cell can be modeled as a resistor in series with a voltage source. The cells are connected in parallel and series to form a battery module or pack (Figure 2.5). The battery losses can be modeled as Ohmic:

$$P_{b,loss} = I_b^2 R_b \quad \textbf{2.16}$$

Where I_b is the current through the battery pack and R_b is the total internal resistance, which can be determined using:

$$R_b = \frac{k}{l} R_c \quad \textbf{2.17}$$

Where R_c is the internal resistance of a single cell and k and l are the number of cells in series and parallel, respectively (Figure 2.5). The power from the battery can be written as:

$$V_{bn} I_b - I_b^2 R_b = P_b \quad \textbf{2.18}$$

Where V_{bn} is the voltage on the battery pack when no current is being drawn. The only remaining unknown is I_b, which can be determined by solving Equation 2.18 using the quadratic equation:

$$I_b = \frac{V_{bn}}{2R_b} - \frac{\sqrt{V_{b,n}^2 - 4R_b P_b}}{2R_b} \quad \textbf{2.19}$$

The total power (including losses) from the battery can be written as:

$$P_{bn} = V_{bn} I_b = \frac{V_{bn}^2}{2R_b} - \frac{V_{bn}\sqrt{V_{b,n}^2 - 4R_b P_b}}{2R_b} \quad \textbf{2.20}$$

The total energy (including losses) from the battery can now be determined using:

$$E_b = \int P_{bn}\, dt \quad \textbf{2.21}$$

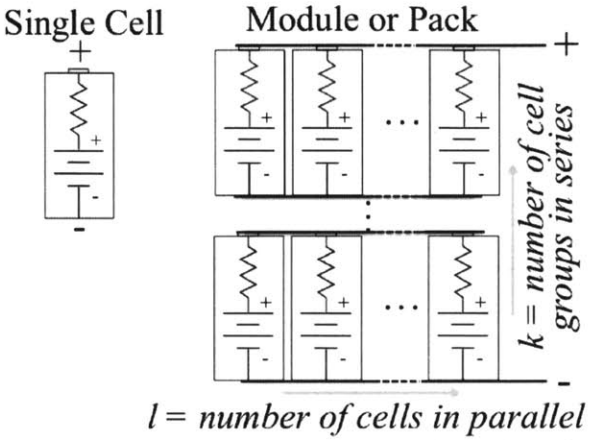

Figure 2.5: A battery cell was modeled as a resistor in series with a voltage source.

2.1.2 Forward-looking Simulations

The motor torque, τ_m, for a DC permanent magnet motor is proportional to the current passing through the motor:

$$\tau_m = K_\tau I_m \quad \textbf{2.22}$$

where K_τ is the torque constant, and I_m is the motor current. Rearranging Equation 2.12 and combining the result with Equation 2.22:

$$F_w = \frac{z\eta_d}{r_w} K_\tau I_m - \frac{m_w}{2}\ddot{x} \quad \textbf{2.23}$$

Now the acceleration of the vehicle can be determined by combining Equations 2.2 and 2.23:

$$\ddot{x} = \frac{1}{m + \frac{m_w}{2}}\left(\frac{z\eta_d}{r_w} K_\tau I_m - {}^1\!/_2\, \rho C_d A(\dot{x} + w)^2 - mgC_{rr}Cos\beta - mgSin\beta\right) \quad \textbf{2.24}$$

The only unknown in Equation 2.24 is the motor current, I_m, which is based on the throttle input. Once I_m is known, the speed and position for the next increment can be determined using numerical integration:

$$\dot{x}_{i+1} = \dot{x}_i + \ddot{x}_i(t_{i+1} - t_i) \quad \textbf{2.25}$$

$$x_{i+1} = x_i + \dot{x}_{i+1}(t_{i+1} - t_i) \quad \textbf{2.26}$$

Determining I_m based on the throttle input is the focus for the remainder of this subsection.

A DC permanent magnet motor can be modeled as a voltage-generating source (V_{emf}) in series with a resistor (R_m) (Figure 2.6). By summing the voltages around the motor model circuit, the following relationship can be derived:

$$I_m = (V_m - V_{emf})/R_m \qquad \textbf{2.27}$$

V_{emf} is proportional to the rotational speed of the motor, $\dot{\theta}_m$, which can be related to the linear speed of the rear wheel, $\dot{x}$, since they are connected. Rewriting Equation 2.27:

$$I_m = \frac{V_m - K_\theta \dot{\theta}_m}{R_m} = \frac{V_m}{R_m} - \frac{zK_\theta}{R_m r_w}\dot{x} \qquad \textbf{2.28}$$

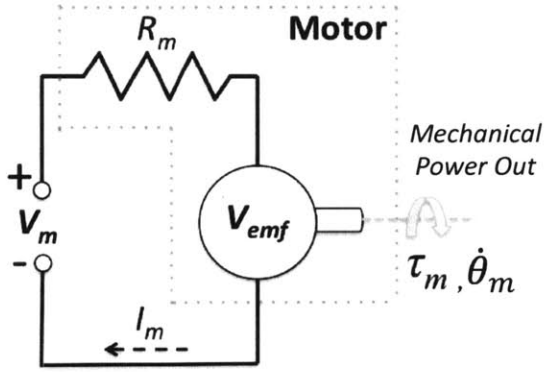

Figure 2.6: It was assumed that a Direct Current (DC) Permanent Magnet (PM) can be modeled as a resistor in series with a back-EMF generating device.

As shown in Equation 2.28, the motor controller continually increases V_m as $\dot{x}$ increases in order to maintain a constant I_m. This is done until (1) the motor current reaches a maximum value, I_m^{limit}, which is a value specified by the engineer based on performance and/or motor thermal considerations, or (2) the motor controller reaches "all-on" conditions (100% duty cycle). When (2) occurs, the batteries are essentially directly connected to the motor and thus $I_m = I_b$, $V_m \approx V_b$[1] and I_m decreases with increasing speed as shown in Figure 2.7 as a solid line. In other words, the motor current is equal to the minimum value of these two scenarios:

$$I_m = minimum\{s \cdot I_m^{limit}, I_b\} \qquad \textbf{2.29}$$

Scenarios (1) and (2) are referred to as current-limited" and voltage-limited, respectively.

[1] When the motor controller is at 100% duty cycle ("all on") there is still a small voltage drop across the transistors.

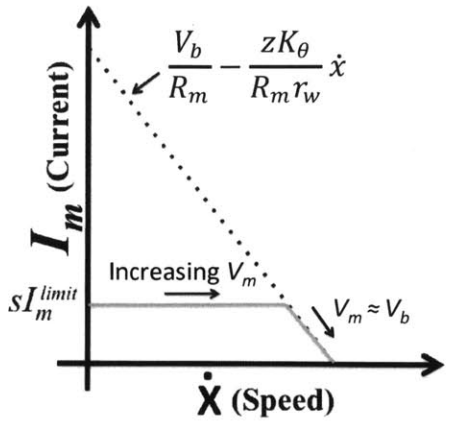

Figure 2.7: This curve shows the relationship between vehicle speed ($\dot{x}$) and motor current (I_m). The motor controller continually increases the motor voltage (V_m) as $\dot{x}$ increases in order to maintain a constant I_m. Eventually the back-EMF becomes large enough that the motor is voltage limited and thus the current decreases with vehicle speed.

The exact values of V_b, I_b, V_m, I_m can be determined by simultaneously solving four equations obtained from the models shown in Figure 2.8. First, conservation of power through the motor controller yields:

$$\eta_{mc} V_b I_b = V_m I_m \qquad \textbf{2.30}$$

Second, summing the voltage drops through the motor model yields:

$$V_m - I_m R_m = K_\theta \dot{\theta}_m \qquad \textbf{2.31}$$

Combing this result with Equation 2.13:

$$V_m - I_m R_m = K_\theta \frac{z\dot{x}}{r_w} \qquad \textbf{2.32}$$

Third, summing the voltage drops within the battery model yields:

$$V_{bn} - I_b R_b = V_b \qquad \textbf{2.33}$$

Thus the four equations are Equations 2.30, 2.32 and 2.33 and:

$$I_m = s \cdot I_m^{limit} \qquad \textbf{2.34}$$

Where s is the throttle signal and varies from 0 to 1. Equations 2.30, 2.32 and 2.33 can be solved simultaneously again, but instead of using 2.34 for the forth equation, the following is assumed (100% duty cycle of motor controller):

$$I_m = I_b \qquad \textbf{2.35}$$

The solutions for V_b, I_b, V_m associated with the minimum motor current are used (Equation 2.29). The total energy consumed from the battery can now be determined:

$$E_b = \int V_{bn} I_b \, dt \qquad \textbf{2.36}$$

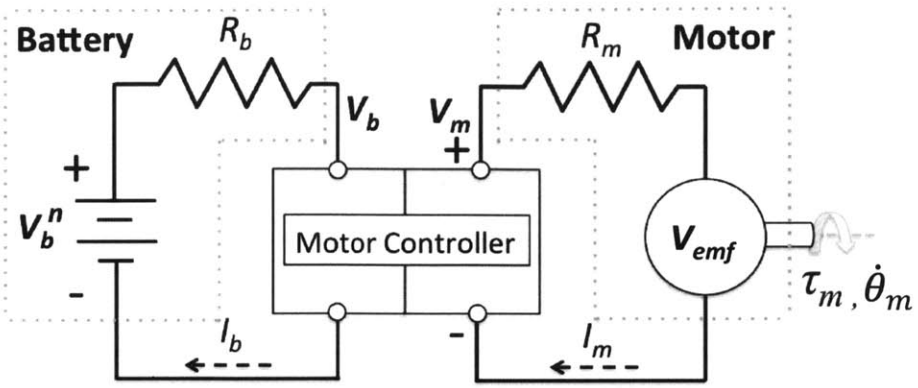

Figure 2.8: Power electronics model consisting of the battery, motor controller and motor.

2.2 Full-throttle Simulations

It is common when studying dynamic systems to excite the system with a "step input" to simulate how it will respond to a maximum input signal. In the case of motorcycle design, a synonymous concept is referred to as a full-throttle simulation. It is assumed that the rider starts at zero speed and applies full-throttle. The motorcycle's speed is then simulated all the way until acceleration is zero, which is the point of maximum speed. It is assumed that the motorcycle is on a straight road and does not experience braking. The forward-looking simulation described in Section 2.1.2 can be used to simulate the motorcycle based on a throttle profile (a step input was used here, though a saw-tooth, ramp, etc. could also be used):

1. Specify the throttle profile (e.g. $s_i = 1$ for full-throttle), calculate $I_{m,i}$ by simultaneously solving Equations 2.29, 2.30, 2.32 and 2.33. Then calculate the motor torque using Equation 2.22.
2. Calculate the wheel force ($F_{w,i}$) using Equation 2.23, obtain a road angle (β_i) from the GPS data, and use Equation 2.24 to calculate the vehicle acceleration ($\ddot{x}_i$).
3. Calculate the battery energy using Equation 2.36.
4. Use Equations 2.25 and 2.26 to step forward in time ($i+1$). Repeat the algorithm for the next increment.

Full-throttle simulations show how maximum acceleration and speed largely depend on the drag forces (e.g. sum of the gravity, rolling, and aero forces) and the motor output power. The motor power that is in excess of the drag power causes the vehicle to accelerate. As the motorcycle increases in speed, the drag forces increase as shown in Figure 2.9a. The motor has a constant torque until the back-EMF from the motor becomes limiting, which is when the

available power from the motor starts to decrease. Once the motor and drag power are equal, the vehicle no longer accelerates and this represents the maximum speed. Thus the intersection of the motor and drag power curves is the maximum speed of the motorcycle and where the vehicle's acceleration is zero.

The behavior of the motor power curve is heavily influenced by both the sprocket ratio and the maximum current from the motor controller (I_{limit}). A larger sprocket ratio and/or I_{limit} will yield higher motor power at a given speed, and thus greater acceleration (Figure 2.9b and c). However, increasing the sprocket ratio decreases the maximum speed. As shown in Figure 2.9d, more current is needed during vehicle acceleration than at steady state/cruise conditions. Simulations like these were used to estimate the appropriate current limit and sprocket ratio.

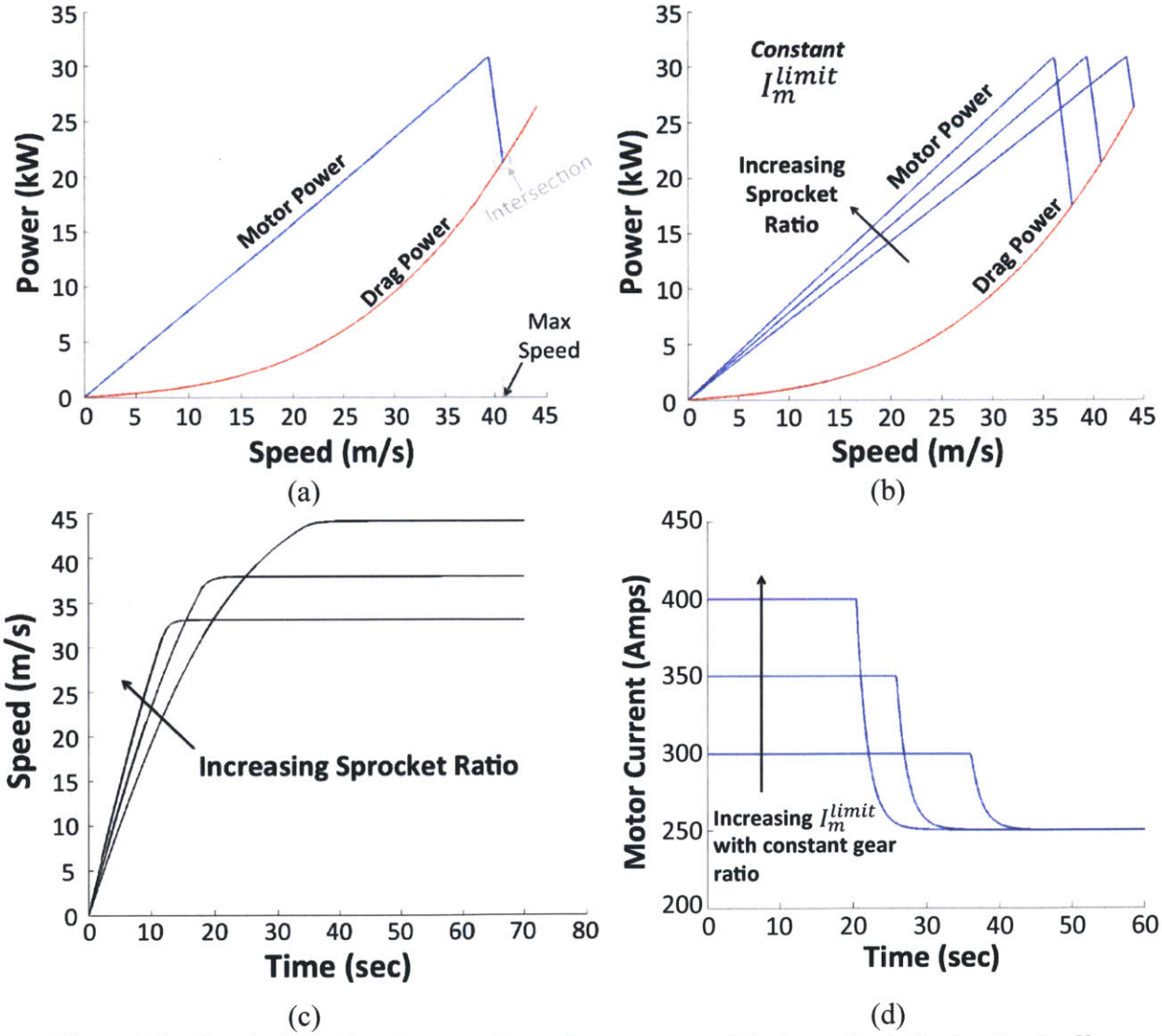

Figure 2.9: Simulations like the ones shown here were used to investigate design tradeoffs.

The main limitation of the algorithm described above is the difficulty in knowing the throttle input, s_i, as a function of distance or time. It is typically infeasible to know the throttle profile for the entire course, since the rider adjusts the throttle in real-time based on personal judgment. Thus this algorithm was not used to estimate the battery energy required to traverse the *entire* course. However, it is useful in exploring maximum power, acceleration and speed during short full-throttle simulations.

2.3 Constant Vehicle Speed Simulations

The backward-looking simulation described in Section 2.1.1 can be used to simulate the motorcycle when it is assumed that a constant speed is maintained throughout the course:

1. Obtain a road angle (β_i) from the GPS data and calculate the wheel force ($F_{w,i}$) using Equation 2.3 with $\ddot{x} = 0$ and $\dot{x}$ = constant.
2. Calculate the power from the battery to the motor controller using Equation 2.15 and the power and energy consumed from the battery using Equations 2.20 and 2.21.

The following subsection proves that it is most energy efficient for a vehicle to maintain a constant speed.

2.3.1 Proof that Constant Speed Minimizes Energy Consumption

The objective of an electric race is to minimize the time it takes to cross the finish line for a fixed amount of battery energy and a specified course. Once the race begins, the only variable the driver can control is the speed of the vehicle, and this section will show that it is most energy efficient to maintain a constant speed. In practice it is impossible to maintain a constant speed since braking is required to safely traverse the corners of the course. But if the braking losses are thought of as a fixed loss that only depend on the average speed, then this derivation is valid. Battery and motor losses are not included in this proof, and it is assumed that the vehicle is traveling at speeds above the terminal velocity (Figure 2.10).

The time it takes to traverse the entire course can be written as:

$$t_f = {}^{x_f}/_{\bar{\dot{x}}} \qquad \textbf{2.37}$$

Where x_f is the distance of the course, and $\bar{\dot{x}}$ is the average speed. The minimum time, $t_{f,min}$, can be written as:

$$t_{f,min} = min\left\{{}^{x_f}/_{\bar{\dot{x}}}\right\} \quad \textbf{2.38}$$

Since x_f is fixed, t_f is minimized by maximizing the average speed. Thus we want to minimize the energy use, E, but maximize the average speed, $\bar{\dot{x}}$. The energy required by the vehicle to travel between positions x_0 and x_f can be written as:

$$E = \int_{x_0}^{x_f} F_w \cdot dx \quad \textbf{2.39}$$

Combining Equations 2.3 and 2.39 yields:

$$E = \int_{x_0}^{x_f} (m\ddot{x} + mgSin\theta + mg\mu Cos\theta + C(\dot{x} + w)^2)dx \quad \textbf{2.40}$$

And expanding the integration:

$$E = \int_{x_0}^{x_f} m\ddot{x}dx + \int_{x_0}^{x_f} mgSin\theta dx + \int_{x_0}^{x_f} mg\mu Cos\theta dx + \int_{x_0}^{x_f} C(\dot{x} + w)^2 dx \quad \textbf{2.41}$$

The first term can be rewritten as:

$$\int_{x_0}^{x_f} m\ddot{x}dx = m\int_{x_0}^{x_f} \frac{d\dot{x}}{dt}dx = m\int_{x_0}^{x_f} \frac{d\dot{x}}{dt}\dot{x}dt = m\int_{x_0}^{x_f} \dot{x}d\dot{x} = {}^1/_2\, m(\dot{x}_f^2 - \dot{x}_0^2) \quad \textbf{2.42}$$

Which is the *kinetic energy* of the vehicle. The second term can be rewritten as:

$$\int_{x_0}^{x_f} mgSin\theta dx = \int_{y_0}^{y_f} mgdy = mg(y_f - y_0) \quad \textbf{2.43}$$

Which is the *potential energy* of the vehicle. The third term of Equation 2.41 can be rewritten as:

$$\int_{x_0}^{x_f} mg\mu Cos\theta dx = mg\mu \int_{x_0}^{x_f} Cos\theta dx \quad \textbf{2.44}$$

Substituting Equations 2.42, 2.43 and 2.44 into Equation 2.41 yields:

$$E = {}^1/_2\, m(\dot{x}_f^2 - \dot{x}_0^2) + mg(y_f - y_0) + mg\mu \int_{x_0}^{x_f} Cos\theta dx + \int_{x_0}^{x_f} C(\dot{x} + w)^2 dx \quad \textbf{2.45}$$

Assuming that $\dot{x}_f = \dot{x}_0$ and $y_f = y_0$, , the only remaining term to be minimized based on the driver control is:

$$E_{min} = min\left\{\int_0^{x_f} C(\dot{x} + w)^2 dx\right\} \quad \textbf{2.46}$$

Defining a new variable (Figure 2.11):

$$\dot{x}^* = \dot{x} - \bar{\dot{x}} \quad \textbf{2.47}$$

Where $\dot{x}^*$ is the speed above the average speed. Thus:

$$\dot{x} = \bar{\dot{x}} + \dot{x}^* \quad \textbf{2.48}$$

Now combining Equations 2.46 and 2.48 and expanding the terms:

$$E_{min} = min\left\{C\int_0^{x_f}(\dot{x}^{*2} + \bar{\dot{x}}^2 + \mathrm{w}^2 + 2\dot{x}^*\bar{\dot{x}} + 2\bar{\dot{x}}\mathrm{w} + 2\dot{x}^*w)dx\right\} \quad \textbf{2.49}$$

Since w cannot be controlled and $\bar{\dot{x}}$ is a constant, they can be ignored in the minimization. The remaining terms are:

$$min\left\{C\int_0^{x_f}(\dot{x}^{*2} + 2\dot{x}^*\bar{\dot{x}} + 2\dot{x}^*w)dx\right\} \quad \textbf{2.50}$$

Which is minimum when:

$$\dot{x}^* = 0 \quad \textbf{2.51}$$

Combining Equations 2.48 and 2.51:

$$\dot{x} = \bar{\dot{x}} \quad \textbf{2.52}$$

This shows that the vehicle should maintain a constant speed in order to minimize the energy it takes to complete the course.

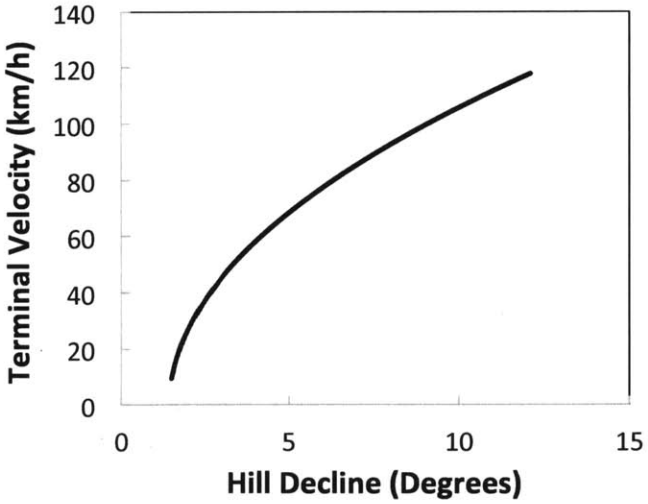

Figure 2.10: The terminal velocity for different hill decline angles. For example, on a hill of 10 degrees, the vehicle could accelerate (without power) all the way until reaching the terminal velocity of 100 km/h. At the terminal velocity, the drag forces will equally balance the gravity hill force and so the vehicle will no longer accelerate. If the vehicle is powered to speeds above the terminal velocity, the vehicle will decelerate down to the terminal velocity when the power is removed. The motorcycle is always above the terminal velocity so it can never accelerate down a hill without motor torque.

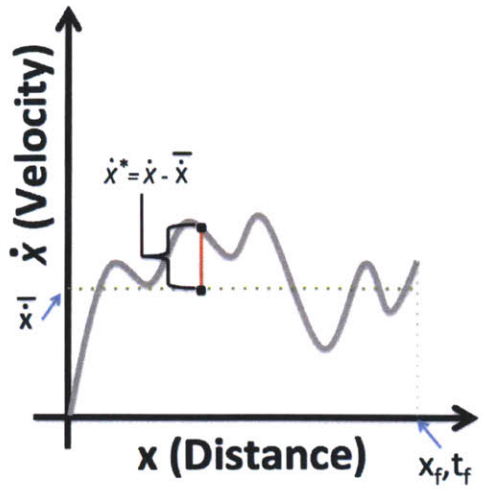

Figure 2.11: The variable $\dot{x}^*$ is defined as the difference between the instantaneous ($\dot{x}$) and average ($\bar{\dot{x}}$) speed.

2.4 Constant Power Simulations

The following equations were used for the assumption that the motor maintains a constant power output throughout the course. Combining Equations 2.6, 2.8 and 2.9 yields:

$$F_w = \frac{P_m \eta_d}{\dot{x}} - \frac{m_w}{2}\ddot{x} \qquad \textbf{2.53}$$

And defining the motor output power, P_m as:

$$P_m = \tau_m \dot{\theta}_m \qquad \textbf{2.54}$$

Combining Equations 2.14 and 2.54 yields:

$$P_b = \frac{P_m}{\eta_{mc}\eta_m} \qquad \textbf{2.55}$$

The following steps were used:

1. Calculate the wheel force ($F_{w,i}$) for a specified constant motor power, P_m, using Equation 2.53. Assume an initial vehicle speed.
2. Obtain a road angle (β_i) from the GPS data, and use Equation 2.2 to calculate the vehicle acceleration ($\ddot{x}_i$).
3. Calculate the battery energy by integrating Equation 2.55 or 2.20 depending on if battery losses are included.
4. Use Equations 2.25 and 2.26 to step forward in time ($i+1$). Repeat the algorithm for the next increment.

2.5 Braking Losses

The calculations so far have not included the energy lost from braking, which will increase the estimates for the battery energy required and decrease the average speed. Thus a braking efficiency, ψ, is defined as:

$$\psi \equiv \frac{avg.speed\ with\ braking}{avg.speed\ without\ braking} \quad \textbf{2.56}$$

For example, it can be assumed that the braking reduces the average speed by 15%, thus ψ =0.85. The average speed when braking is included can now be written as:

$$\bar{\dot{x}}^B = \psi\bar{\dot{x}} \quad \textbf{2.57}$$

where $\bar{\dot{x}}$ is the average speed without braking and the superscript "B" denotes values after braking estimates are included. Also by definition:

$$\bar{\dot{x}}^B = \frac{x_f}{t_f^B} \quad \textbf{2.58}$$

Where x_f is the distance of the course and t_f^B is the time to finish the course when braking is included. Also:

$$\bar{\dot{x}} = \frac{x_f}{t_f} \quad \textbf{2.59}$$

Where t_f is the time required to finish the course when braking is not included. Combining Equations 2.57, 2.58 and 2.59 yields:

$$\bar{\dot{x}} = \frac{x_f}{\psi t_f^B} \quad \textbf{2.60}$$

Thus this higher speed would be used in the constant speed simulations.

An alternative approach is to estimate the amount of energy lost because of changes in kinetic energy while braking through the turns. For example, let us assume that the motorcycle enters *n* turns at 150 km/h and exits after braking at 100 km/h. The change in kinetic energy from braking is:

$$\Delta KE = n\frac{1}{2}m({v_1}^2 - {v_2}^2) \quad \textbf{2.61}$$

Substituting in values for this course and motorcycle (assuming n = 50 turns):

$$\Delta KE = 50\frac{1}{2}300(150^2 - 100^2) \approx 2.6\ kWh \quad \textbf{2.62}$$

Thus ~2.6 kWh of energy could be attributed to braking losses.

2.6 Estimating the Required Motor Power and Battery Capacity

The following algorithm uses the methods described in Sections 2.2 through 2.5 to estimate the required motor power and battery capacity:

1. Choose a desired average finishing time, t_f^B and then use Equation 2.60 to determine the corresponding average speed without braking, $\bar{\dot{x}}$.
2. Use the value of $\bar{\dot{x}}$ with the algorithm described in Section 2.3 to estimate the battery energy, E_b. This serves as a lower-bound (best-case) estimate for the actual battery energy.
3. Put the equations described in Section 2.4 into a spreadsheet, and iterate (or numerically solve for) the value of P_m until the average speed equals $\bar{\dot{x}}$ (the same value used above). This serves as an upper-bound (worst-case) estimate for the actual battery energy.
4. Perform the full-throttle simulations in Section 2.2 to ensure that the maximum acceleration, speeds and power are adequate.

For the final estimates it was assumed that an average speed of 137 km/h (27 minutes) would be competitive. Based on the simulations described above, this would required 25 to 30 kW of average power from the motors and ~10 to 11 kWh of battery energy (Figure 2.12). The braking constant, ψ, was assumed to be 0.8 for the constant power driving cycle and 0.82 for the constant speed driving cycle[2].

Table 2.2: Parameter specifications used for the vehicle simulations.

Description	Variable	Value	Unit
Total Mass	m	311	kg
Drag Area	C_dA	0.41	m^2
Rolling Resistance	C_r	0.025	-
Motor Speed Constant	K_θ	42	RPM/V
Motor Torque Constant	K_τ	0.207	Nm/A

[2] It was assumed that the constant power simulation would require more braking since there are more speed fluctuations.

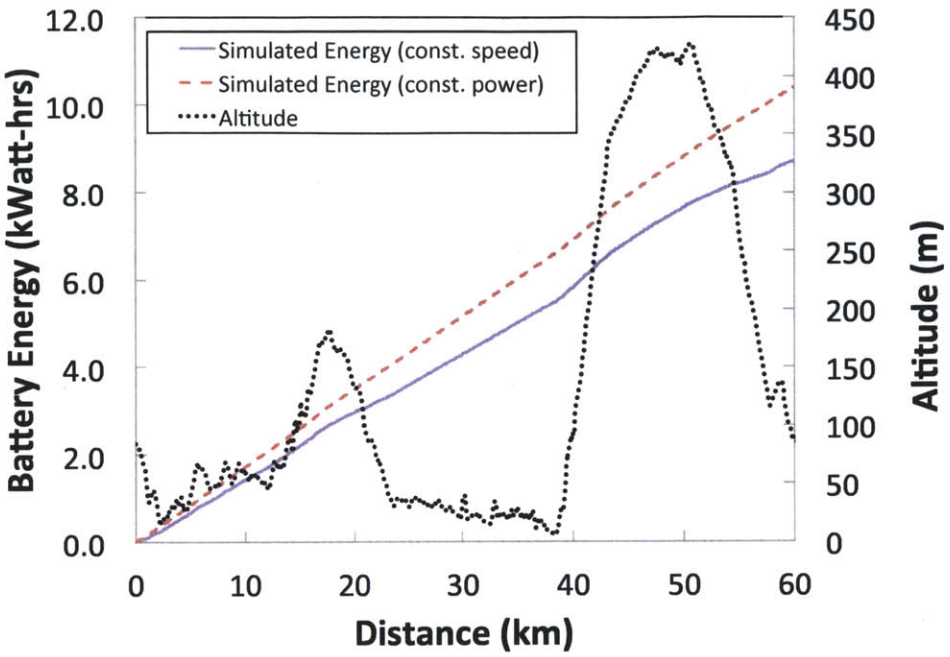

Figure 2.12: Simulation of the battery energy consumed during the race assuming a 137 km/h average speed.

3. Motorcycle Design and Testing

A 2010 BMW S1000RR motorcycle was used as the base chassis. The CAD of the final design is shown in Figure 3.1, and the component specifications are listed in Table 3.1. Two motors were combined with a rigid shaft to provide a maximum of 32 kWh of continuous power. The energy storage consisted of 106 kg of lithium-ion batteries totaling 11.9 kWh. This chapter describes the electrical (Section 3.1) and mechanical designs (Section 3.2) including the justification for critical design decisions.

Figure 3.1: CAD of the final motorcycle design.

Table 3.1: Final component specifications.

Masses			
Rolling Chassis	*Battery Modules*	*Motors*	*Other*
77kg	106kg	25kg	23kg
Mass Distribution w/out Rider			
Front Wheel	*Rear Wheel*	*Total Mass*	
122kg	109kg	231kg	
Mass Distribution w/ 80kg Rider			
157kg	154kg	311kg	
Battery Specifications			
Paral./series	*Voltage*	*Capacity*	
6/30	99V	11.9 kWh	
Motor Specifications (2 motors combined)			
Cont. Power	*Cont. Current*	*Model Number*	
32 kW	400A	D135RAG	
Motor Controller Specifications			
Voltage	*Cont. Current*	*Model Number*	
18-136V	540A	KDH12121E	
Drivetrain Specifications			
Sprocket Ratio	*Chain Size*	*O-Rings*	
53/16T	428	No	

3.1 Electrical Design

The systems engineering described in Section 2.6 estimated that 25 to 30 kW of average power would be required from the motors and ~10 to 11 kWh of battery energy would be consumed over the entire course. Due to cost, availability, volume, and mass constraints, it was decided to use two DC, permanent magnet, air-cooled motors from the Lynch Motor Company. The motor selection set the maximum voltage on the battery pack to ~100V. The battery pack was designed with help from A123 Systems; a custom version of their prismatic lithium-ion Nanophosphate® modules was used (Figure 3.2). The corresponding volumes of the batteries and motors were modeled in CAD to ensure adequate space on the motorcycle chassis (Figure 3.3). Note that the lean angle and ground clearance surfaces were added to the CAD. The battery and motor masses were also calculated and included within an overall mass budget. A single motor controller from Kelly Controls was used to regulate the energy to both motors.

The motorcycle was instrumented with sensors to measure acceleration, speed, location, current, voltage, and temperature (Table 3.2). A battery management system (BMS) was used to measure the voltage of each cell and perform cell balancing. A safety monitoring system from A123 Systems checked for vitals such as ground faults, the condition of the fuse, and over current. All of the sensing was integrated via a CAN-bus and an open-source microcontroller made by Arduino. The data was transmitted to a laptop via xBee wireless transmitters/receivers. The data was displayed off-board in real-time via a Graphical User Interface written in an open-source environment by Processing.org, and logged on-board. The rider display consisted of a series of simple LEDs to indicate the state of the motorcycle and a single LCD screen displayed digital real-time values for battery power, battery energy consumed and vehicle speed.

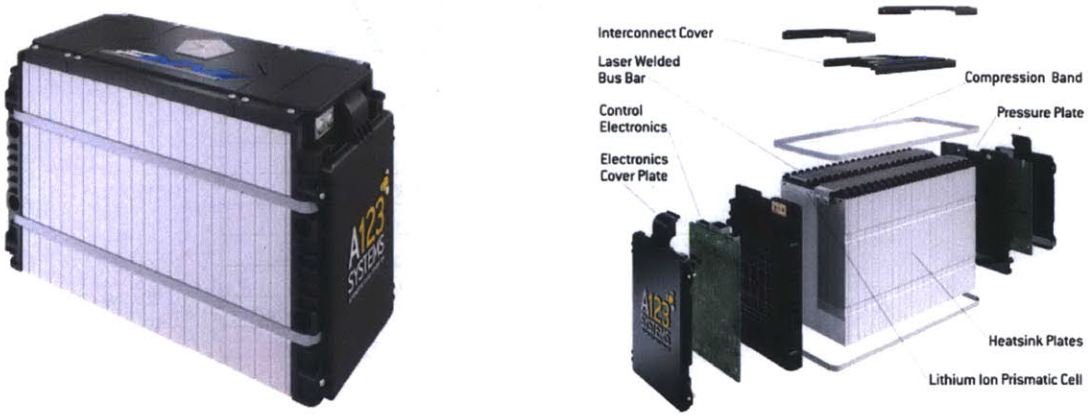

Figure 3.2: Battery module assembly (left) and exploded view (right). Images from A123 Systems.

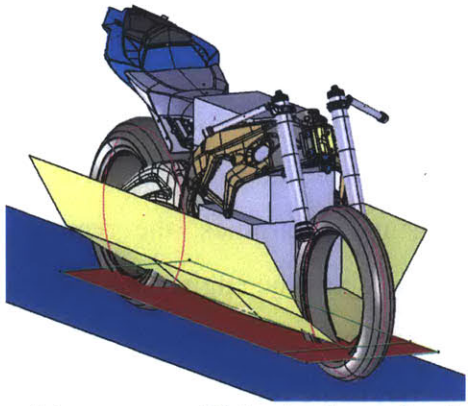

Figure 3.3: CAD was used to ensure sufficient volume for the batteries and motors.

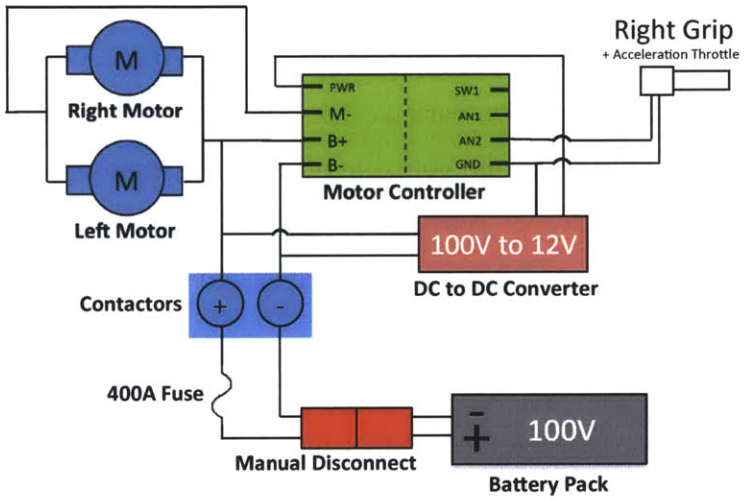

Figure 3.4: Wiring diagram of the motorcycle's power electronics.

Table 3.2: Sensors used on the motorcycle.

Subsystem	Measurement	Specific Location
Batteries	Temperature	Between battery cells
	Temperature	Cell interconnections
	Current	Around battery cable
	Continuity	Across main fuse to sense if fuse has blown
	Continuity	Attached to frame chassis to check for ground fault
	Voltage	Each cell group and entire pack
Motors	Temperature	Back side of brush holder (1 per motor)
	Current	Main power cable from motor controller (1 per motor)
System	Accelerometer	Mounted in motorcycle tail
	GPS	Mounted in motorcycle tail
	Distance	Magnet mounted on the front disk brake, sensor on front suspension fork to count wheel rotations

3.2 Mechanical Design

The entire motorcycle was designed in CAD, which enabled the various subsystems to fit inside the motorcycle with ~0.5 millimeter accuracy.[3] A structural frame was needed to support the batteries, motor, and supporting electronics; the removal of the engine needed to be considered in the mechanical design, since the engine was originally a structural element (Figure 3.5). Instead of a more common space-frame weldment, it was decided to design a frame that could be made purely on the waterjet using aluminum plates. The waterjet was chosen because it is rapid, economical, and provides significant design flexibility. The final frame design is shown in Figure 3.6. Designing a set of 2D plates also made prototyping easy; a laser cutter was used to cut wood and cardboard into quick prototypes (Figure 3.7). The frame was assembled like puzzle pieces with small tabs connecting the various 2D plates together (Figure 3.8a). The frame, including the tab-slots, was welded while bolted in place on the motorcycle chassis. A rigid steel jig was made to preserve the proper spacing and parallelism for the motors during welding (Figure 3.8b). It should also be noted that an integrated design was used to house both the motors and batteries in one weldment assembly.

The motors were connected via a custom designed drive shaft (Figure 3.9). Finite Element Analysis (FEA) was used to ensure that the shaft could handle the maximum torque loads of the motors and chain. Typically there is a flexible element in the drive shaft to provide compliance for misalignment, though in this case it was assumed that the flexture in the frame mounting was sufficient.[4]

---

[3] CAD of the S1000RR chassis was provided by BMW.
[4] Based on a discussion with the motor designer (Cedric Lynch).

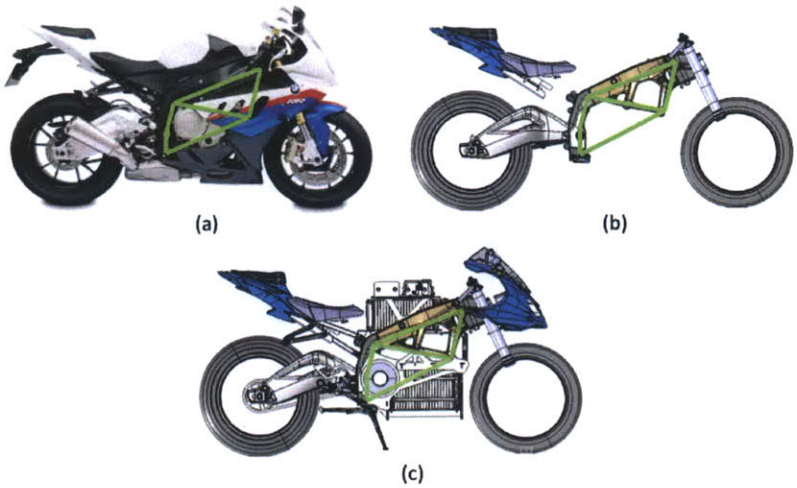

Figure 3.5: The structural loop needed to be preserved when the gasoline engine was replaced by batteries and electric motors.

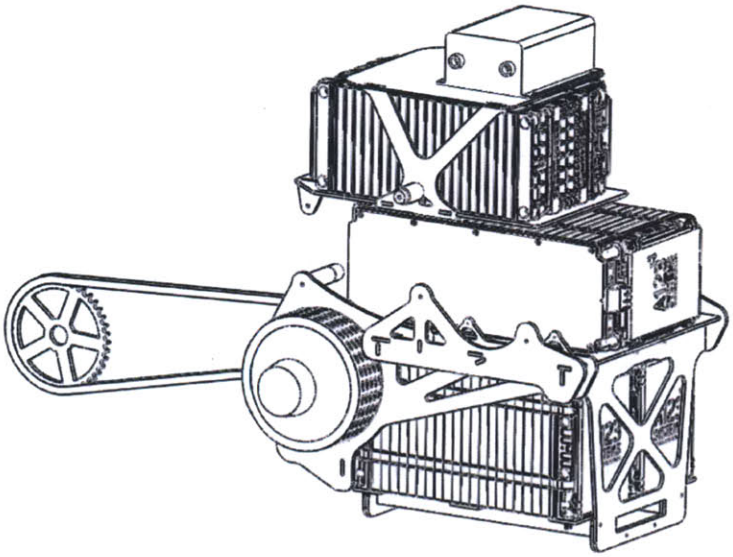

Figure 3.6: The final design of the battery and motor structural frame (shown with motors and batteries). An integrated design was used to house both the motors and batteries.

Figure 3.7: The frame and battery assemblies were prototyped using cardboard and wood cut on a laser-cutter according to the CAD files.

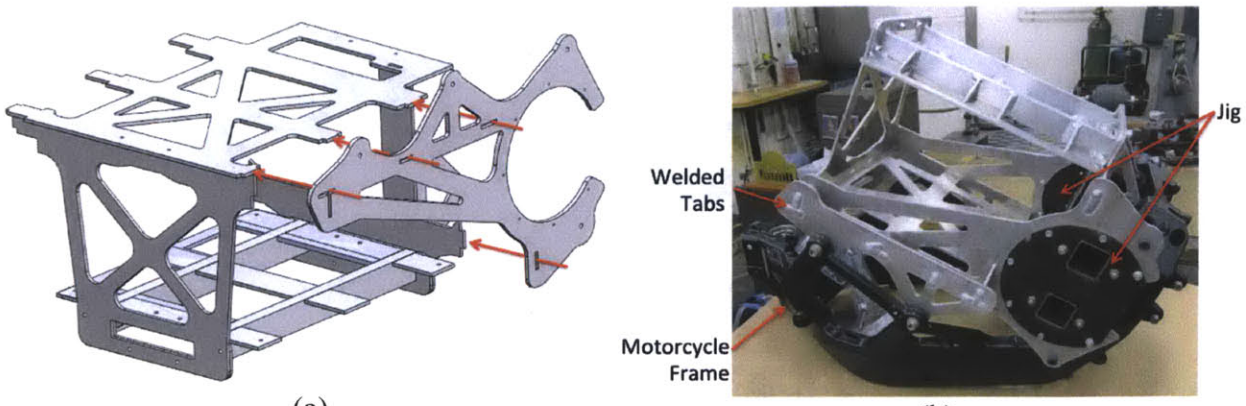

(a) (b)

Figure 3.8: The frame was designed to be fabricated using a waterjet. The tab-slots of the frame were welded while bolted to the actual motorcycle chassis (a). A rigid steel jig was used to set the proper motor spacing during welding (b).

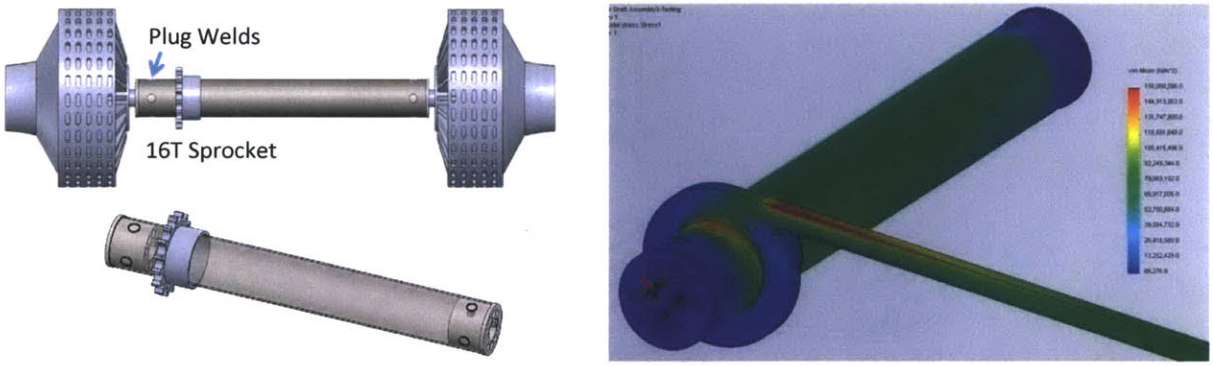

(a) (b)

Figure 3.9: A rigid shaft was designed to connect the two motors together (a). FEA was used to ensure that the designs were adequate under maximum motor loading (b).

3.3 Testing

A series of incremental tests was performed to ensure that each subsystem operated as predicted. This included the following tests: bench-top, wind tunnel, chassis dynamometer, track, and finally road. The methods, results and usefulness of these tests are discussed in this subsection.

Bench-top tests were performed to ensure that each subsystem was functioning as expected before it was integrated into the rest of the motorcycle. The motorcycle chassis, main fairings, and cardboard mock-ups of the batteries and motors were assembled and tested in the MIT wind tunnel to estimate the aerodynamic coefficient (Figure 3.10).

The fully assembled motorcycle was then tested extensively on a chassis dynamometer (Figure 3.11). The main function of a dynamometer is to measure the power output as the motorcycle is strapped on a stationary stand. The front wheel is held rigidly, while the rear wheel is free to spin on a drum that provides resistance. A sensor and computer measures and records the torque and speed of the drum, which can be translated to power, torque, and speed curves. The dynamometer was used to do the following:

1. **Ensure that the drivetrain, and other components were able to withstand full load and speed:** Since safety was a main consideration, it was important to ensure that the motorcycle would not have failures – especially under heavy load and high speeds. The heavy loading and high speeds were tested on the dynamometer while there was easy visual and physical access.
2. **Match the current going to each motor:** A single motor controller was used and the motors were wired in parallel. Thus the motors needed to be adjusted (timed) so that a nearly equal amount of current was going to each motor. The brushes were advanced or retarded by a very small amount depending on the conditions (Figure 3.12c).
3. **Understand the thermal characteristics of the batteries and motor:** Initially it was uncertain how the temperature of the motors and batteries would change with time. The dynamometer represented a worst-case scenario, since the actual airflow at 140+ km/h would provide much more cooling than the dynamometer fans (Figure 3.12a and b).
4. **Use the data obtained from the dynamometer to validate and tune the analytical models:** The dynamometer generated the curve shown in Figure 3.12d, which was used to validate and tune the models discussed in Section 2.1.
5. **Measure the drive-train efficiency:** The dynamometer is able to measure power output at the rear wheel (P_{dyno}). The current (I) and voltage (V) can be measured at the motor leads (power terminals/connections) to determine the power going into the motor. The drivetrain efficiency (motor shaft to rear wheel) can then be estimated as:

$$\eta_{drivetrain} \approx \frac{P_{dyno}}{VI\eta_{motor}} \qquad \textbf{3.1}$$

It should be noted that this method also includes the rolling resistance of the rear wheel since the wheel is rolling on the dynamometer drum.

6. **Test the microelectronics and software:** The motorcycle had multiple microprocessors and sensors that were wirelessly streaming data to on- and off-board data loggers and computers. The dyno enabled testing of the full microelectronic system and software.

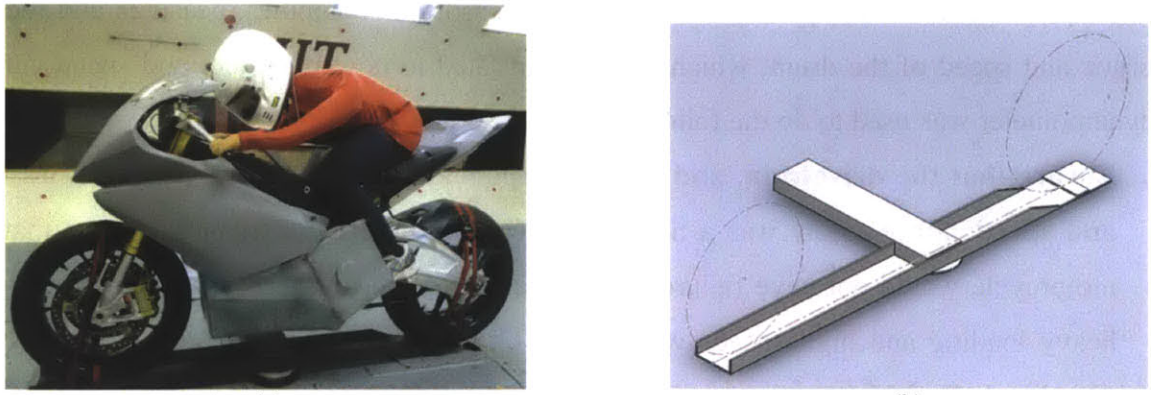

(a) (b)

Figure 3.10: The motorcycle was put in a wind tunnel. A manikin was used to simulate the rider (a). A custom mount secured the motorcycle to the wind tunnel test stand (b).

After multiple dynamometer tests, upgrades, and fixes, the motorcycle was tested on a track at New Hampshire Motor Speedway where it performed as previously predicted (Table 3.3 and Figure 3.13). The motorcycle was then sent by air from Boston to the Isle of Man inside a wooden crate. Partial disassembly was required since import/export regulation required the batteries to be shipped separately by the manufacturer (A123 Systems). The motorcycle was reassembled on the Isle of Man and a locally available dynamometer was used to run the motorcycle under full load and speed. Finally, the motorcycle was road-tested on the Isle of Man before the races (Figure 3.14).

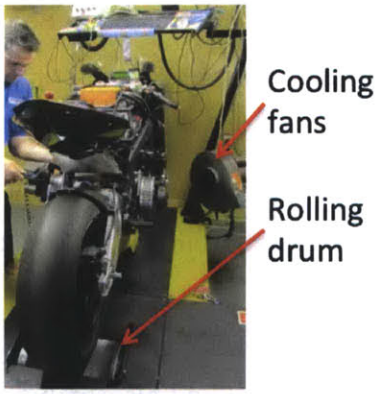

Figure 3.11: The motorcycle on a dynamometer.

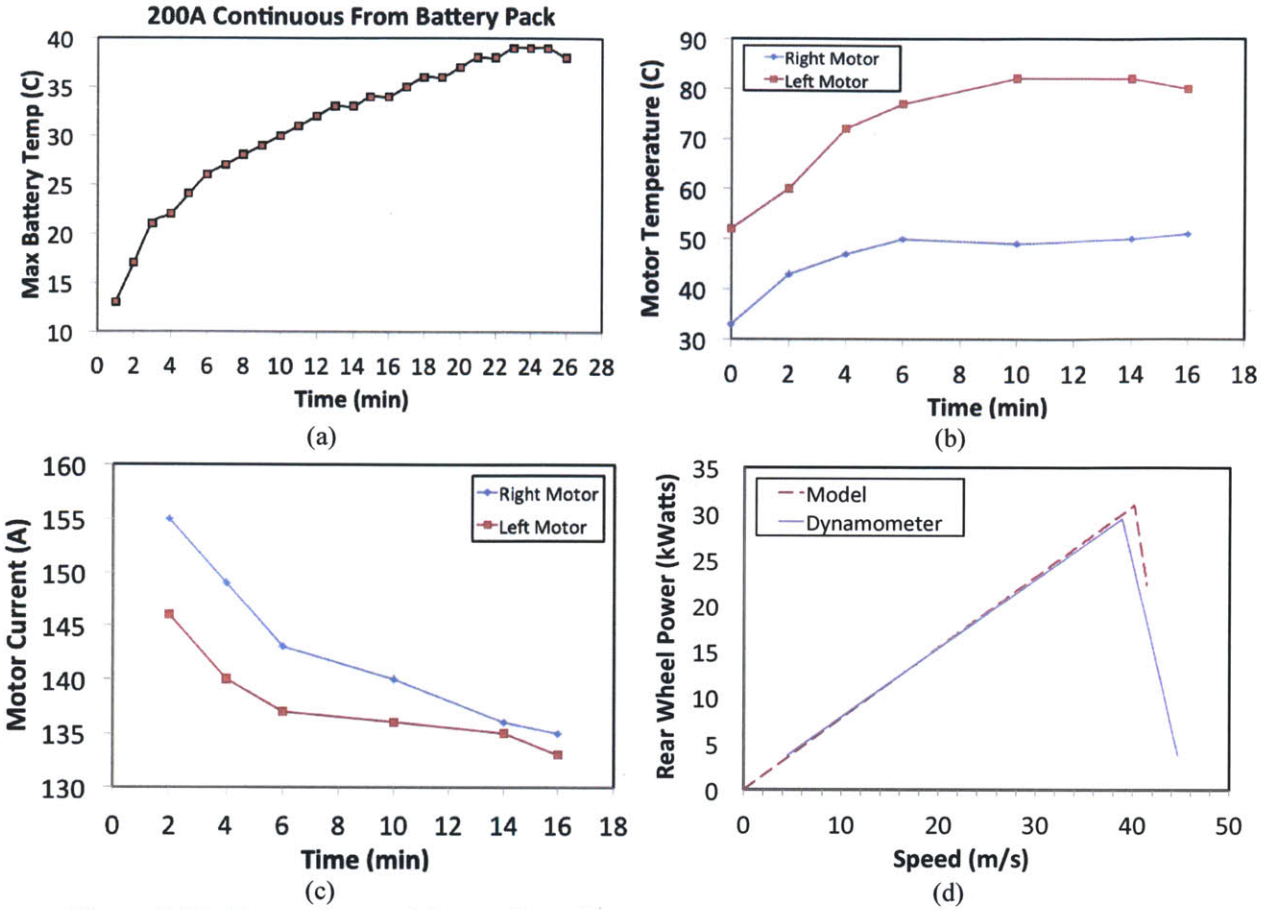

Figure 3.12: Example set of data collected on the dynamometer: battery (a) and motor (b) temperature, and motor current (c) data taken while the motorcycle was under load. The dynamometer can also be used to validate and tune models; plot (d) shows a full-throttle run, and thus the maximum power available at the given speed.

Table 3.3: Motorcycle performance specifications obtained from testing and simulation.

0 to 90 MPH (sprocket ratio = 3.3)	25 sec
Maximum Speed (sprocket ratio = 3.3)	44 m/s
0 to 60 MPH time (sprocket ratio = 5.3)*	8 sec
0 to 60 MPH time (sprocket ratio = 5.3, max motor output)*	4.3 sec

*Simulation only

Figure 3.13: Track testing at New Hampshire Motor Speedway.

Figure 3.14: Road testing on the Isle of Man.

4. Motorcycle Race Results and Analysis

The motorcycle and rider competed in two qualifying races and one final race (Figure 4.1). The following subsections analyze the race data to understand the motorcycle performance (Section 4.1) and validate the models and assumptions made during the design process (Section 4.2). The final section reflects on the racing experience to outline a set of guidelines for designing zero emission races with the aim of promoting innovation (Section 4.3).

Figure 4.1: The motorcycle during the TT race.

4.1 Analyzing the Motorcycle Performance

The average vehicle speed and energy consumption increased with each race (Table 4.1), which was likely caused by: (1) adjustments in the motor controller settings (2) changes in the sprocket ratio between each race, and (3) the rider learning to better control the motorcycle with each additional race. The speed versus distance over the entire course is shown in Figure 4.2 and each dip in the curve represents a point in the course where the rider slowed down to enter a turn. The speed data is shown with the corresponding altitude, which highlights the speed reduction while traversing up the mountain. The motors were closely matched as measured by current during the final race (Figure 4.4), though the left motor was nearly 20°C warmer than the right

(Table 4.1). The temperature differences likely resulted from one motor having a different gap between the commutator and magnets. The gap differed because the motors were rebuilt between each race and the reassembly process was modified each time. The motors were operated within their current limits (Table 3.1) and the battery power fluctuated about a safe nominal value of ~22 kW (Figure 4.3). Finally, the battery cells, interconnects and terminals stayed at ambient temperatures throughout the race, which indicates that sufficient cooling was achieved.

Table 4.1: Comparing the qualifying and final race results.

Parameter	Units	*Qual. 1*	*Qual. 2*	*Race*
Average Speed	[km/hr]	122	126	127
Finishing Time	[mins]	29:54	28:50	28:58
Battery Energy	[kWh]	9.4	9.7	9.8
Average Battery Power	[kW]	19	20	20
Average Battery Current	[A]	198	215	220
Battery Energy/Distance	[Wh/km]	147	155	161
Left Motor Temp*	[°C]	72	63	52
Right Motor Temp*	[°C]	68	87	35
Average Current to Left Motor	[A]	-	-	149
Average Current to Right Motor	[A]	-	-	142

*Temperature taken at the end of the race using infrared temperature gun

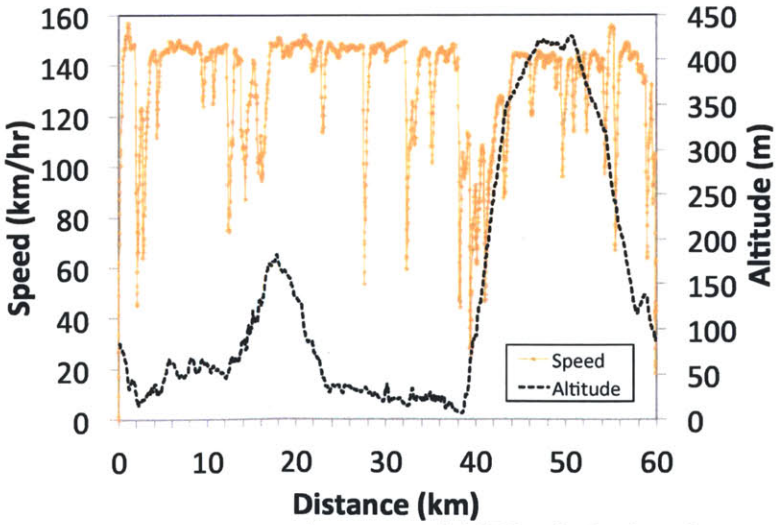

Figure 4.2: The motorcycle averaged 127 km/h during the race.

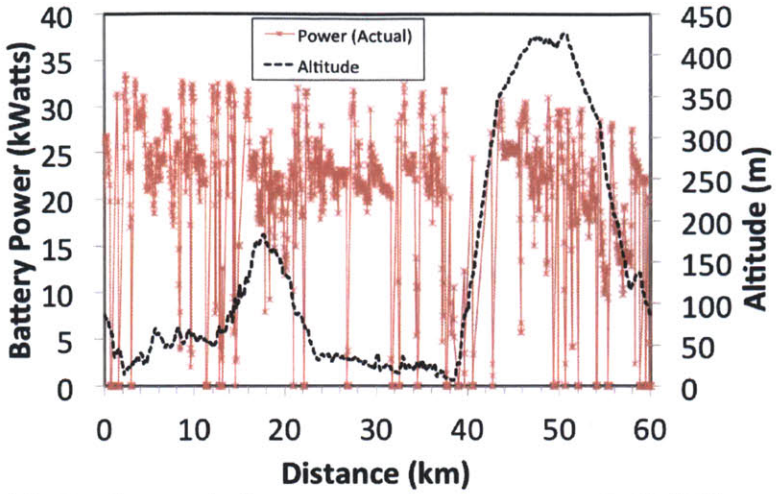

Figure 4.3: The battery had an average power output of ~20 kW.

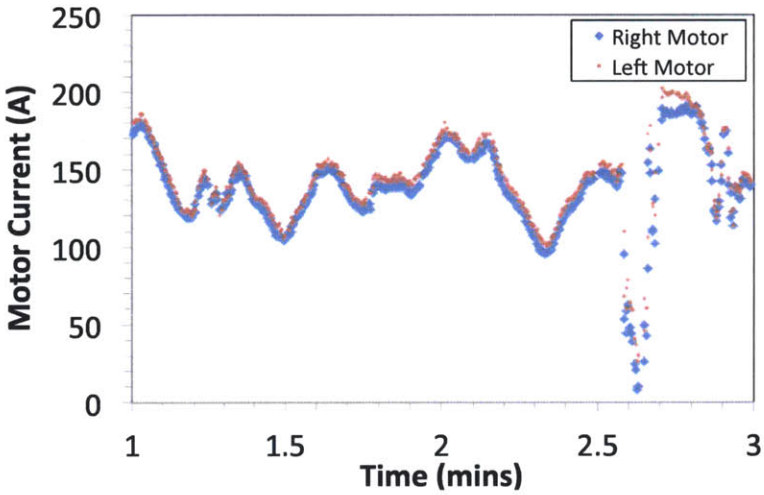

Figure 4.4: The race data shows that the motors were equally matched.

4.2 Model Validation

The speed versus distance plot in Figure 4.5 shows that the models derived in Section 2.2 closely match the real world data when full-throttle was applied during the race. The parameters shown in Table 2.2 were used in the simulations. Additionally, Figure 4.6 shows that the racing data supports the hypothesis described in Section 2.6 that the actual battery energy required to traverse the course is in between best and worst cases of constant speed and power, respectively. Interestingly, an arithmetic mean of the constant speed and power curves matches the actual race data at the finish with <5% error (Figure 4.7). It should be noted that the battery energy was

measured by a shunt and voltage measurement at the output of the battery and thus internal battery losses were not included. Table 4.2 lists the comparisons between the models and racing data. The conclusive result is that the models and assumptions were able to sufficiently predict motorcycle performance.

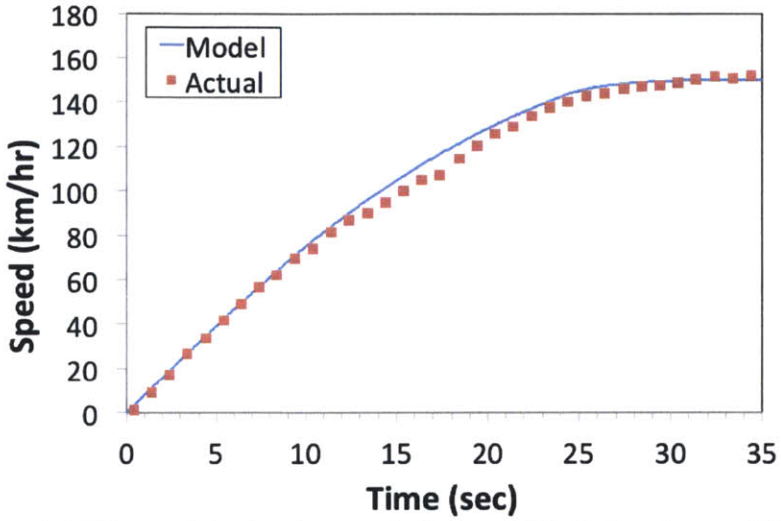

Figure 4.5: The models closely match the actual full-throttle conditions.

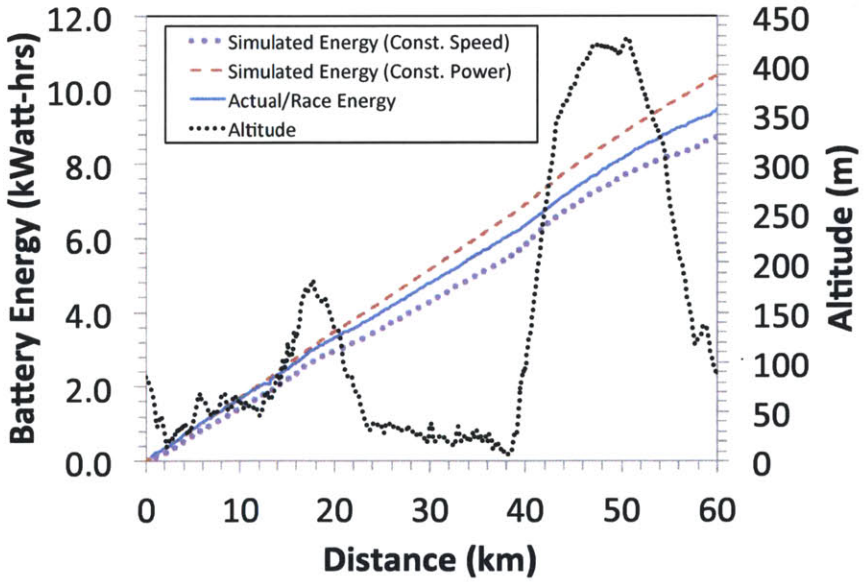

Figure 4.6: The race data supports the hypothesis described in Section 2.6 that the actual battery energy required to traverse the course is in between best and worst cases of constant speed and power, respectively.

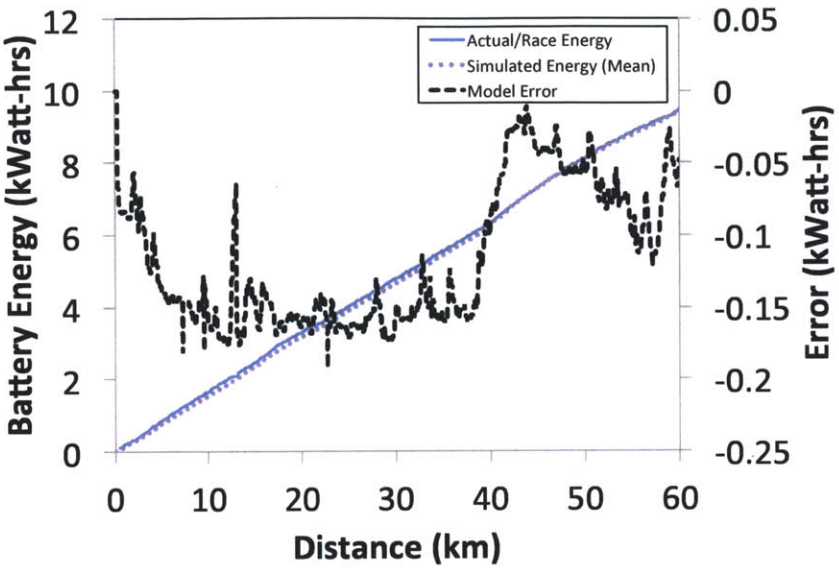

Figure 4.7: An arithmetic mean of the constant speed and power curves matches the actual race data at the finish to within 5% error.

Table 4.2: A comparison between the model predictions and final race results.

Parameter	Units	*Model*	*Race*	*Error*
Battery Energy	[kWh]	*9.6*	*9.8*	*2%*
Battery Energy/Distance	[Wh/km]	*158*	*161*	*2%*
Average Speed	[km/h]	*127**	*127*	*N/A**
Maximum Speed	[km/h]	*148*	*155*	*5%*
0 to 144 km/hr (z = 3.3)	[sec]	*24*	*25*	*4%*

*the average speed used in the simulation was set equal to the actual race speed

4.3 Framework for Spurring Innovation Through Racing

The Isle of Man TT Zero is an example of a new breed of "zero emission" races. The aim of these races is to spur innovation that will reduce the environmental impact of consumer vehicles. Racing has historically been a catalyst for innovation, particularly in the early years of motorcycles and automobiles [15]. New concepts were tested on the track and the desire to win drove companies to produce superior technology. Consumer demand for better performance motivated companies to transfer the technology from the racetrack to the mass market.

The fundamental question is whether or not zero emission racing will yield the desired outcome. With the goal of contributing to the success of zero emission racing, this subsection outlines a set of guidelines for designing zero emission races that will yield relevant innovation.

Innovation in this context is defined as the act of generating a product or service that (1) reduces the environmental impact of vehicles and (2) consumers want to purchase.

4.3.1 Consider the Historical Context

Gasoline vehicle racing has evolved dramatically over the past 100 years. Because of this, caution should be used when copying a modern gasoline race with a zero emission equivalent. Zero emission racing might require a different approach and lessons may be learned from looking back into the beginnings of gasoline racing.

Patience will also be required when directly comparing modern gasoline and zero emission racing. It is easy to forget that it took decades for gasoline engines to make dramatic improvements. For example, it took 50 years for the first gasoline motorcycle to reach a 100 mph average lap at the TT. The electric motorcycles reached this same milestone within 4 years from the start of electric motorcycle racing at the TT.

4.3.2 Utilize the Power of Regulation

Regulations should be used as the fundamental tool to engineer a race for a desired outcome. For example, assume that consumers want to refuel their vehicle quickly; if winning a zero emission race is dependent on fast refueling, then the regulations are successfully guiding development. A successful racing innovation platform must focus on technology relevant to the consumer market.

4.3.3 Drive Technology

Many diverse participants, including inventors, academia, and corporate research labs contribute to generating and developing innovative ideas. Consumer-focused companies choose relevant developments, refine them, and promote them to the consumer market. Identifying which ideas will succeed is a challenge facing all vehicle companies. Resources are often not available to invest in multiple emerging technologies. For example, it is costly for an automobile company to invest in batteries, fuel cells, and super capacitors simultaneously. Racing competitions should be structured to accelerate the transition from ideas to mass production and simultaneously facilitate the development of multiple technologies.

4.3.4 Provide Valued Entertainment

Any repeated event that the public finds entertaining will draw a large number of spectators both in person and through the media (e.g. internet, TV, etc.). Spectators and media

drive advertising, which creates an influx of funds through team, rider and event sponsorship. These funds help finance the teams who in turn develop the technology. Thus valued entertainment is drawing in extra research and development funds *that would otherwise not be available for that purpose* (Figure 4.8). For example, an energy drink manufacturer might be indirectly funding battery research. This could translate into significant funds spent on zero emission innovation [16].

The influx of available sponsorship also reduces the risk that the team with the most personal wealth will win. In other words, sponsorships are typically chosen based on which team is likely to win; if the teams generating the most innovative vehicles are more likely to win, these teams would be rewarded through sponsorship funds to develop even better technology.

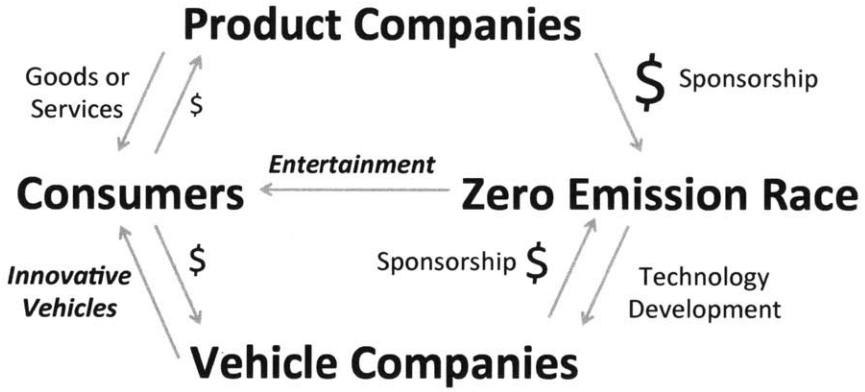

Figure 4.8: This diagram illustrates how the entertainment from racing can indirectly generate research and development funds and drive Technology Development. A Zero Emission Race provides entertainment to Consumers and the associated advertising at the race motivates consumers to purchase vehicles and products from race sponsors. This money eventually flows back into the Zero Emission Race through sponsorship. The race generates Technology Development that goes back into Vehicle Companies, which in the long run will provide consumers with more advanced vehicles.

4.3.5 Inspire Consumer Demand

It is critical that the races inspire consumers to purchase the technology that is found superior on the racetrack. Otherwise, true innovation will not be achieved through racing and the objective of reducing the environmental impact of vehicles will not be achieved. One way this can be accomplished is through styling, and ensuring that the race vehicle has brand identity. For example, a motorcycle company should use styling that is distinct and that connects their race vehicle to their commercially available vehicles.

Secondly, inspiration can be found through education. The race should strive to inform the consumer of the environmental effects and implications of the various technologies.

Finally, races can inspire consumer demand by building confidence in new technologies. For example, racing could prove that rapid charging is feasible, which might convince the skeptical consumer that the technology will satisfy their needs.

Part II: Estimating an Electric Vehicle's Distance to Empty

5. Introduction to Part II

An electric vehicle's Distance to Empty (D_{TE}) is defined as the distance the vehicle can be driven before recharging is required. A real-time *estimate* of D_{TE} is commonly displayed on the vehicle's dashboard and is used by the driver for route planning (Figure 5.1). The objective of Part II of this thesis is to introduce a new D_{TE} algorithm that uses measurements from the past along with knowledge of the future route. For example, if the driver provides their destination(s) beforehand, a navigation system could obtain route, traffic and weather information via the internet and this information could be used to improve the D_{TE} estimate. Instead of physics-based models, a multivariate linear regression model is used that adjusts a historical average of energy consumption based on estimated changes in speeds, traffic and temperature. This approach could be implemented as a cloud-based mobile phone application since it is computationally light and fitted using historical driving data.

The new D_{TE} algorithm was quantitatively compared to conventional methods. To perform this comparison using real driving data, a large set of driving data would be needed that contains speed, energy, traffic and temperature information. Since this dataset is not currently available, a large variety of driving conditions were simulated using a set of physics-based models. The models were based on the motorcycle work (Part I) and data from a fleet of electric vehicles. The input to the models is a Markov-based stochastic speed profile generator, which attempts to capture the stochastic nature of driving. Example simulations show that including future driving conditions in the D_{TE} algorithm can significantly reduce error.

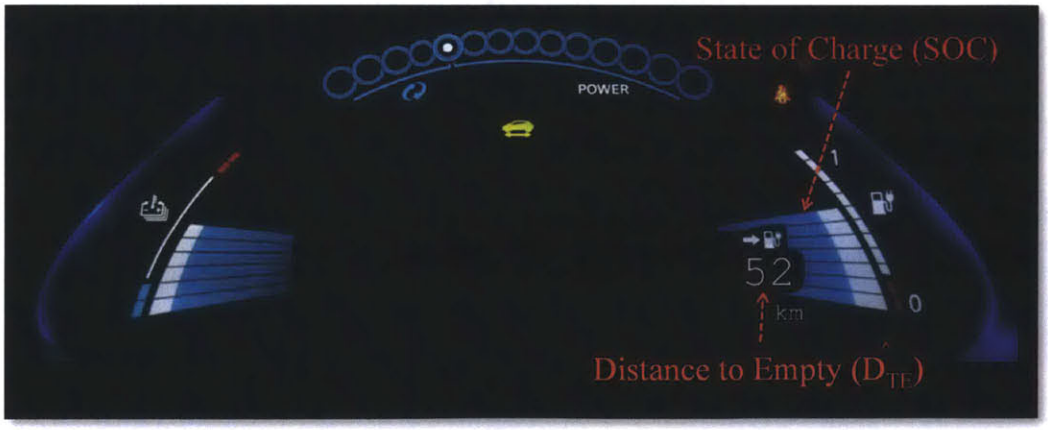

Figure 5.1: The dashboard of the Nissan Leaf displays the D_{TE} and the SOC.

5.1 Motivation

The maximum D_{TE} for electric vehicles (EV), also referred to as range, is typically 100 to 400 km less than gasoline vehicles and a full recharge usually takes hours instead of minutes (Table 5.1). Also, the energy consumption of EVs is more influenced by auxiliary loads (e.g. heating) [17]. An undesirable scenario is one where the driver is left stranded on the side of the road without the ability to quickly recharge. For these reasons it is important to provide an accurate D_{TE} estimate. Studies have shown that current D_{TE} algorithms are insufficient and often cause "range anxiety" among drivers [18][19]. Estimating D_{TE} is difficult because of the stochastic nature of driver behavior and the environment, the lack of a quantitative understanding for how these factors affect energy use, and the fairly basic algorithms currently being used. Recent studies have shown that the maximum D_{TE} can vary by as much as 55% depending on the driving conditions [20]. The usefulness and importance of the D_{TE} estimate was confirmed by a study of EV users, which concluded that "providing drivers with a reliable usable range [estimate] may be more important than enhancing maximal range in an electric mobility system" [18]. In other words, a more accurate D_{TE} estimate may be more useful than increasing the size of the battery pack.

Table 5.1: Comparing the energy storage, recharging times, fuel economy and range of various vehicles. The approximate values were obtained from the manufacturer's websites.

Vehicle Type	Make/Model	Energy Storage	Recharge (km per hour of charging)	Fuel Economy (L/100km or EV-equivalent)	Range (km)
Gasoline	Honda Civic	50 Liters	N/A	7.4	680 (gas)
Plug-in Hybrid (PHEV)	Toyota Prius Plug-in	4.4 kWh 40 Liters	11	2.5 (EV) 4.7 (hybrid)	18 (EV) 870 (total)
Plug-in Hybrid (PHEV)	GM Volt	16 kWh 35 Liters	14	2.5 (EV) 6.4 (gas)	56 (EV) 655 (total)
Battery Electric (BEV)	Nissan Leaf	24 kWh	23	2.4	160 (EV)
Battery Electric (BEV)	Tesla Model S	40-85 kWh	50-480	2.6	258-483 (EV)

5.2 Overview

Chapter 6 develops a stochastic vehicle simulation environment that was used to compare D_{TE} algorithms. This approach captures the random nature of driving and can be used to simulate an unlimited number of full battery discharges. Chapter 7 introduces key concepts and equations

that aid in developing and evaluating D_{TE} algorithms. Chapter 8 proposes a new approach that uses estimates of future driving conditions to more accurately predict D_{TE}. Instead of using physics-based models, a multivariate linear regression-based model is derived, which adjusts a historical average of energy consumption up or down based on estimated changes in route, traffic and traffic. Both the conventional and new algorithms are compared in Chapter 9 using the stochastic vehicle simulation environment.

5.3 Related Work

A previous study used a basic vehicle model combined with static assumptions about auxiliary use to estimate the maximum D_{TE} [21]. Though their simulations and experimentation closely matched the expected values published by the manufacturers, they did not take into account the true stochastic nature of the driving conditions nor did they investigate the accuracy of D_{TE} with distance. Some have approached the more general topic of estimating the energy consumed between two points [22][23]; they used commercially available simulation software with historical traffic and road data. There are similar approaches that require physics-based models to estimate energy use and/or D_{TE} [24]. Others describe a method where historical data is used to predict the energy required for future trips [25][26]. Many of the techniques related to energy estimation were applied to power-split control algorithms for plug-in hybrids or gasoline vehicles [27]. Finally, there are many patents issued by automobile companies that describe various averaging techniques used to estimate D_{TE} [32][33][34].

None of the research described above shows results of a D_{TE} simulation or experimentation, nor do they explain how their approaches would be implemented. They also all stop short of measuring the quality of the D_{TE} estimates and making comparisons to other methods. Finally, there has been little effort to understand the fundamental relationship between energy estimation and D_{TE} error. This chapter aims to contribute in these areas and start a more open and in-depth discussion of D_{TE} algorithms.

6. Stochastic Vehicle Simulations for Evaluating D_{TE} Algorithms

This chapter derives a parametric physics-based electric vehicle simulation, which was used to simulate an unlimited number of full battery discharges under realistic driving conditions. The overall simulation architecture is discussed in Section 6.1. The simulation uses a stochastic speed profile (speed versus time) as input, which is discussed in Section 6.2. The subsystem models (e.g. vehicle, motor, etc.) are discussed in Section 6.3. Finally, Section 6.4 summarizes how the models were used together to generate a stochastic vehicle simulation.

6.1 Simulation Architecture

The models derived in this section form a backward-looking simulation similar to the methods described for the motorcycle in Section 2.1.1. The main differences are the (1) stochastic speed profile generator and (2) auxiliary model (Figure 6.1). The speed profile generator produced a speed versus time dataset, $\dot{x}(t)$, that was used as input to the vehicle model. The vehicle model then determined the wheel force (F_w) required to follow the prescribed profile based on a set of design parameters. Similarly, the transmission and motor models determined the amount of electric power needed by the motor (P_m) in order to generate the desired wheel force. Next, the motor power combined with the Auxiliary Power (P_a) was the net electrical energy needed from the battery (P_b). The battery model translated the total electrical need (P_m + P_a) to battery energy (E_b) and included internal losses. The battery losses depended on the battery current (I_b). The following subsections derive each of these models.

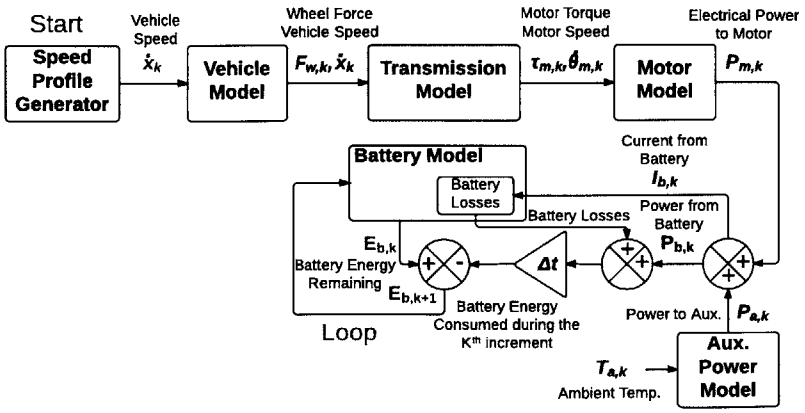

Figure 6.1: The backward-looking vehicle simulation.

6.2 Stochastic Speed Profile Generator

Backward-looking simulations require a speed profile (speed versus time) as input. It is most common to use standardized Environmental Protection Agency (EPA) *driving cycles* as inputs, which specify the speed profile and auxiliary use (e.g. A/C and heater use). The following are the most commonly used EPA driving cycles:

- City driving (FTP-75)
- Highway driving (HWFET) See Figure 6.2
- Aggressive driving (SFTP US06)
- Air conditioning test (SFTP SC03)

The following are key limitations to using EPA driving cycles for D_{TE} simulations:

- **Short Length:** The EPA driving cycles are short in length (~10 km) and thus would have to be repeated multiple times in order to simulate a full battery discharge (~100 to 300 km).
- **Lack of Randomness:** A D_{TE} algorithm could be tuned to work well with EPA driving cycle(s), but it might not work well under broader (more realistic) conditions.

For these reasons, it is undesirable to use standard EPA driving cycles as the input to the D_{TE} simulations. Instead, this section derives a method for generating stochastic speed profiles that can be of any length with specified conditions (e.g. city or highway).

Various methods for generating stochastic speed profiles have been described in literature [36][37][38][39][40][41]. The general approach used in this thesis is to view any time-series speed profile as a Markov process, which is a stochastic process with no memory [42]. The selection of the next state only depends on the current state and not on prior states. In this case the *states* are sequential sets of data that represent deceleration, cruise, acceleration or idle events – or states. These *states* are referred to as *modes* (Figure 6.3a) since they represent particular operating modes of the vehicle. Since there are different intensities of acceleration and deceleration at difference speeds (e.g. low acceleration at high speeds and high acceleration at low speeds), the acceleration and deceleration modes were more finely divided for a total of 10 states in the Markov model: 4 deceleration, 1 cruise, 4 acceleration and 1 idle state.

A large set of driving data (speed versus time) was parsed, and the Markov Transition Probability Matrix (TPM) was determined by observing the transitions between states (e.g.

counting the number of times the state transitioned from the cruise to deceleration mode). The TPM along with a random number generator was used to string together a stochastic speed profile of any length. To simulate a variety of conditions, the TPM matrix was modified to give preference to certain modes (e.g. less aggressive driving was simulated by putting zeros in the columns of the TPM associated with the largest acceleration and deceleration modes). This section will describe the details of this approach.

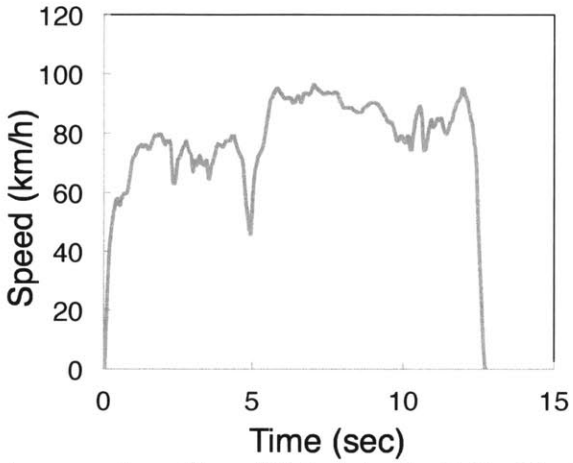

Figure 6.2: The above plot is a speed profile published by the EPA. The EPA speed profiles are too short and lack variety in conditions and thus are not adequate for D_{TE} simulations.

6.2.1 Raw Driving Data

The speed profiles are derived from a large set of driving data collected by the EPA in Kansas City in 2004 [43]. The data contains over 400 hours of GPS-based speed data logged at 1 Hz for 480 randomly selected light duty vehicles in the Kansas City metropolitan area. An EPA subcontractor performed extensive statistical analysis to ensure that a variety of ages, genders, races and vehicle types were considered. However, the method derived in this section is independent of the data collected, so any large set of speed traces could be used.

6.2.2 Categorizing and Grouping Data

A *speed trace* is defined as the raw speed data collected by GPS. The large database of speed traces was converted to a readable format for Matlab, and an extensive set of checks were performed to remove erroneous data (e.g. loss of GPS signals or general errors). Next, the speed traces were divided into "micro-trips," which are defined as the speed data collected in between moments when the speed was zero (Figure 6.4). Each micro-trip was further categorized as either highway or city based on maximum speed.

Each micro-trip is composed of a series of deceleration, cruise, acceleration and/or idle "modes." It is necessary to develop an algorithm that determines the sequence of modes for each micro trip as shown in Figure 6.3a. To this end, Lin [36] derived a method based on Maximum Likelihood Estimation (MLE). However, the MLE method was implemented and tested as part of this research and found to yield inconsistent and unreliable results. Thus the following approach was developed that used the fractional increase in speed between each 1 Hz speed data point was calculated:

$$\Delta\dot{x}_i = \frac{\dot{x}_{i+1} - \dot{x}_i}{\dot{x}_i} \qquad \textbf{6.1}$$

Where $\dot{x}_i$ is the speed of data point i. Then the mode was selected based on the values outlined in Table 6.1.

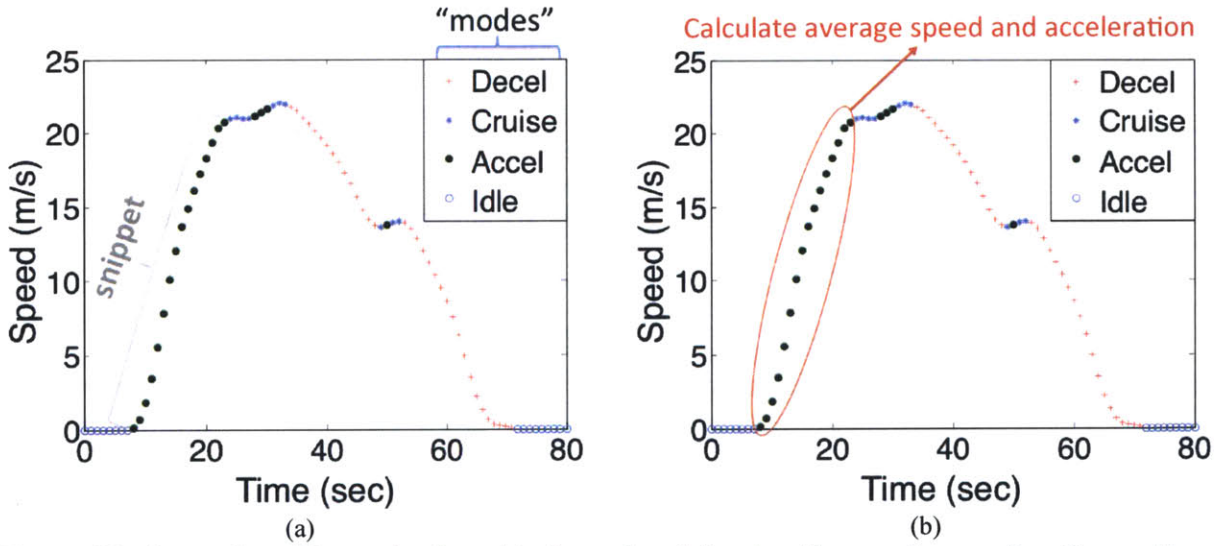

Figure 6.3: A speed profile can be thought of a series of deceleration, cruise, acceleration and/or idle "modes." Each set of points that compose a mode is called a "snippet" (a). The average speed and acceleration were calculated for each snippet (b).

Each sequential string of mode data is referred to as a "snippet" (Figure 6.3a). A snippet is discarded if it contains fewer than 3 data points. The average speed and acceleration are calculated for each snippet and the speed-acceleration pairs for each snippet are grouped by mode (Figure 6.3b). The snippets that are acceleration or deceleration modes are further subdivided to form a total of ten modes: Deceleration (1 through 4), Cruise (5), Acceleration (6-9) and Idle (10). The subdivision is done with a k-means clustering algorithm (Figure 6.5) [44]. Thus each snippet is assigned to one of the ten possible modes based on the snippet's average

acceleration and speed. The entire categorizing and grouping method is summarized in Figure 6.6.

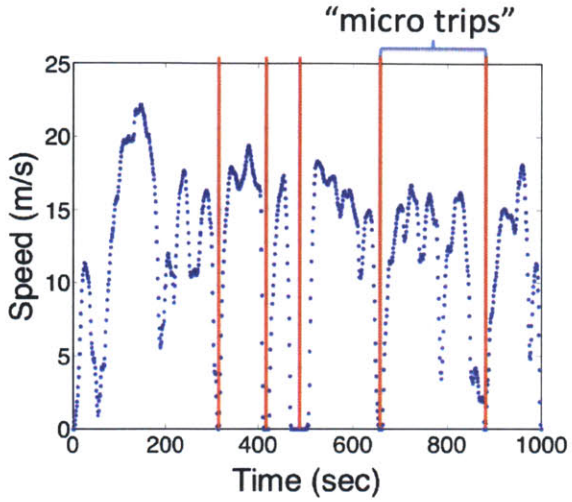

Figure 6.4: The speed traces were divided into micro-trips.

Table 6.1: Criteria for assigning the driving "mode" to each data point.

$\Delta\dot{x}$	Mode
=<-0.01	Deceleration
>-0.01 & <0.01	Cruise
>=0.01	Acceleration
0	Idle

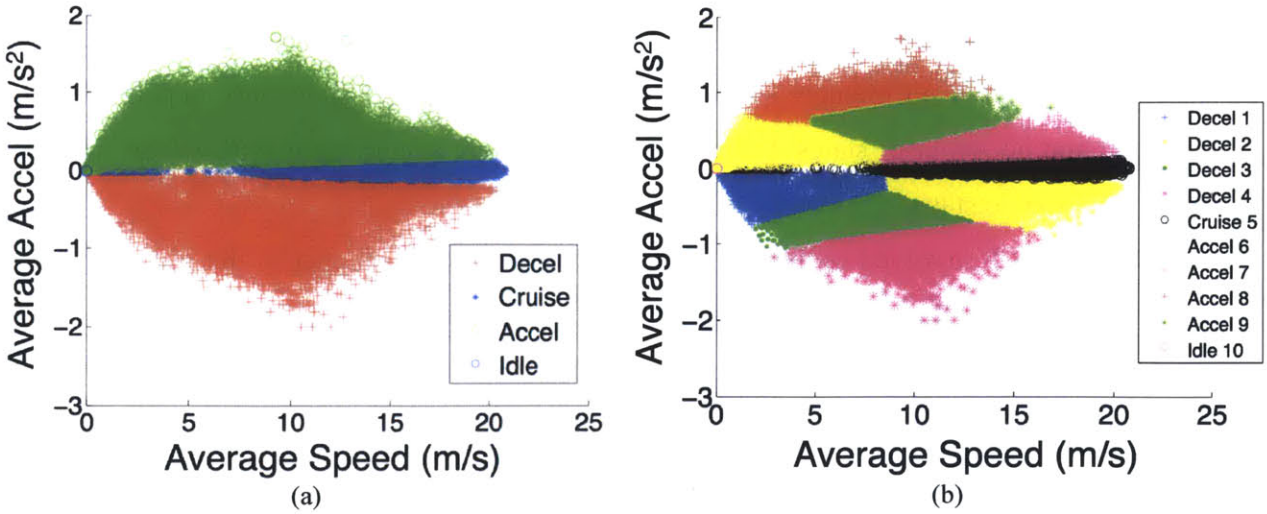

Figure 6.5: The speed-acceleration pairs for all of the snippets were grouped by mode (a). The deceleration and acceleration groups were further subdivided using a k-means clustering technique (b). The result is 10 distinct modes that were used in the Markov model.

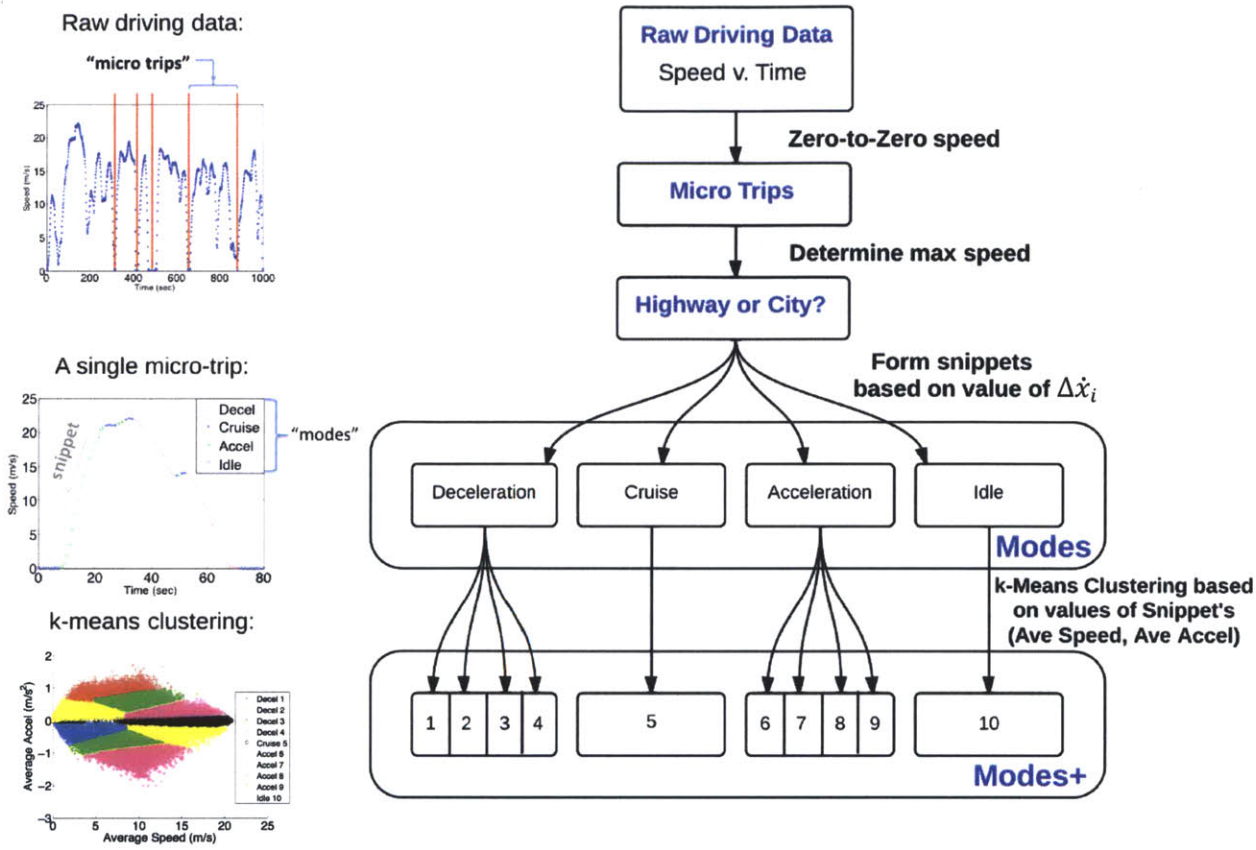

Figure 6.6: A summary of the method used to categorize data into snippets, and then assign each snippet to one of ten modes.

6.2.3 Markov Model

It was assumed that speed profiles can be modeled as a Markov process, which is a stochastic process with no memory [42]. The selection of the next state only depends on the current state and not on prior states. In this case the *states* are synonymous with *modes* and thus there are ten possible states.

The approach involved sequentially stepping through each snippet in the order that they occurred and counting the mode transitions. For example, the micro trip shown in Figure 6.3a transitions from Mode 10 (idle) to Mode 9 (accel), Mode 5 (cruise), Mode 7 (accel), Mode 5 (cruise), Mode 2 (decel) etc. The goal was to determine the probability of transitioning from one mode to another. These are referred to as *transition probabilities* and were calculated using:

$$\Pi_{ij} = \frac{\pi_{ij}}{n_i} \qquad \textbf{6.2}$$

Where π_{ij} is the number of times a snippet transitioned from Mode i to Mode j and n_i is the total number of snippets in the Mode i group. $\mathbf{\Pi}$ is the *transition probability matrix* and by definition the following is true for all values of i:

$$\sum_{j=1}^{10} \Pi_{ij} = 1 \qquad \textbf{6.3}$$

An example transition probability matrix (TPM) is shown in Figure 6.7.

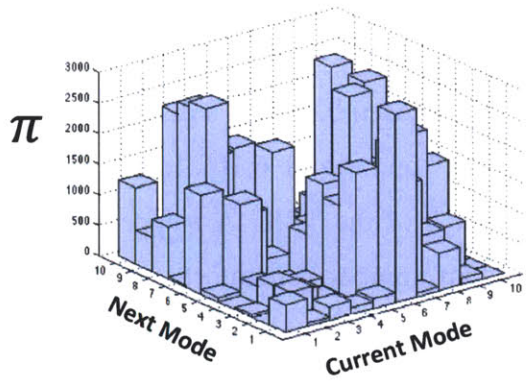

$$\Pi_{ij} = \begin{bmatrix}
0.092 & 0.000 & 0.007 & 0.000 & 0.015 & 0.332 & 0.006 & 0.176 & 0.114 & 0.257 \\
0.010 & 0.074 & 0.073 & 0.049 & 0.254 & 0.004 & 0.479 & 0.002 & 0.057 & 0.000 \\
0.027 & 0.000 & 0.026 & 0.000 & 0.002 & 0.137 & 0.006 & 0.220 & 0.303 & 0.278 \\
0.020 & 0.000 & 0.002 & 0.024 & 0.000 & 0.053 & 0.005 & 0.342 & 0.325 & 0.229 \\
0.020 & 0.265 & 0.182 & 0.210 & 0.092 & 0.002 & 0.229 & 0.000 & 0.001 & 0.000 \\
0.616 & 0.007 & 0.135 & 0.006 & 0.020 & 0.129 & 0.040 & 0.012 & 0.035 & 0.000 \\
0.008 & 0.220 & 0.175 & 0.131 & 0.359 & 0.000 & 0.108 & 0.000 & 0.001 & 0.000 \\
0.088 & 0.111 & 0.323 & 0.161 & 0.137 & 0.034 & 0.111 & 0.025 & 0.010 & 0.000 \\
0.016 & 0.120 & 0.245 & 0.167 & 0.252 & 0.001 & 0.172 & 0.000 & 0.027 & 0.000 \\
0.000 & 0.000 & 0.000 & 0.000 & 0.000 & 0.148 & 0.000 & 0.330 & 0.191 & 0.330
\end{bmatrix}$$

Figure 6.7: An example transition probability matrix.

6.2.4 Simulating Highway, City and Aggressive Driving Conditions

When generating a speed profile it was desirable to choose "city" or "highway" driving conditions. This was accomplished by splitting the micro-trips into two groups based on maximum speed as shown in Figure 6.6. All micro-trips with a maximum speed greater than or equal to 65 km/h were considered highway driving and all of the slower traces were considered city driving. Separate TPMs were made for both the city and highway data.

Next, to create a TPM representing less aggressive driving, the values in column 4 and 8 were replaced by zeros, which effectively removed the largest deceleration and acceleration modes, respectively. In general the TPM can be modified to yield various outcomes. Thus four TPMs were generated: city, less aggressive city, highway and less aggressive highway. All four matrices were used to generate a variety of mixed combinations as discussed in the next section.

6.2.5 Creating a Stochastic Speed Profile

The TPMs were used to join snippets together to form a speed profile of a specified length. Below is a summary of the algorithm:

1. One of four TPMs was chosen: city, less aggressive city, highway and less aggressive highway (see Section 6.2.4).
2. A snippet was chosen at random with an initial speed equal to zero and an average speed greater than zero. The random initial snippet selection shown in Figure 6.8 was from Mode 6 through 9 (accel).
3. The subsequent mode was chosen based on a distribution formed from the corresponding row of the TPM (Figure 6.7 and Figure 6.10). In this example, Mode 9 has the transition probabilities listed in row 9 of the TPM. A snippet of this mode type was then chosen randomly (using a random number generator) – though it must satisfy the requirement that the initial speed was within a specified percentage of the final speed from the previous snippet.
4. Step 3 was repeated until the desired speed profile length was obtained (Figure 6.9).

Switching between highway and city TPMs can generate speed profiles with varying conditions. For example, half of a speed profile could be city and the highway. The proportion of highway versus city driving for a given speed profile was set using a random number generator. The same concept was applied to varying aggressiveness. Thus each speed profile was unique, stochastic and simulated a mix of highway and city driving conditions.

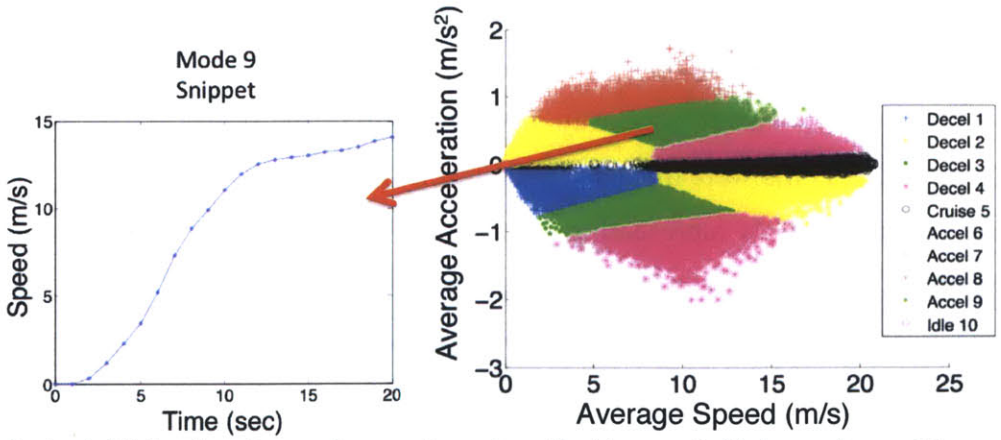

Figure 6.8: An initial snippet was chosen at random that has an initial speed equal to zero and an average speed greater than zero.

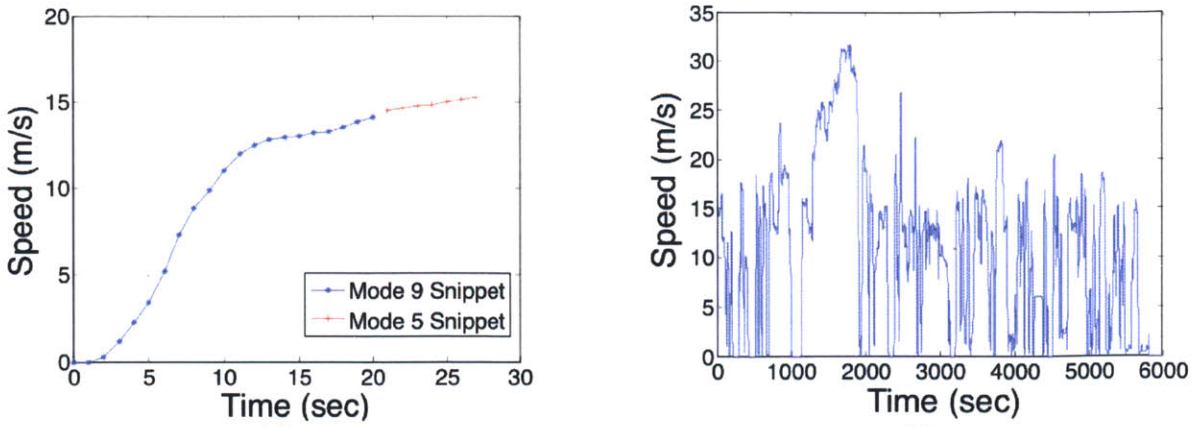

Figure 6.9: The TPM was used to select subsequent snippets (a). The process was repeated until a specified length of time was achieved (b).

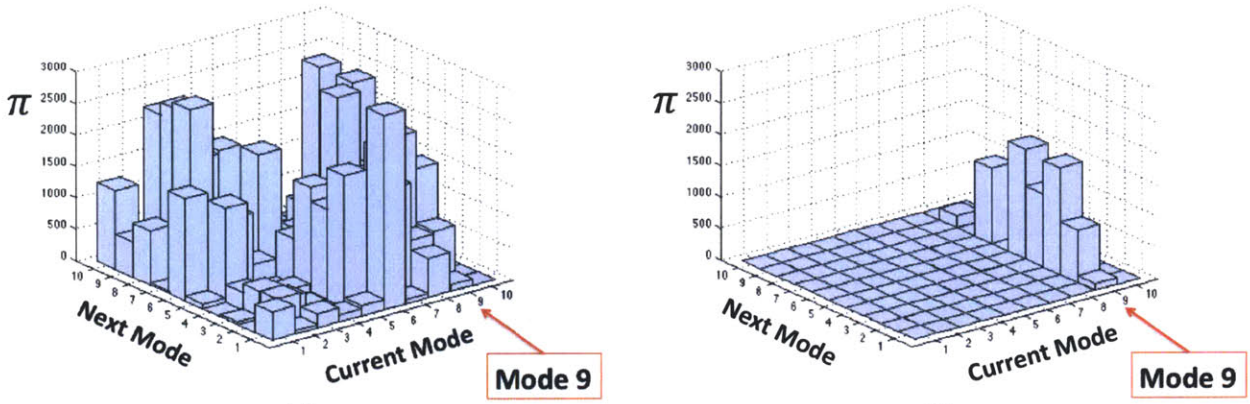

Figure 6.10: The transition histogram (non-normalized) of all modes (a) and only Mode 9 (b).

6.3 Subsystem Models

6.3.1 Vehicle Model

An electric vehicle can be modeled as a mass on an incline with externally applied forces (Figure 6.11). It is propelled forward by an electric motor acting through the front and/or rear wheel with a force, F_w, but slowed down by the aerodynamic drag, F_{aero}, the rolling resistance from all four wheels, $F_{rolling}$, and the horizontal component of weight, $F_{gravity}$. Rewriting Equation 2.3, which was derived in Section 2.1.1:

$$F_w = m\ddot{x} + {}^1/_2\,\rho C_d A(\dot{x} + w)^2 + mgC_{rr}Cos\beta + mgSin\beta \qquad \textbf{2.3}$$

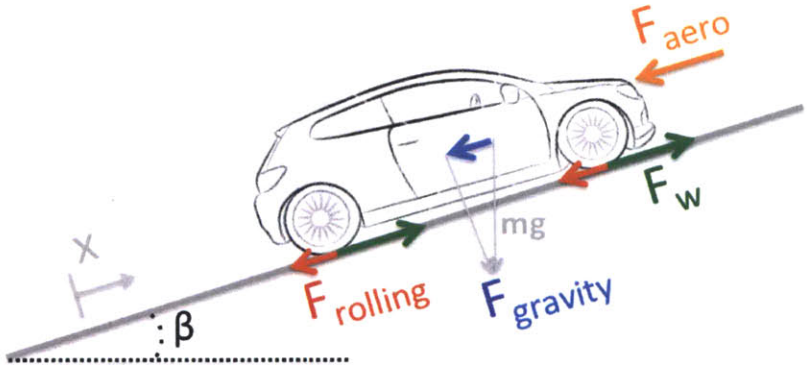

Figure 6.11: A vehicle can be modeled as a mass on an incline with externally applied forces.

6.3.2 Transmission Model

The force on the wheel(s), F_w, originates from a motor acting through a transmission. The transmission generates a torque on the wheels, τ_w. Summing the torques around the wheel yields (Figure 6.12) the same as Equation 2.12:

$$\tau_m = \left(\frac{\ddot{x}m_w}{2} + F_w\right)\frac{r_w}{z\eta_d} \qquad \textbf{2.12}$$

Figure 6.12: Torques and forces on the wheel.

6.3.3 Motor Model

The same motor model derived in Section 2.1.1 was used. Rewriting Equation 2.15 with P_{mc} defined as the power going to the motor controller:

$$P_{mc} = \frac{\left(\frac{\ddot{x}m_w}{2} + F_w\right)\dot{x}}{\eta_{mc}\eta_m\eta_d} \qquad \textbf{6.4}$$

6.3.4 Battery Model

The battery model derived in Section 2.1.1 was used, though auxiliary loads must be considered for non-racing consumer applications. The total power from the battery is the sum of the power to the motor and the power to the accessories (Power In – Losses = Power Out):

$$P_b - I_b^2 R_b = P_m + P_a \tag{6.5}$$

Where P_a is the power going to the auxiliary loads. The power from the battery can be written as:

$$P_b = V_{bn} I_b \tag{6.6}$$

Where V_{bn} is the voltage on the battery pack when no current is being drawn. Combining Equations 6.5 and 6.6 yields:

$$V_{bn} I_b - I_b^2 R_b = P_m + P_a \tag{6.7}$$

The only remaining unknown is I_b, which can be determined using the quadratic equation. Thus:

$$I_b = \frac{V_{bn}}{2R_b} - \frac{\sqrt{V_{b,n}^2 - 4R_b(P_m + P_a)}}{2R_b} \tag{6.8}$$

Combining Equation 6.6 and 2.44:

$$P_{bn} = \frac{V_{bn}^2}{2R_b} - \frac{V_{bn}\sqrt{V_{b,n}^2 - 4R_b(P_m + P_a)}}{2R_b} \tag{6.9}$$

The energy consumed from the battery can now be determined by integrating Equation 6.9:

$$E_b = \int P_{bn}\, dt \tag{6.10}$$

6.3.5 Auxiliary Model

The auxiliary model was meant to simulate the energy used to run the heating, air-conditioner, radio, headlights, etc. [17]. The model is shown in Figure 6.13 and is based on measurements taken with an electric sedan similar but not identical to the Nissan Leaf. This simple model assumes that the auxiliary energy use only depends on the outside (ambient) air temperature. It also assumes that heating and cooling take the same amount of energy for a given change in ambient air temperature. This increase is meant to simulate the energy use required to keep the inside air (cabin) at a comfortable temperature. Other factors (e.g. defrosting) are lumped into this model.

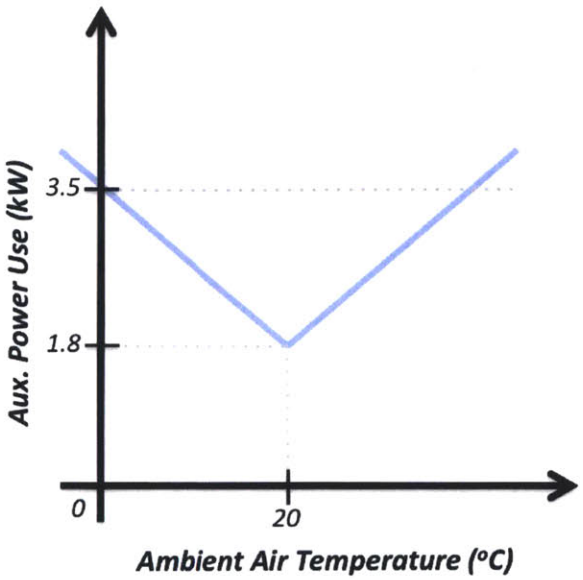

Figure 6.13: Auxiliary power model used for the vehicle simulations.

6.4 Generating Stochastic Vehicle Simulations

This section summarizes the process of simulating an unlimited number of full battery discharges (see Figure 6.1). The inputs to the simulation are the speed profile, ambient air temperature, and vehicle parameters (drag coefficient, mass, battery voltage, etc.). The speed profile, $\dot{x}(t)$, is generated using the algorithm described in Section 6.2.5. The following equations can be used to numerically solve for the force, torque, power and energy values for each increment in time. The force on the wheel is:

$$F_w = m\ddot{x} + {}^1/_2\,\rho C_d A(\dot{x} + w)^2 + mgC_{rr}Cos\beta + mgSin\beta \qquad \textbf{2.3}$$

Then the corresponding torque from the motor:

$$\tau_m = \left(\frac{\ddot{x}m_w}{2} + F_w\right)\frac{r_w}{z\eta_d} \qquad \textbf{2.12}$$

And the power going to the motor from the batteries:

$$P_m = \frac{\left(\frac{\ddot{x}m_w}{2} + F_w\right)\dot{x}}{\eta_{mc}\eta_m\eta_d} \qquad \textbf{6.4}$$

Where the efficiencies are obtained from experimental data. The battery power, which includes the internal losses, can be determined using:

$$P_b = \frac{V_{bn}^2}{2R_b} - \frac{V_{bn}\sqrt{V_{b,n}^2 - 4R_b(P_m + P_a)}}{2R_b} \qquad \textbf{6.9}$$

The auxiliary energy, P_a, is determined using the model shown in Figure 6.13. And the total battery energy consumed is:

$$E_b = \int P_{bn}\, dt \qquad \textbf{6.10}$$

The vehicle parameters (e.g. C_dA) are fixed and the ambient air temperature is selected based on the specific scenario. The simulations used in this thesis assumed a generic sedan EV – similar but not identical to the Nissan Leaf and BMW ActiveE. The output is the simulated battery energy, speed and distance with time for a full battery discharge.

7. Fundamental D_{TE} Concepts

This chapter first derives key equations that quantify D_{TE} error and aid in formulating D_{TE} algorithms (7.1). It is shown that these equations take on an analytical form that is similar to other applications such as predicting the time remaining until a vehicle reaches a destination (7.2). Next, conventional D_{TE} algorithms are derived to serve as examples of algorithms being used in practice today (7.4). Conventional algorithms blend together a long-term and short-term average of past energy use. It is shown that this approach works well *except* in cases when significant changes in driving conditions occur for sustained periods of time (e.g. changes in traffic or auxiliary energy use). These conventional algorithms are compared to a new algorithm in Chapter 9.

7.1 Key D_{TE} Equations

The energy stored in the battery, E_b, is consumed as the vehicle is driven a distance x (Figure 7.1a). An important metric used frequently in this discussion is the *average energy use*, $\bar{p}$, which is defined as the quantity of energy ΔE_b consumed over a distance Δx and has units of Wh/km:

$$\bar{p} \equiv \frac{\Delta E_b}{\Delta x} \tag{7.1}$$

The *future* average energy use, $\bar{p}_f(t)$, can be determined by evaluating Equation 7.1 between the current time, t, and final time, t_f:

$$\bar{p}_f(t) = \frac{E_b(t)}{x(t_f) - x(t)} \tag{7.2}$$

Where $t \rightarrow \mathbb{R} \in \{t_0, t_f\}$, t_0 is the time when the battery is fully charged and t_f is the time when the battery is fully discharged. $E_b(t)$ is the battery energy remaining at time t. By definition, D_{TE} can be written as (Figure 7.1a):

$$D_{TE}(t) = x(t_f) - x(t) \tag{7.3}$$

Combining Equations 7.2 and 7.3 yields:

$$D_{TE}(t) = \frac{E_b(t)}{\bar{p}_f(t)} \tag{7.4}$$

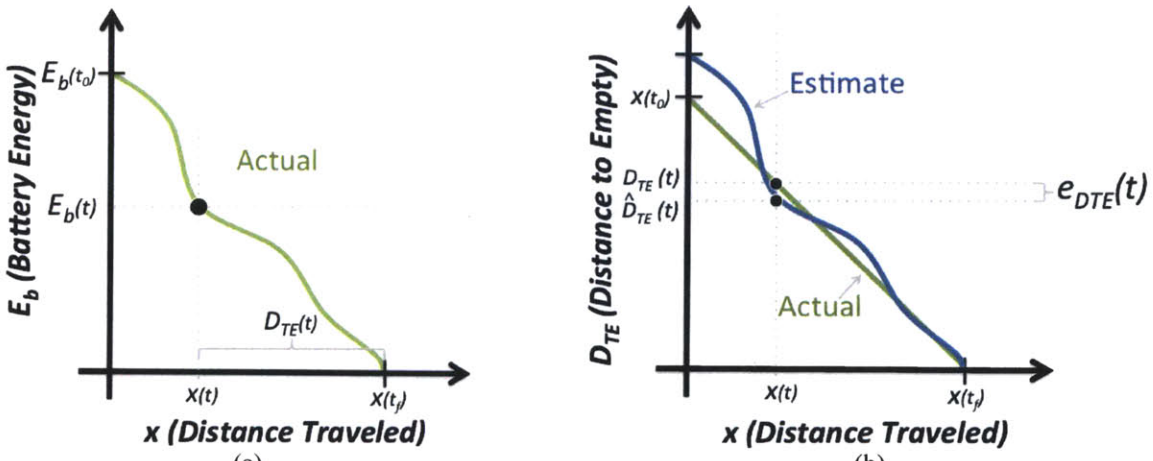

Figure 7.1: A schematic of the vehicle's battery energy (a) and D_{TE} (b) with distance. The actual D_{TE} is a straight line with distance traveled.

Evaluating Equation 7.2 at t_0 yields:

$$\bar{p}_f(t_0) = \frac{E_b(t_0)}{D_{TE}(t_0)} = \frac{E_b(t_0)}{x(t_f)} \quad \textbf{7.5}$$

Now solving for $x(t_f)$:

$$x(t_f) = \frac{E_b(t_0)}{\bar{p}_f(t_0)} \quad \textbf{7.6}$$

Combining Equations 7.3 and 7.6 yields a different form of D_{TE}:

$$D_{TE}(t) = \frac{E_b(t_0)}{\bar{p}_f(t_0)} - x(t) \quad \textbf{7.7}$$

Conceptually, both Equations 7.4 and 7.7 show that D_{TE} can be determined if the *current* battery energy and the *future* energy consumption are known. An onboard Battery Management System (BMS) measures $E_b(t)$ and was assumed to be known perfectly. Thus the task of a D_{TE} algorithm is to estimate the *future* energy consumption, $\bar{p}_f$. Also, Equation 7.7 reveals that a perfect algorithm would predict a linear relationship for D_{TE} with distance (Figure 7.1b).

Errors in D_{TE} are caused by the algorithm's inability to perfectly predict $\bar{p}_f$. Thus it is desirable to quantify how errors in estimating $\bar{p}_f$ relate to errors in D_{TE}. Assume that a D_{TE} algorithm estimates $\bar{p}_f(t)$ and the associated error is defined as:

$$e_{\bar{p}_f}(t) \equiv \hat{\bar{p}}_f(t) - \bar{p}_f(t) \quad \textbf{7.8}$$

Where ^ designates an estimate of the actual value.

The corresponding error in the D_{TE} estimate is then (Figure 7.1b):

$$e_{DTE}(t) \equiv \widehat{D}_{TE}(t) - D_{TE}(t) \tag{7.9}$$

Substituting Equations 7.4 and 7.8 into Equation 7.9 yields:

$$e_{DTE}(t) = E_b(t)\left[\frac{1}{\bar{p}_f(t) + e_{\bar{p}_f}(t)} - \frac{1}{\bar{p}_f(t)}\right] \tag{7.10}$$

Rearranging:

$$e_{DTE}(t) = -\frac{E_b(t)}{\bar{p}_f(t)}\left[\frac{e_{\bar{p}_f}(t)/\bar{p}_f(t)}{\frac{e_{\bar{p}_f}(t)}{\bar{p}_f(t)} + 1}\right] \tag{7.11}$$

Combining with Equation 7.4 results in:

$$e_{DTE}(t) = -D_{TE}(t)\left[\frac{e_{\bar{p}_f}(t)/\bar{p}_f(t)}{\frac{e_{\bar{p}_f}(t)}{\bar{p}_f(t)} + 1}\right] \tag{7.12}$$

Equation 7.12 shows that when Equation 7.4 is used the error in estimating D_{TE} will attenuate to zero towards the end of the discharge. Equation 7.12 can be rearranged as:

$$\frac{e_{DTE}(t)}{D_{TE}(t)} = -\left[\frac{e_{\bar{p}_f}(t)/\bar{p}_f(t)}{\frac{e_{\bar{p}_f}(t)}{\bar{p}_f(t)} + 1}\right] \tag{7.13}$$

Now defining the fractional error, E, as:

$$E_{DTE}(t) \equiv \frac{e_{DTE}(t)}{D_{TE}(t)} \text{ and } E_{\bar{p}_f}(t) \equiv \frac{e_{\bar{p}_f}(t)}{\bar{p}_f(t)} \tag{7.14}$$

Combining Equations 7.13 and 7.14:

$$E_{DTE}(t) = -\left[\frac{E_{\bar{p}_f}(t)}{E_{\bar{p}_f}(t) + 1}\right] \tag{7.15}$$

Equation 7.15 is plotted in Figure 7.2. The plot quantifies the relationship between errors in estimating $\bar{p}_f$ and the resulting D_{TE} errors. It can be seen that the relationship is linear for small errors (~10%) but becomes increasingly non-linear for larger errors. The plot also shows that D_{TE} error is greater when $\bar{p}_f$ is underestimated versus when it is overestimated (e.g. when $\bar{p}_f$ is underestimated by 30% the corresponding D_{TE} error is ~43% while when $\bar{p}_f$ is overestimated by 30% the corresponding D_{TE} error is ~23%).

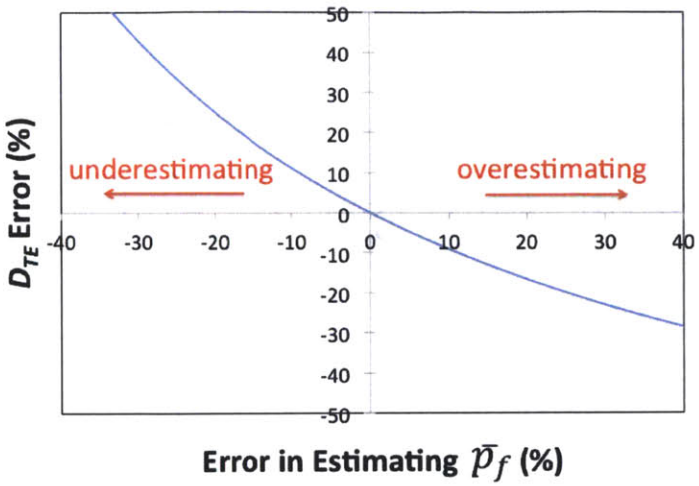

Figure 7.2: A plot of Equation 7.15 shows quantitatively how errors in estimating $\bar{p}_f$ result in D_{TE} errors. D_{TE} error is larger when $\bar{p}_f$ is overestimated.

7.2 Measuring the Remaining Battery Energy

As mentioned in the previous section, it was assumed that the BMS is able to perfectly measure the remaining battery energy, $E_b(t)$, which has units of Watt-hrs (Wh). The value of E_b is analogous to the battery's State of Charge (SOC), which is defined as the *percentage* of battery energy remaining. There is a large amount of literature related to SOC estimation, which describes both model- and empirical-based methods [45]. An alternative approach is to use SOC (%) instead of Wh and thus E_b would have units of percentage and $\bar{p}_f$ would have units of SOC (%) per kilometer. A subtle but very important distinction assumed in this thesis is that E_b and SOC includes the energy that will be consumed by internal battery losses. For example, if 12 kWh of battery energy is remaining, some fraction of this energy will be lost as heat within the battery.

Another common measurement of battery capacity is Amp-hours (Ah). Both Ah and Wh, as measured at the output of the battery, depend on the rate of discharge (e.g. fast discharge results in fewer Ah and Wh). So neither are fixed quantities in this case. However, if the control volume is drawn around the entire battery to include internal losses then both Ah and Wh are fixed quantities. Wh are used in this thesis because they can be directly converted to Joules (J) which is more useful in the mechanical domain. Also, the battery losses are modeled as a resistor and the losses have units of J (or Watts) and not Ah.

7.3 Other Applications with a Similar Formulation

It should be noted that there are other applications that attempt to solve a problem similar to Distance to Empty. For example, estimating the time remaining on a battery for mobile phones or computers takes on a similar form as Equation 7.4:

$$T_{TE}(t) = \frac{E_b(t)}{\bar{b}_f(t)} \tag{7.16}$$

Where T_{TE} is the time (minutes) remaining until the battery is empty, E_b is the remaining battery energy and $\bar{b}_f$ is the future average energy use (Wh/min). Similar to conventional approaches for estimating D_{TE}, the past work in this area has used historical averages to estimate the future [45].

Another example is the time required to reach a destination, T_{TD}, which is estimated by navigation and mapping software:

$$T_{TD}(t) = \frac{D(t)}{\bar{v}_f(t)} \tag{7.17}$$

Where D is the distance (km) remaining until the destination is reached and $\bar{v}_f$ is the future average speed (km/hour). Past work in this area uses posted speed limits and crowd-sourced information to estimate $\bar{v}_f$ [47]. Even though each vehicle will accelerate slightly differently, the average speed is approximately the same and thus it is possible to estimate $\bar{v}_f$ based on crowd-sourced information. Crowd-sourcing $\bar{p}_f$ for Distance to Empty, however, is more difficult because each vehicle will consume energy differently over an identical path based on the vehicle type and driver. Crowd-sourced data has been used for predicting fuel consumption in gasoline vehicles by adjusting the crowd-sourced values based on vehicle and driver type [27]. A similar approach might be possible for electric vehicles, though further research is required.

7.4 Conventional D_{TE} Algorithms

Conventional D_{TE} algorithms assume that the future energy use will be similar to the past. In other words, the following is assumed:

$$\bar{p}_f \approx \bar{p}_p \tag{7.18}$$

Where $\bar{p}_p$ is the average energy use of *past* driving, which can be determined using past (historical) driving energy data (e.g. 1 km, running, or blended averages as defined below). The D_{TE} can then be estimated by combining Equations 7.4 and 7.18:

$$\widehat{D}_{TE}(t) = \frac{E_b(t)}{\bar{p}_p(t)} \tag{7.19}$$

The values of $\widehat{D}_{TE}$ will deviate from D_{TE} according to Equation 7.12 and the amount depends on the validity of Equation 7.18 (Figure 7.1b). This is considered a conventional approach since it is likely very similar to the methods being used in EVs today based on the limited amount of related literature [32][33][34]. The average energy use over the past 1 km is defined as:

$$\bar{p}_{1km}(t) = \frac{E_b(t_{1km}) - E_b(t)}{x(t) - x(t_{1km})} \tag{7.20}$$

where t is the current time and t_{1km} is the time 1 km in the past. And the running average is defined as:

$$\bar{p}_{running}(t) = \frac{E_b(t_0) - E_b(t)}{x(t) - x(t_0)} \tag{7.21}$$

A "blended" average uses a long-term average energy use, $\bar{p}_{long}$, during the beginning of discharge but blends to a more recent short-term average energy use measurement, $\bar{p}_{short}$, as the battery is discharged. This can be written as:

$$\bar{p}_{blend}(t) = \bar{p}_{long}(t) - b(\bar{p}_{long}(t) - \bar{p}_{short}(t)) \tag{7.22}$$

Where b is a "blending factor," $b \rightarrow \mathbb{R} \in \{0,1\}$. The value of b is typically chosen based on a linear function that changes with State of Charge (SOC):

$$b(t) = 1 - SOC(t)/100 \tag{7.23}$$

SOC is defined as the percentage of battery energy remaining:

$$SOC(t) \equiv \frac{E_b(t)}{E_b(t_0)} \cdot 100 \tag{7.24}$$

These historical averages work well as long as the future conditions are similar to the past. However, there are cases when changes in energy use will cause significant errors. For example, Figure 7.3a shows that switching on auxiliary loads could have significant impacts on energy use. Each curve represents a constant auxiliary load and was obtained by simulating a sedan-sized vehicle at constant driving speeds. For example, a 2 kW constant auxiliary load will cause a 30% increase in energy consumption when driving at a constant speed of 45 km/h. Figure 7.3b-d are meant to show how a 30% change in energy consumption would impact D_{TE} error. To this end, assume that a vehicle has been consuming energy at a constant rate of 210 Wh/km for the long and short-term past. When the vehicle is ~50 km into a full discharge, a heater load is turned on, which causes a 30% increase in energy consumption (Figure 7.3a and

b). Figure 7.3c shows the actual and estimated D_{TE} when the running average or blend algorithms were used. Figure 7.3d shows that the corresponding D_{TE} error for the blended algorithm ranges from 0 to 30% depending on the distance traveled.

Figure 7.4a and b show a similar situation, where the energy consumption is increased due to auxiliary loads part way through the discharge, though this time a stochastic vehicle simulation is used instead. The stochastic vehicle simulation is described in a Chapter 6, and uses stochastic speed profiles and physics-based models to more accurately represent a vehicle's energy consumption. The simulation runs multiple discharges in order to generate a long-term average energy use, $\bar{p}_{long}$, which in this case is the Wh/km averaged over the past 300 km. A final example is shown in Figure 7.4c and d, and for this case there is no change in auxiliary use or traffic.

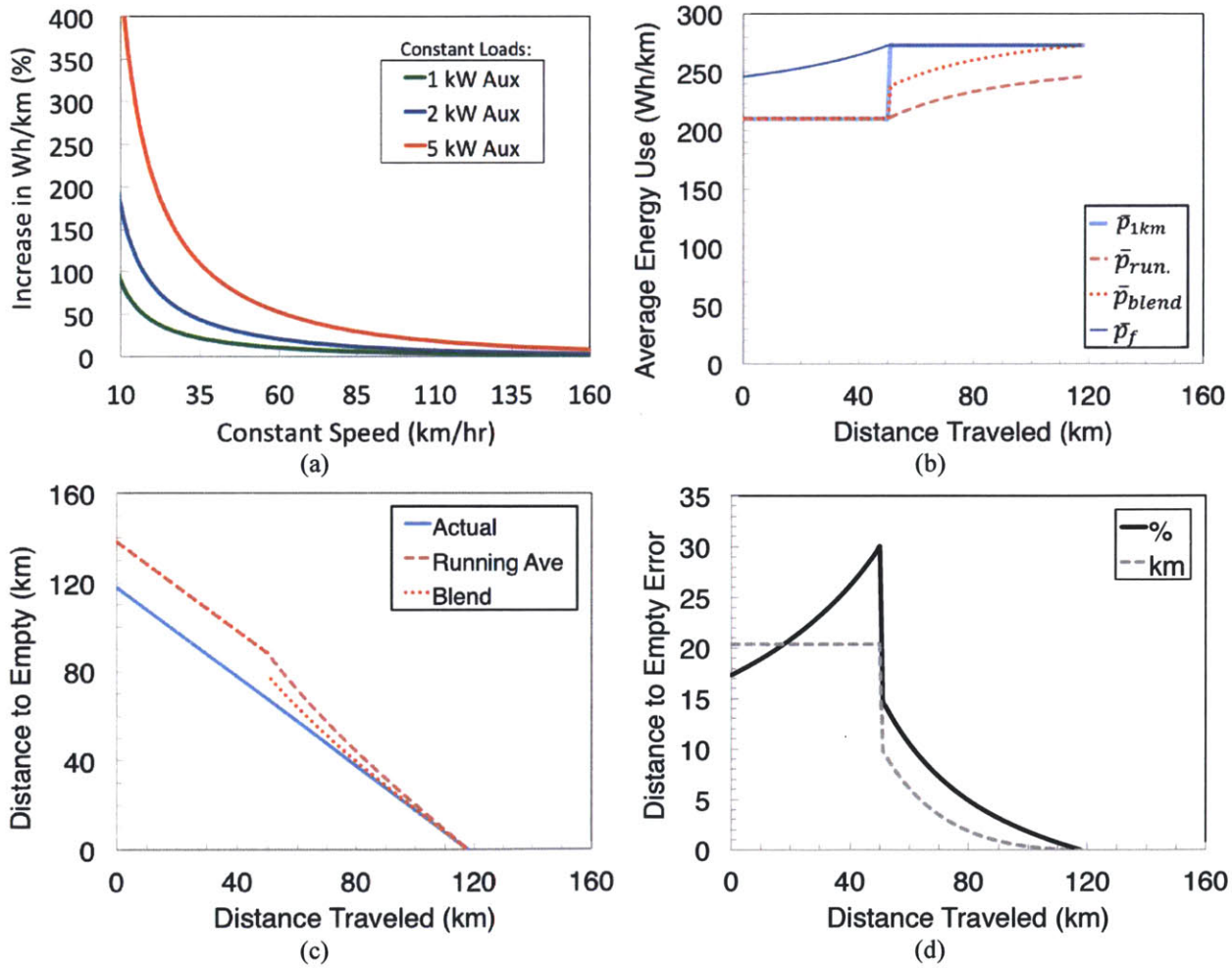

Figure 7.3: A simple example showing how auxiliary use can cause errors in the D_{TE} estimate when the running average or blended algorithms are used.

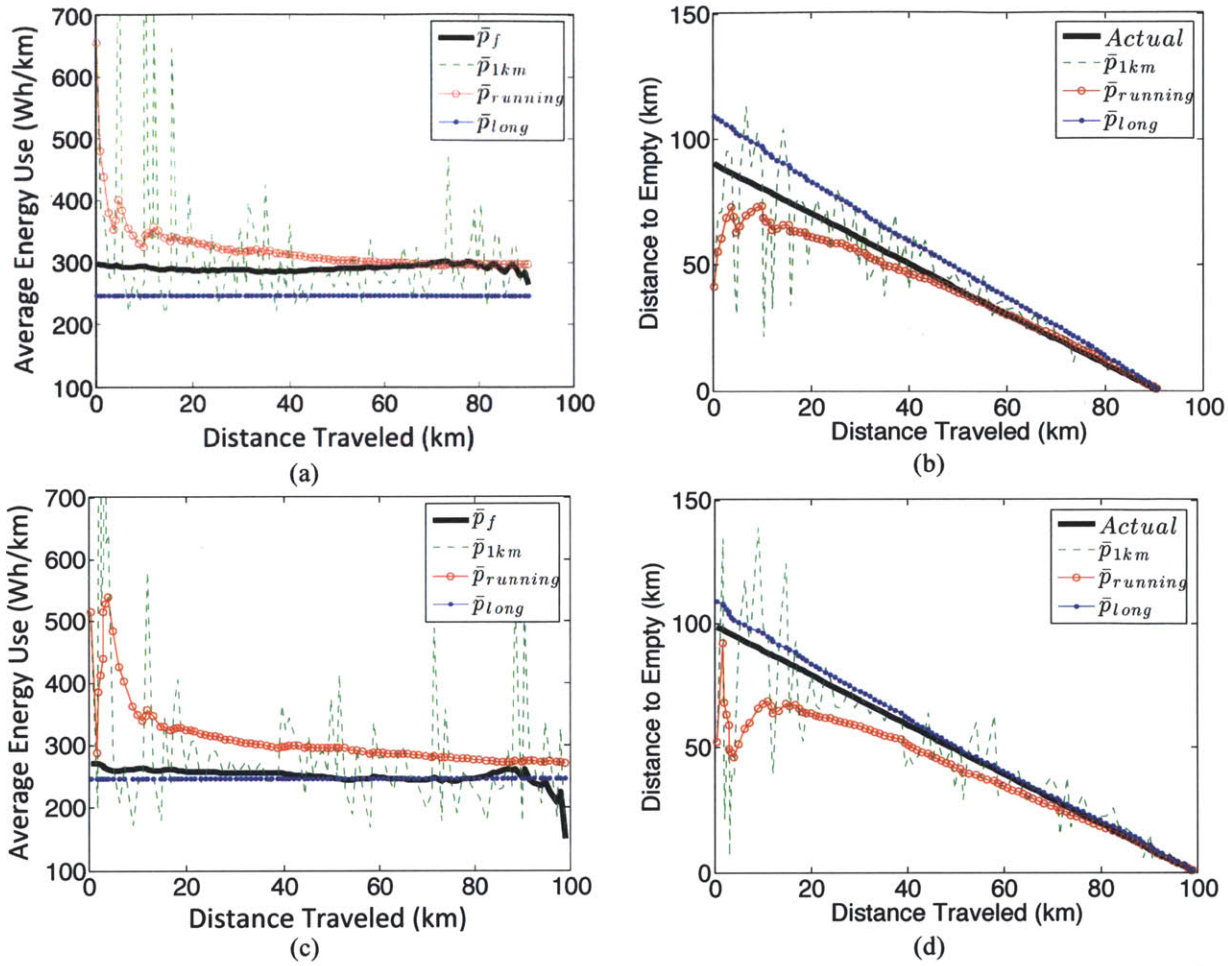

Figure 7.4: Example output from a stochastic vehicle simulation. The plots show the corresponding $\hat{D}_{TE}$ using Equation 7.19 with $\bar{p}_p$ equal to $\bar{p}_{1km}$, $\bar{p}_{running}$ and $\bar{p}_{long}$. For these examples $\bar{p}_{long}$ is defined as the energy use averaged over the previous 300 km. Figures a and b simulate an increase in auxiliary load part way through the discharge while c and d have a constant auxiliary load. The above simulations show that using past data and assuming $\bar{p}_f \approx \bar{p}_p$ works well as long as there are no sustained changes in driving conditions.

All three of these examples support the following conclusion: using averages and blends of past data and assuming that $\bar{p}_f \approx \bar{p}_p$ works well as long as there are no sustained changes in driving conditions between the past average and the future average (e.g. sudden use of heater for a sustained period of time). It is interesting to note that in Figure 7.4c the assumption that $\bar{p}_f \approx \bar{p}_{long}$ is especially true at the beginning to middle of discharge since $\bar{p}_{long}$ is a measure of average energy use over a similar length scale as $\bar{p}_f(t_0)$. In other words, both $\bar{p}_{long}$ and $\bar{p}_f(t_0)$ are aggregates of a large amount of varying and stochastic conditions (temperature, traffic, etc.) over a similar distance.

The examples above reveal that D_{TE} algorithms could be improved if future changes in driving conditions were anticipated, which is a concept described in the next section.

7.5 Using Estimates of Future Conditions and Models to Improve D_{TE} Predictions

The previous section showed that D_{TE} errors occur when the average energy use changes significantly from the past. This section describes the concept of detecting these changes beforehand and using this information, along with a model, to improve the D_{TE} estimate. For example, assume that the driver provides their destination(s) to an on-board navigation system before departure. The navigation system could then obtain navigation, traffic and weather information via the internet. Thus changes in driving conditions could be detected before they occur and fed into a model that estimates $\bar{p}_f$. The physics-based modeling methods described in Chapter 2 could be used, though there are differences between racing and consumer driving that make that approach less feasible. For example, there are more factors that significantly influence energy consumption of consumer vehicles and thus additional models would be required (Table 7.1).

Figure 7.5 shows that auxiliary energy has a much larger impact on the total energy use (Wh/km) at lower speeds. Since the motorcycle race is at high speeds (~150 km/hr), the total energy use is less impacted by auxiliary energy consumption. Consumer vehicles, on the other hand, are driven at lower speeds and thus more impacted by auxiliary use. The conclusion is that a fluctuation in auxiliary power has a larger impact on energy use, which causes larger errors in D_{TE} estimates.

Figure 7.6 attempts to capture all of the factors that affect energy use in consumer EVs. Modeling each of these factors using physics-based models would be complex, require vehicle-specific parameters and can be computational intensive for real-time applications. To avoid these shortcomings, the following section will derive a method that uses a model that can be "learned" as the vehicle is driven.

Table 7.1: Comparing factors that influence energy use for motorcycle racing and consumer vehicle applications.

Factors	Motorcycle Race	Consumer Vehicle
Route	A single trip in a single battery discharge	Multiple trips in a single battery discharge
Average Speed	Steady ~150 km/hr	Variable <110 km/hr
Auxiliary Loads	Insignificant	Variable and significant
Traffic	None	Variable and significant
Driver Behavior	Steady and repeatable	Variable and significant
Cargo Mass	Constant	Variable and significant

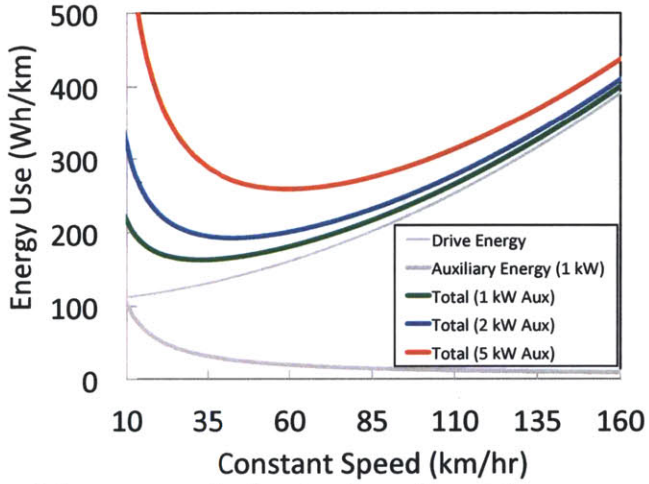

Figure 7.5: A simulation of the motorcycle showing how the total energy use (Wh/km) changes with speed and auxiliary load. Constant speed driving on a flat road and a constant auxiliary load were assumed. The exact shape of the curve depends on many factors specific to the vehicle's loss parameters (e.g. drag coefficient, rolling resistance)

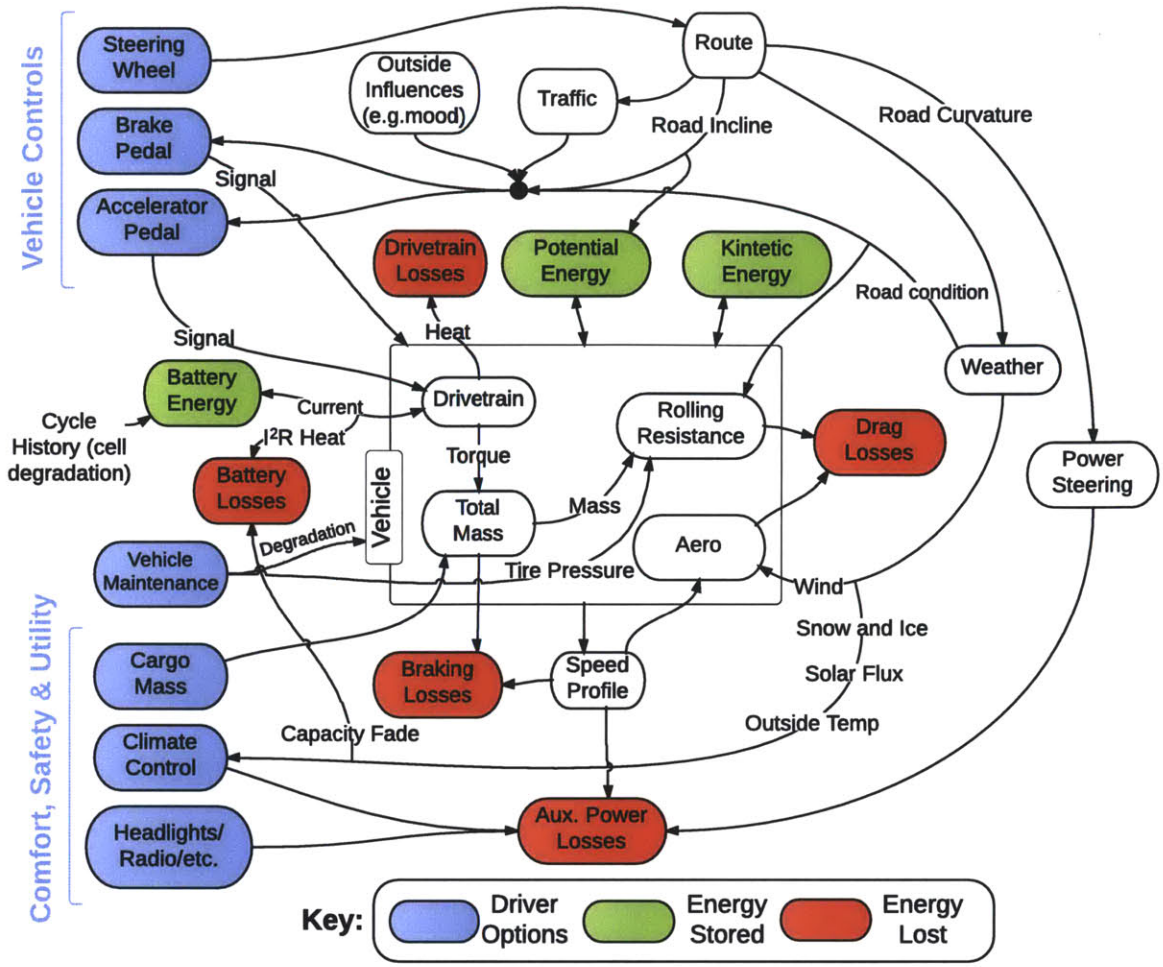

Figure 7.6: This diagram attempts to show all of the factors that influence a consumer vehicle's energy consumption and specifically how various driver decisions and options (purple) lead to energy losses (red) and storage (green).

8. A Regression-based D_{TE} Algorithm

This chapter derives an algorithm that uses estimates of future driving conditions to more accurately predict D_{TE}. As discussed in Chapter 7.2, the past energy use, $\bar{p}_{long}$, is often a good estimate for future energy consumption as long as there are no significant changes in driving conditions. *An improved algorithm is one that adjusts the value of* $\bar{p}_{long}$, *based on estimated changes in future driving conditions, to yield a better estimate of* $\bar{p}_f$. The approach is to multiply $\bar{p}_{long}$ by an adjustment factor, y, that makes the following true:

$$\bar{p}_f(t) = y(t)\,\bar{p}_{long}(t) \qquad \textbf{8.1}$$

Combing Equations 7.4 and 8.1 yields:

$$D_{TE}(t) = \frac{E_b(t)}{y(t)\,\bar{p}_{long}(t)} \qquad \textbf{8.2}$$

Since y cannot be determined perfectly beforehand, an estimate $\hat{y}$ can be made when an unknown residual error, ε, is included:

$$y(t) = \hat{y}(t) + \varepsilon(t) \qquad \textbf{8.3}$$

Rearranging:

$$\hat{y}(t) = y(t) - \varepsilon(t) \qquad \textbf{8.4}$$

Then an estimate for D_{TE} can be written as:

$$\hat{D}_{TE}(t) = \frac{E_b(t)}{\hat{y}(t)\,\bar{p}_{long}(t)} \qquad \textbf{8.5}$$

Section 8.1 proposes a multivariate linear regression model for determining $\hat{y}$. The regression model uses a training set to learn (fit) the relationship between explanatory variables and $\hat{y}$. Section 8.2 defines the explanatory variables as changes in ambient temperature, traffic and average speed. Section 8.3 describes how the training set is obtained using historical driving data and Section 8.4 checks the validity of the regression model.

The advantage to this new approach is that there is no need for physics-based models. In other words, instead of precisely predicting the future energy consumption using physics-based models, a past measurement is simply adjusted up or down based on estimates of future conditions and a regression model.

8.1 Multivariate Linear Regression Model

A regression model uses a training dataset to learn the relationship between explanatory variables, χ, and the response variable, $\hat{y}$. Assuming a linear model of the form [29]:

$$\hat{y}(t_i) = \beta_0 + \beta_1 \chi_{i1} + \beta_2 \chi_{i2} + \cdots + \beta_m \chi_{nm} \quad \textbf{8.6}$$

Where β_i is a set of m unknown coefficients that are determined from historical data (training set). The variables χ must be measurable and predictable factors that cause differences in energy use between the past and future. For the sake of this derivation, the values of χ are assumed to be known. Equation 8.6 can be written in matrix form:

$$\hat{\boldsymbol{y}} = \boldsymbol{\chi\beta} \quad \textbf{8.7}$$

Once $\hat{y}$ is known, Equation 8.5 can be used to determine $\widehat{D}_{TE}$. Rewriting Equation 8.3 in matrix form:

$$\boldsymbol{y} = \hat{\boldsymbol{y}} + \boldsymbol{\varepsilon} \quad \textbf{8.8}$$

Combining Equations 8.7 and 8.8:

$$\boldsymbol{y} = \boldsymbol{\chi\beta} + \boldsymbol{\varepsilon} \quad \textbf{8.9}$$

Solving for the residual error:

$$\boldsymbol{\varepsilon} = \boldsymbol{y} - \boldsymbol{\chi\beta} \quad \textbf{8.10}$$

The residual error can be minimized through a least squares estimator, which can be written as a function *S(c)*:

$$S(\boldsymbol{c}) = \sum \varepsilon_i^2 = \boldsymbol{\varepsilon}^T\boldsymbol{\varepsilon} = (\boldsymbol{y} - \boldsymbol{\chi\beta})^T(\boldsymbol{y} - \boldsymbol{\chi\beta}) \quad \textbf{8.11}$$

Expanding the right side of the equation:

$$S(\boldsymbol{c}) = \boldsymbol{y}^T\boldsymbol{y} - \boldsymbol{y}^T\boldsymbol{\chi\beta} - \boldsymbol{\beta}^T\boldsymbol{\chi}^T\boldsymbol{y} + \boldsymbol{\beta}^T\boldsymbol{\chi}^T\boldsymbol{\chi\beta} \quad \textbf{8.12}$$

Setting the derivative of *S(c)* to zero solves for the minimum residual error:

$$\frac{\partial S}{\partial \boldsymbol{c}} = -2\boldsymbol{\chi}^T\boldsymbol{y} + 2\boldsymbol{\chi}^T\boldsymbol{\chi\beta} = 0 \quad \textbf{8.13}$$

Rearranging Equation 8.13 yields the *Normal Equation:*

$$\boldsymbol{\chi}^T\boldsymbol{y} = \boldsymbol{\chi}^T\boldsymbol{\chi\beta} \quad \textbf{8.14}$$

Solving for $\boldsymbol{\beta}$:

$$\boldsymbol{\beta} = (\boldsymbol{\chi}^T\boldsymbol{\chi})^{-1}\boldsymbol{\chi}^T\boldsymbol{y} \quad \textbf{8.15}$$

The strategy is to "learn" values of $\boldsymbol{\beta}$ using known historical values of $\boldsymbol{y}$ and $\boldsymbol{\chi}$ and Equation 8.15 (training set). Then the learned values of $\boldsymbol{\beta}$ and the real-time values of $\boldsymbol{\chi}_i$ can be used to calculate

$\hat{y}(t_i)$ using Equation 8.6. The following subsection will explain how the explanatory variables χ are defined and calculated.

8.2 Explanatory Variables

The explanatory variables χ must be (1) measurable and predictable factors that (2) cause differences in energy use between the past and future. The *past* is defined by $\bar{p}_{long}$. For example, if $\bar{p}_{long}$ is the energy use over the past 300 miles, then the *past* is defined as the past 300 miles worth of driving. The value of $\bar{p}_{long}$ compresses a large amount of microstructure driving data into a single measurement that quantifies how energy has been used historically. When using $\bar{p}_{long}$ to estimate the future, the value needs to be adjusted up or down if the future is different from the past. The *future* is the data contained between $x(t_i)$ and $x(t_f)$. *(1) The Explanatory Variables must be factors that indicate a difference in average energy use between the past ($\bar{p}_{long}$) and future ($\bar{p}_f$).* For example, assume that the energy and distance values used to determine $\bar{p}_{long}$ were collected while the average ambient temperature was 15°C, while it is predicted that the future will contain a average ambient temperature of 5°C. Since auxiliary heater use at 15°C ambient will be less than that at 5°C, it can be assumed that the change in ambient temperature may cause a change in future energy use. Thus the change in the ambient temperature's arithmetic mean can be one of the explanatory variables. (2) *The Explanatory Variables should be measured from past data and estimated (predicted) into the future:* The ambient temperature serves as a good example of a factor that can be easily measured using a temperature sensor. The future temperature can be predicted using weather forecasts and/or by assuming that the temperature at t_0 will be equal to the arithmetic mean of the future temperature.

There are other factors that might cause a difference in energy use but few can be directly measured and predicted. For example, the driver's mood might cause an increase in future energy use though it cannot be easily measured and predicted. Given these constraints, the following explanatory variables were used:

(1) Change in Ambient Temperature: As described previously, the change in the arithmetic mean of the ambient temperature is defined as:

$$\Delta T_a(t_i) \equiv \left|\bar{T}_{a,f}(t_i) - 20\right| - \left|\bar{T}_{a,p}(t_i) - 20\right| \qquad \textbf{8.16}$$

Where $\bar{T}_{a,p}(t_i)$ is the arithmetic mean of the past ambient temperature and $\bar{T}_{a,f}(t_i)$ is the estimated arithmetic mean of the future ambient temperature. The difference from 20°C is taken since it is assumed that temperatures above and below 20°C cause an increase auxiliary energy.

(2) Change in Traffic Conditions: Traffic conditions have a significant influence on energy use and recent advances in traffic sensing techniques make traffic measurements and predictions possible. For example, Google Maps is able to provide a quantitative measure of the upcoming (future) traffic delay and corresponding estimates of average speeds over distance segments [35]. This information is accessible in real time via their internet-based Application Programming Interface (API). If the future route is specified, an estimate for future traffic conditions can be made. However, to reduce the scope of this project, it was assumed that the traffic conditions can be captured through the percentage of time spent at idle conditions (i.e. zero speed):

$$\Delta t_{idle}(t_i) \equiv \bar{t}_{idle,f}(t_i) - \bar{t}_{idle,p}(t_i) \quad \textbf{8.17}$$

Where $\bar{t}_{idle,p}(t_i)$ is the arithmetic mean of the percentage of time spent at idle in the past and $\bar{t}_{idle,f}(t_i)$ is the estimated arithmetic mean of the percentage of time spent at idle in the future.

(3) Change in Average Speed: It is well known that high speeds require more energy [30]. It was assumed that the arithmetic mean of the future speed can be estimated using route information from Google Maps (or equivalent). Thus a difference in mean speed was used as an explanatory variable:

$$\Delta v_{ave}(t_i) \equiv \bar{v}_f(t_i) - \bar{v}_p(t_i) \quad \textbf{8.18}$$

Where $\bar{v}_p(t_i)$ is the arithmetic mean of the past speed and $\bar{v}_f(t_i)$ is the estimated arithmetic mean of the future speed.

8.3 Creating a Training Dataset

Assume that multiple historical discharges are being analyzed with each discharge starting at 100% SOC and data is available to calculate both $\bar{p}_{long}$ and $\bar{p}_f$. The actual values of $y(t_i)$ can be determined by rewriting Equation 8.1:

$$y(t_i) = {\bar{p}_f(t_i)}/{\bar{p}_{long}(t_i)} \quad \textbf{8.19}$$

Since there are n discrete values of t_i, the values of $y(t_i)$ can be written as a $nx1$ vector:

$$\boldsymbol{y} = \begin{pmatrix} y(t_1) \\ \vdots \\ y(t_n) \end{pmatrix} \quad \textbf{8.20}$$

The values of ΔT_a, Δt_{idle} and Δv_{ave} for each time t_i form the explanatory matrix:

$$\boldsymbol{\chi} = \begin{bmatrix} 1 & \Delta T_a(t_1) & \Delta t_{idle}(t_1) & \Delta v_{ave}(t_1) \\ \vdots & \vdots & \vdots & \vdots \\ 1 & \Delta T_a(t_n) & \Delta t_{idle}(t_n) & \Delta v_{ave}(t_n) \end{bmatrix} \quad \textbf{8.21}$$

The following section describes how this process is repeated for multiple discharges to build a training set with a sufficient regression fit and to avoid extrapolation [29].

8.4 Algorithm Simulation

It was necessary to first train the multivariate regression model by simulating ~300 km of vehicle driving (Chapter 6) to generate an initial *historical* dataset (e.g. $\bar{p}_{long}$, $\bar{T}_{a,p}$, $\bar{t}_{idle,p}$, and $\bar{v}_p$) based on the specified vehicle and environmental conditions. A constant ambient temperature of 20°C was assumed though other scenarios could be easily used.

Next, multiple full-discharge simulations with varying conditions were used as a "training dataset." For example, a random speed profile was generated with an ambient temperature of 10°C. This process was repeated for different temperatures (e.g. 15°C, 20°C, etc.) to generate a training dataset large enough that extrapolation does not occur when the regression is used. The temperatures were held constant for each discharge though the speed profile was generated stochastically with a variety of city, highway and aggressiveness conditions. The values of ΔT_a, Δt_{idle} and Δv_{ave} and y were determined for each 1% SOC increment in the discharge. The full training dataset was used with Equation 8.15 to determine the values of β_i.

Once values of $\bar{p}_{long}$ and β_i were calculated, an *actual discharge dataset* was obtained and used to simulate D_{TE} algorithms. A new stochastic speed profile and a random constant ambient temperature were used to simulate the actual discharge dataset. The D_{TE} algorithm then used all of the collected datasets. This process can be repeated multiple times using different parameters and conditions.

In summary, there were three datasets used:

Historical Dataset: Multiple full battery discharges used to determine the *past driving* energy consumption data.

Training Dataset: Multiple full battery discharges with varying conditions used to *train* the regression model and thus determine β_i values.

Actual Discharge Dataset: A single discharge that is meant to be the observed discharge for simulating D_{TE} algorithms.

In practice, the values of $\bar{T}_{a,f}(t_i)$, $\bar{t}_{idle,f}(t_i)$, and $\bar{v}_f(t_i)$ will need to be estimated using Google Maps, weather information, etc. However, the simulations shown in this thesis had perfect knowledge of the future.

Finally, it is best to discretize the problem based on State of Charge (SOC), since the range of values is constant {0,100} between the various training sets (unlike time and distance, which have a range of values that change based on driving conditions). In discretized form: $SOC_i \rightarrow \mathbb{Z} \in \{0,100\}$:

$$SOC(t_i) = SOC_i \tag{8.22}$$

For example, t_{50} is the time when SOC = 50%.

8.5 Validating the Assumptions and Fit of the Regression Model

The assumptions and fit of the regression model were tested using the output from the simulations described in Section 8.4. The assumptions of the multivariate linear regression model can be summarized as follows [29]:

- Assumption 1: The linear model adequately describes the behavior of the data.
- Assumption 2: The residual error, ε (Equation 8.3), is an independent and normally distributed random variable, with a zero mean and variance σ^2.

There are various checks commonly used to evaluate these underlying assumptions for a given training dataset. An observation with Cook's distance larger than three times the mean Cook's distance might be an outlier [31] and the fit might be improved if the outliers are removed. Figure 8.1a shows that < 3% of the data points for this training dataset are considered outliers. The second is to perform a significance test on each of the coefficients, β_i (Equation 8.6), to ensure that the model is not over-specified. This is done by testing the null hypothesis that each coefficient is zero, which yields a pValue (Table 8.2). The small pValues (<< 0.05) and large R^2 indicates that the model is valid (Table 8.3). To verify the conditions in Assumption 2, a

frequency distribution of the residual error was used to verify normality. It can be seen from Figure 8.1b that the distribution has a normal shape.

Given the results from the above analysis, there is sufficient evidence to support the assumptions made in the multivariate linear regression model. The following sections will investigate whether or not the regression model improves D_{TE} estimates over the conventional blend approach.

Table 8.2: Metrics used to determine significance of coefficients.

	Estimate of β_i	Standard Error	tStat	pValue
Intercept	1.08	0.00381	283	0
ΔT_a	0.00868	0.000161	53.9	3.82E-296
Δt_{idle}	0.0306	0.000746	41.1	1.24E-215
Δv_{ave}	0.0291	0.000629	46.34	9.05E-250

Table 8.3: Metrics used to determine significance of coefficients and fit of regression.

Metric	Value
Root Mean Squared Error	0.035
R^2	0.86
F-Statistic (v. constant model)	2.0e+03
pValue	0

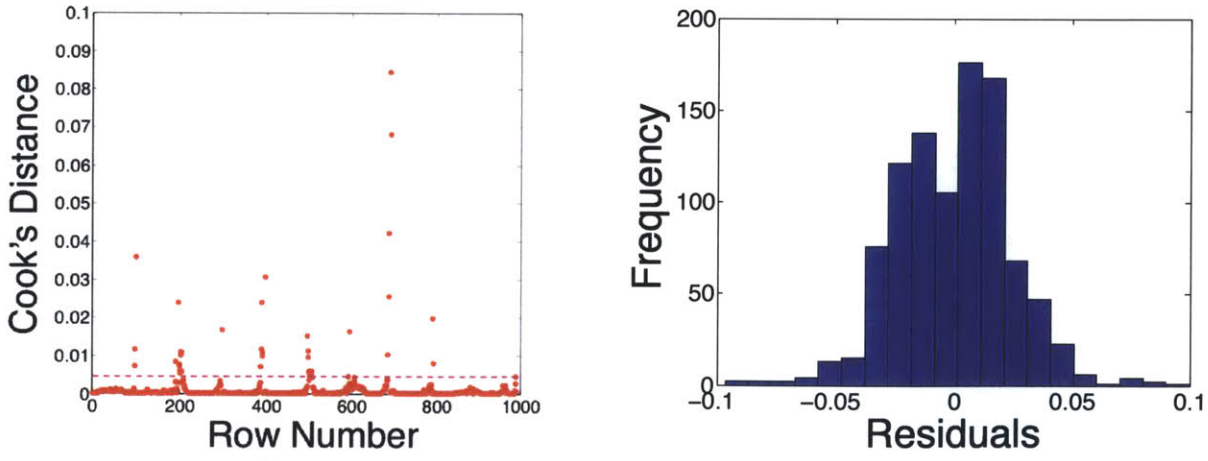

(a) (b)

Figure 8.1: The Cook Distance (a) and a histogram of residuals (b) are used to evaluate the assumptions of the regression analysis.

9. Comparing D_{TE} Algorithms

This chapter uses the stochastic vehicle simulation (Chapter 6) to quantitatively compare the conventional (Section 7.2) and new regression-based D_{TE} algorithms (Chapter 8). Section 9.1 describes the metrics used for comparing the quality of D_{TE} algorithms and the results are shown in Section 9.2.

9.1 Measuring the Performance of D_{TE} Algorithms

The error in estimating D_{TE} was defined in Section 7.1 as:

$$e_{DTE}(t) \equiv \hat{D}_{TE}(t) - D_{TE}(t) \tag{7.9}$$

Figure 7.1 illustrates this same concept schematically. The performance of the D_{TE} algorithm can be determined by visually inspecting plots such as Figure 7.1 or more quantitatively by determining the arithmetic mean (average) error over sections of the discharge. It is useful to discretize the problem so that each i^{th} value of error is written as $e_{DTE,i}$. The algorithm can both over-estimate ($e_{DTE,i} > 0$) and under-estimate ($e_{DTE,i} < 0$). Thus the average over-estimation error is:

$$\frac{1}{n_1}\sum_{i=1}^{n_1} e_{DTE,i} \mid e_{DTE,i} > 0 \tag{9.1}$$

Where n_1 is the number of increments that have $e_{DTE,i} > 0$. And the average under-estimation error is:

$$\frac{1}{n_2}\sum_{i=1}^{n_2} e_{DTE,i} \mid e_{DTE,i} < 0 \tag{9.2}$$

Where n_2 is the number of increments that have $e_{DTE,i} < 0$.

The accuracy of the D_{TE} algorithm changes as the battery is discharged. For example, the D_{TE} estimate may be less accurate at the beginning of the trip but more accurate as the battery pack is drained. Thus the discharge was divided into three sections: start, middle and end, and the average error was calculated within these sections (Figure 9.1b).

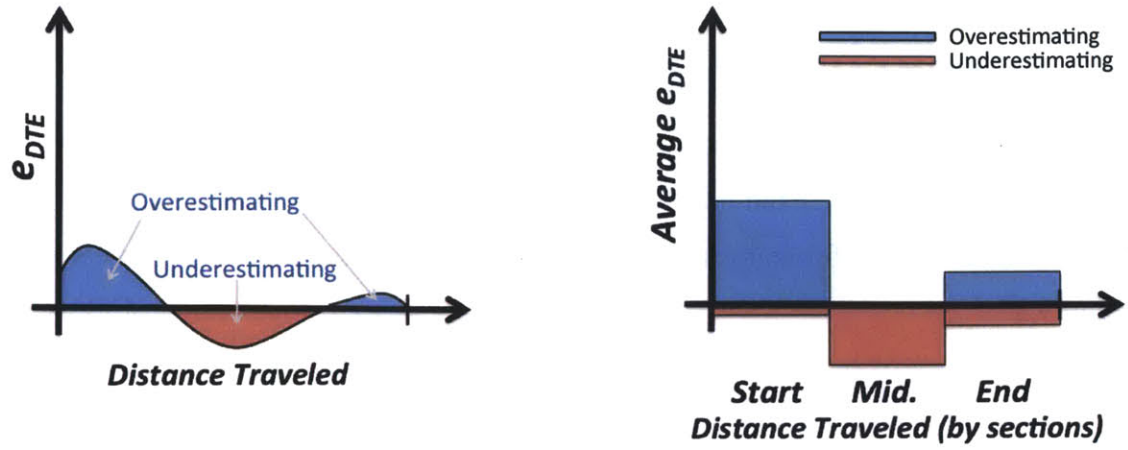

(a) (b)

Figure 9.1: The over- and under-estimation error is shown for the entire interval (a) or averaged by the start, middle and end sections of the full discharge (b).

9.2 Results

The stochastic vehicle simulation (Chapter 6) was used to quantitatively compare the conventional (Section 7.2) and new regression-based D_{TE} algorithms (Chapter 8). The training set was first obtained as described in Section 8.3. Figure 9.2 shows one example full discharge, though more scenarios are simulated later in this section. The speed and battery energy profiles are shown in Figure 9.2a and b and the resulting D_{TE} plots are shown in Figure 9.2c and d. This particular simulation assumed that the discharge dataset occurred with an ambient temperature of 10°C as to simulate a drop in temperature from the past (which had an ambient temperature of 20°C as described in Section 7.2). The graphical representation of D_{TE} error, as discussed in Section 9.1, provides a quantitative comparison of the algorithms. Figure 9.2c shows that, for this example simulation, the regression-based approach reduced the error at the beginning of discharge by ~15%. It is important to note that the ability to accurately estimate D_{TE} at the start of a full charge (*key-on*) is likely the most critical task of an algorithm since the driver uses this estimate to plan their route.

To better understand how the algorithms perform for a wider variety of conditions, 1000 full battery discharges were simulated using stochastic speed profiles and randomly generated ambient temperatures (0 to 22°C) for the *actual discharge dataset*. For each case the same *historical and training datasets* described in Section 8.3 were used. To simplify the analysis, only the D_{TE} error at the beginning of the discharge (key-on) was used for comparison (Figure 9.3). Figure 9.4a shows that the error for the regression-based approach has a smaller arithmetic

mean. A t-test showed that there is statistical significance between the two means [29]. The probability density plots were estimated using the simulation data and built-in Matlab functions [45][49].

Another approach to comparing the two algorithms is to measure the reduction in D_{TE} error at the beginning of discharge, which is defined as:

$$Reduction\ in\ D_{TE}\ Error\ (key-on) \equiv \frac{|e_{DTE,r}(t_0)| - |e_{DTE,b}(t_0)|}{|e_{DTE,b}(t_0)|} * 100 \qquad \textbf{9.3}$$

Where $e_{DTE,r}(t_0)$ and $e_{DTE,b}(t_0)$ are the D_{TE} error at key-on for the regression and blended algorithm, respectively. This measures the percentage reduction that the regression algorithm has over the blended algorithm. For example, a -100% reduction in error corresponds to a situation where the regression-based algorithm eliminated all of the error. The error reduction was calculated for the 1000 full battery discharges and a frequency distribution of the results is shown in Figure 9.4b. The regression-based algorithm performed better than the blend algorithm for cases when the error reduction is in between -100% and zero, and worse when the reduction is greater or equal to zero. Overall it can be seen that the regression-based algorithm reduced the error, and thus improved the D_{TE} estimate ~90% of the time.

Next, it was of interest to plot $e_{DTE}(t_0)$ versus the explanatory variables (ΔT_a, Δt_{idle} and Δv_{ave}) to explore how changes in the explanatory variables affect errors at the very beginning of a full discharge (i.e. $e_{DTE}(t_0)$). For example, assume the vehicle was driven for 300 km in low traffic with an ambient temperature of 20°C. Now imagine that the vehicle is being driven, starting with a full battery, in higher traffic conditions with a hotter ambient temperature of 27°C. This would result in a ΔT_a = 7°C. It is expected that $e_{DTE}(t_0)$ would increase for the blended algorithm since it is not able to anticipate these changes. The results from the 1000 simulations are shown in Figure 9.5. Analysis of Covariance (ANCOVA) was performed for each dataset, which showed statistical significance between the least-squares slopes [50]. In other words, *the D_{TE} error for the regression-based algorithm is less impacted by changes in driving conditions.*

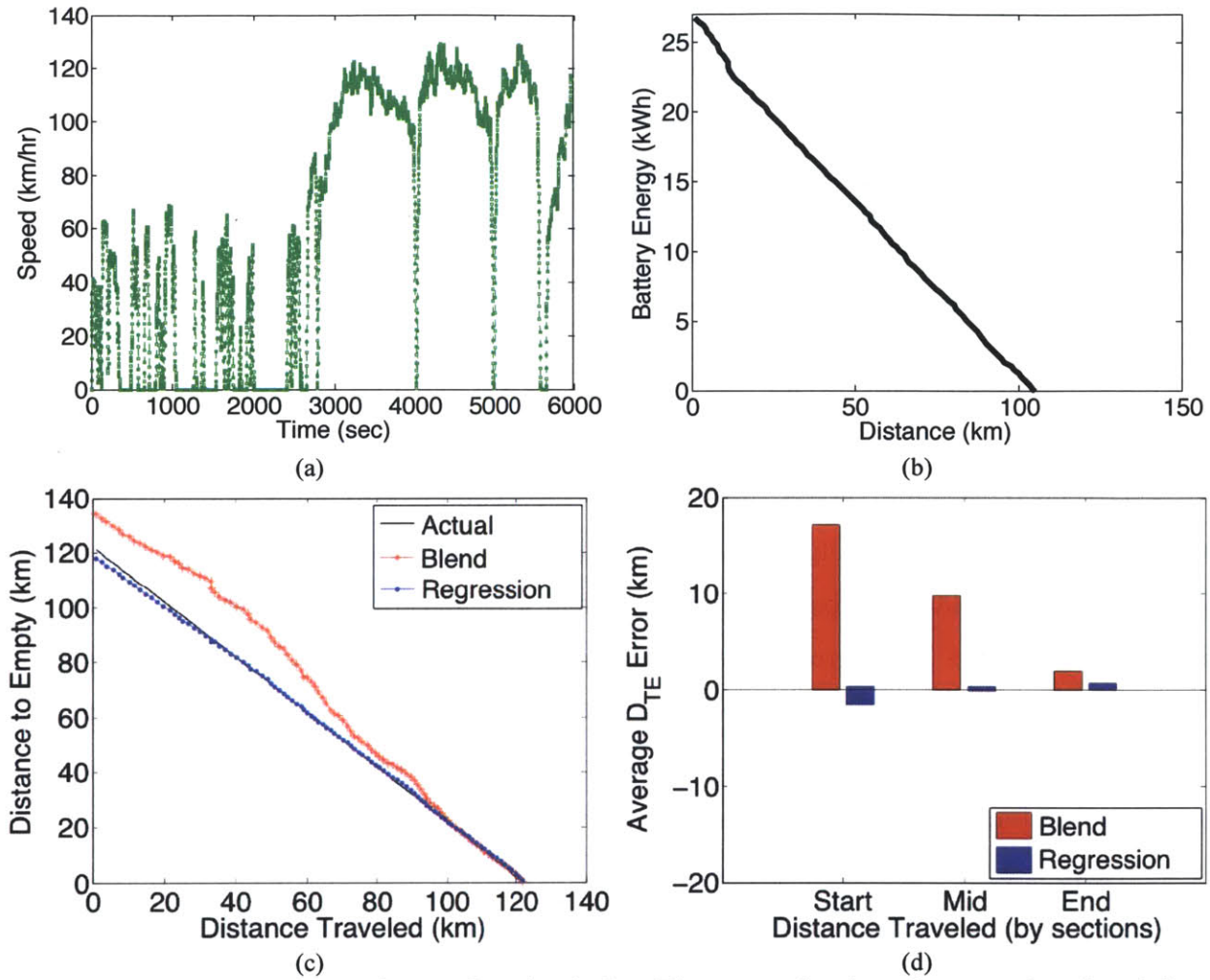

Figure 9.2: Example output from a D_{TE} simulation. The regression-based approach reduced the error at the beginning of discharge by ~15%.

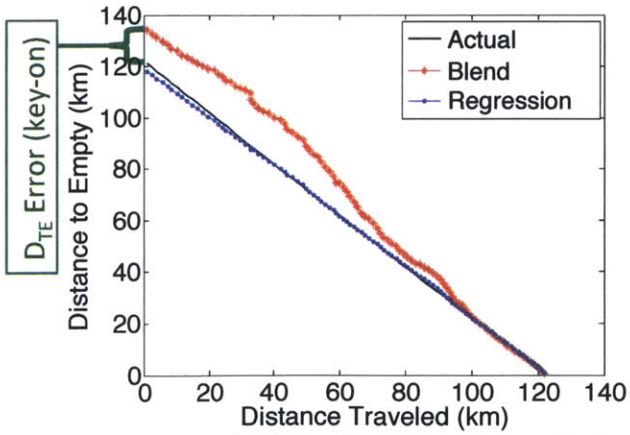

Figure 9.3: The D_{TE} error at key-on is defined as the error at the beginning of discharge.

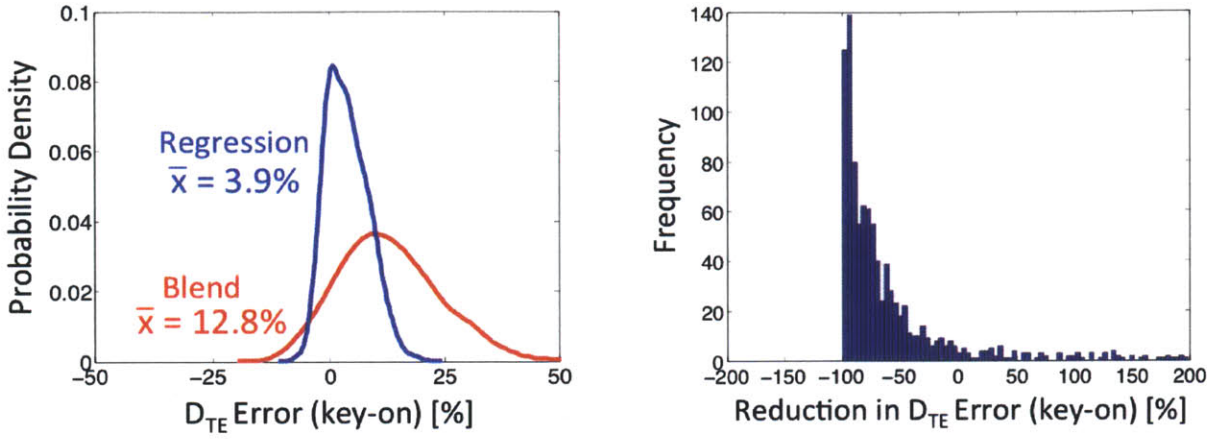

Figure 9.4: The arithmetic mean error is significantly less for the regression-based algorithm (a). A frequency plot of the reduction in error, as defined in Equation 9.3, shows that the regression-based algorithm reduced the error ~90% of the time (b).

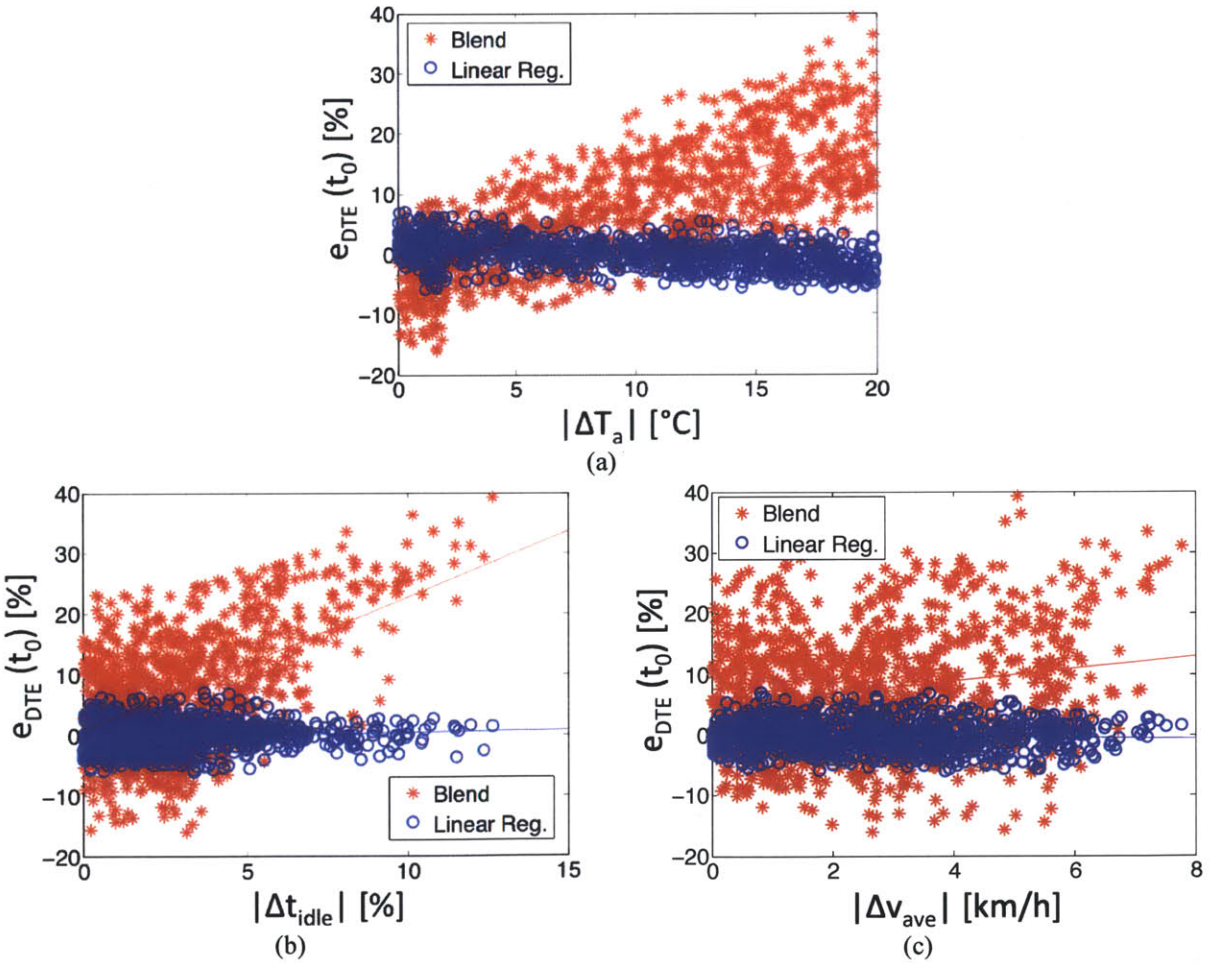

Figure 9.5: Multiple simulations show how the key-on error in D_{TE} is affected by changes in driving conditions (explanatory variables). These plots show that the linear regression algorithm is less sensitive to changes in driving conditions.

Part III: Summary and Contributions

10. Conclusions

This chapter contains a summary of the entire thesis, a list of the original contributions made to the field of electric vehicles and a description of ongoing and future work.

10.1 Summary of Thesis

Part I described the process of designing, building, testing and racing a high performance electric motorcycle for the 2011 Isle of Man Tourist Trophy (TT) Zero race. Systems engineering was used to size the batteries and motors, predict vehicle speeds and predict the time required to finish the race. Two types of simulations were considered. The first estimated the motor and battery power and vehicle speed when full-throttle is applied. The second simulation type estimated upper and lower bounds for the battery energy required to traverse the entire course. The lower bound, or best case, was determined by assuming the motorcycle maintained a constant vehicle speed throughout the course, which was shown to be the most energy efficient way to drive. The upper bound, or worst case, was determined by assuming the motorcycle maintained a constant motor power throughout the course, which would yield large speed fluctuations.

Two motors were combined with a rigid shaft to provide a maximum of 32 kWh of continuous power. The energy storage consisted of 106 kg of lithium-ion batteries totaling 11.9 kWh. A structural frame was needed to support the batteries, motor, and supporting electronics. The removal of the engine needed to be considered in the mechanical design, since it was originally a structural element. Instead of a more common space-frame weldment, it was decided to design a frame that could be made on the waterjet using aluminum plates. The waterjet was chosen because it is rapid, economical, and provides significant design flexibility. Designing a set of 2D plates also made prototyping easy; prototypes were made quickly with a laser cutter using wood and cardboard. The frame was assembled like a puzzle with small tabs connecting the various 2D plates. The final aluminum frame, including the tab-slots, was welded while bolted in place on the motorcycle chassis.

The motorcycle was instrumented with sensors to measure acceleration, speed, distance, current, voltage, and temperature. A battery management system (BMS) was used to measure the

voltage of each cell and perform cell balancing. A safety monitoring system from A123 Systems checked for ground faults, the condition of the fuse, and over current. The data was transmitted wirelessly to an off-board real-time display and logged on-board. The rider display consisted of LEDs to indicate the state of the motorcycle and a single LCD screen. The screen displayed digital real-time values for battery power, battery energy consumption and vehicle speed.

A series of incremental tests were performed to ensure that each subsystem operated as predicted. This included the following tests: bench-top, wind tunnel, chassis dynamometer, track, and finally road. In June 2011 the motorcycle design and simulations were tested in three races on the Isle of Man. Post-race analysis showed that the predictions had less than 10% error.

The energy estimation methods that were developed for the motorcycle were subsequently modified and applied to non-racing electric vehicles (EV). Instead of predicting the energy required to traverse a known route (or race course), it is more useful for non-racing applications to consider the reverse scenario, which is the distance the vehicle can travel before charging is required. This is referred to as the Distance to Empty (D_{TE}) and an estimate is displayed in real-time in the vehicle's dashboard. It was shown that a D_{TE} algorithm must predict the future energy consumption of a vehicle. Future energy can be predicted reliably if either (i) future energy consumption is sufficiently similar to the past or (ii) applicable information about the future is known beforehand. A conventional D_{TE} algorithm assumes (i) by "blending" both a long-term and short-term average of past energy use. However, significant changes in driving conditions (e.g. traffic or auxiliary energy use) for sustained periods of time can cause large errors in D_{TE} estimates. This thesis showed that D_{TE} error can be reduced if future changes are detected beforehand and used by the algorithm. Instead of using a complex parametric physics-based model, a multivariate linear regression-based model was derived that adjusts the value of $\bar{p}_{long}$ up or down based on estimated changes in driving conditions (temperature, traffic and speeds). In practice the driver would specify their destination(s) and a service such as Google Maps would provide an estimate of the future driving conditions to the algorithm. When compared to the conventional blend algorithm, it was shown that the D_{TE} error for the new regression-based algorithm is less sensitive to changes in driving conditions.

There are two additional advantages to the proposed regression-based algorithm. The first is that it is computational light and thus can be run in real-time with a variety of processor speeds. The second is that it does not require vehicle-specific calibration and validation. In other

words, the algorithm can be learned (fitted) over time by simply capturing data that is already available on the CAN-bus of most EVs. These unique advantages make the approach conducive to mobile phone and cloud-based computing services currently being developed [49].

The D_{TE} algorithms were compared using a stochastic, parametric and physics-based electric vehicle simulation. Though real driving data could be used, the simulation approach yields an unlimited number of full battery discharges under a wide variety of realistic driving conditions. Instead of using EPA speed profiles as input, a method for generating stochastic speed profiles using a mode-based Markov model was derived. A large set of driving data (speed versus time) was parsed into sequential Markov *states*, which were defined by deceleration, cruise, acceleration or idle events. The Transition Probability Matrix (TPM) was determined by observing the transitions between states (e.g. counting the number of times the state transitioned from cruise to deceleration). The TPM along with a random number generator was used to string together a stochastic speed profile of any length. To simulate a variety of conditions, the TPM matrix was modified to give preference to certain modes (e.g. less aggressive driving was simulated by putting zeros in the columns of the TPM associated with the largest acceleration and deceleration modes). The algorithm is capable of providing speed versus time profiles that are stochastic, variable in length (e.g. full discharge), and based on actual driving data.

10.2 Summary of Contributions

Below is a summary of the original research and contributions presented in this thesis.

(1) Derived and validated a method for estimating the battery energy required for electric vehicle racing.

Predicting the exact amount of energy required to traverse the Isle of Man course is difficult since the speed profile is unknown beforehand. So lower- and upper-bound scenarios were estimated with the hypothesis that the actual required energy lay somewhere in between these values. The lower bound, or best case, was determined by assuming the motorcycle maintained a constant vehicle speed throughout the course, which was proven to be the most energy efficient way to drive. The upper bound, or worst case, was determined by assuming the motorcycle maintained a constant motor power throughout the course, which would yield large speed fluctuations and is thus inefficient. These scenarios were simulated using first-order

physics-based models of the motorcycle system. It was shown that the racing data supports this hypothesis.

(2) Developed fundamental concepts critical to understanding D_{TE} algorithms.

Equations were derived to aid in the understanding of Distance to Empty (D_{TE}) algorithms. It was shown that the main objective of a D_{TE} algorithm is to predict the future average energy use of the vehicle ($\bar{p}_f$). Future energy can be predicted reliably if either (i) future energy consumption is sufficiently similar to the past or (ii) applicable information about the future is known beforehand. Equations were derived to show that D_{TE} error is larger when $\bar{p}_f$ is underestimated versus when it is overestimated by the same percentage amount.

(3) Formulated an improved D_{TE} algorithm that uses a past energy consumption measurement and future route information.

It was shown that D_{TE} error can be reduced if the future route is known beforehand and thus changes in temperature, traffic and speed are used by the algorithm. Specifically, a multivariate linear regression-based model was derived that adjusts the past average energy use based on estimated changes in driving conditions (temperature, traffic and speed).

(4) Created a stochastic vehicle simulation environment that was used to compare D_{TE} algorithms.

In order to compare D_{TE} algorithms it was necessary to develop a stochastic, parametric and physics-based electric vehicle simulation. The simulation approach provided an unlimited number of full battery discharges under a wide variety of realistic driving conditions. Instead of using EPA speed profiles as input, a method for generating stochastic speed profiles using a mode-based Markov model was derived.

10.3 Ongoing Work

Below is a summary of the ongoing work related to the research presented in this thesis.

10.3.1 Increasing Average Speeds at the Isle of Man TT Zero

The speeds of the Isle of Man TT Zero race are limited by the energy density of currently available batteries. In other words, the race is a battery energy-limited design problem where the motors are able to output larger amounts of energy and power than the batteries can actually store given the volumetric limitations of the motorcycle. Given this situation, it is useful for teams to (i) increase vehicle efficiency and (ii) ensure that all of the available battery energy is consumed during the race (i.e. no battery energy remains when the motorcycle crosses the finish line). The best approach to improving efficiency is to reduce aerodynamic and rolling drag. But it is also possible to increase efficiency by following the most efficient speed profile given the terrain. For example, the overall energy efficiency might be improved by driving more quickly during certain portions of the course than others. This has been discussed in the literature for other applications and could be applied and tested in the Isle of Man race [8][9].

The second (ii) could be accomplished by performing real-time estimates of D_{TE}, which is currently not being done with any level of sophistication. It was shown in this thesis that the fast and consistent speeds and low auxiliary loads of the motorcycle yield fairly constant energy use. This means that a fairly simple past-averaging D_{TE} algorithm would likely yield accurate results. This is supported by the race data shown in Figure 10.1, which shows the energy use averaged over 1 km ($\bar{p}_1$) and 10 km ($\bar{p}_{10}$). It can be seen that the average energy use does a fairly good job at predicting the future energy use, $\bar{p}_f$, especially at the beginning of the race. Thus a basic algorithm could use the past 10 km average of energy use to predict the future energy use and thus D_{TE} (see Equation 7.4).

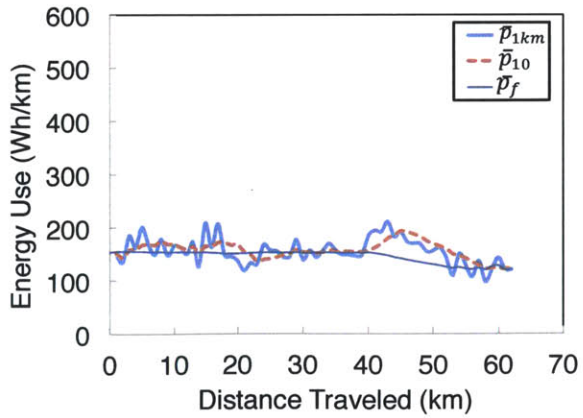

Figure 10.1: Average energy use of the motorcycle during the Isle of Man race. This figures shows that the fast and consistent speeds and low auxiliary loads of the motorcycle yielded fairly constant energy use. A basic algorithm could use a past 10 km average of energy use to predict the future energy use and thus D_{TE}.

10.3.2 Advancing D_{TE} Algorithms

When simulating the regression-based algorithm, it was assumed that the future driving conditions (temperature, traffic and speed) were known perfectly. It would be useful to add noise (errors) to these values to more accurately simulate the uncertainty that will exist in real-world applications. It is also important to better understand the accuracy and utility of real traffic and route data (e.g. provided by Google Maps). For example, traffic was quantified in this thesis by measuring the average time at idle, $\bar{t}_{idle}$. In practice there are other metrics used to measure traffic (e.g. a number ranging from 0 to 10 depending on the amount of traffic).

There are other regression methods that could be used to adjust $\bar{p}_{long}$ based on estimates of future conditions. For example, historical data could be used to track energy use of repeated routes and/or conditions. Trip types could be categorized and $\bar{p}_{long}$ could be adjusted accordingly.

10.3.3 Comparing D_{TE} Algorithms

The Distance to Empty algorithms were compared in this thesis using a stochastic vehicle simulation, though it is desirable to begin testing the algorithms using real driving data. This would require an integrated cloud-based approach that simultaneously measures vehicle speed, energy use, ambient temperature and traffic. This information could be obtained by recording data from the vehicle's CAN-bus while also obtaining real-time information from Google Maps (traffic). Though it would be a significant research effort, recent advances in cloud-based automotive hardware make this task feasible [51][52].

References

[1] Honda Isle of Man TT Race Declaration, Retrieved May 4, 2013, from http://world.honda.com/MotoGP/history/Man-TT-Declaration/

[2] Frank, A., 2003, Honda Motorcycles, MBI Publishing.

[3] Stuecke, P., 2011, "Development of a Racing Motorbike with Electric Power Train," SAE International.

[4] Dorrell, D., 2012, "Design of brushless permanent-magnet DC motors for racing motorcycles," IEEE International Symposium.

[5] Cavaiuolo, D., 2012, "Design of an Electric Motor Controller with Embedded Dynamic Thermal Control Logic for Motorbike Racing Application," Electric Vehicle Conference (IEVC).

[6] Pudney, P., 2000, "Optimal energy management for solar-powered cars," PhD Thesis, University of South Australia.

[7] Pudney, P., 2002, "Critical Speed Control of a Solar Car," Optimization and Engineering.

[8] Dib, W., 2011, "Optimal Control to Minimize Trip Time and Energy Consumption in Electric Vehicles," IEEE Vehicle Power and Propulsion Conference (VPPC).

[9] Petit, N., 2011, "Optimal drive of electric vehicles using an inversion-based trajectory generation," 8th IFAC World Congress Milano.

[10] Hutcheson, R., 2010, "Conceptual Design of a Formula Hybrid Powertrain System Utilizing Functionality-based Modeling Tools," ASME IDETC/CIE.

[11] Same, A., 2010, "A study on optimization of hybrid drive train using Advanced Vehicle Simulator (ADVISOR)," Journal of Power Sources.

[12] Markel, T., 2002, "ADVISOR: a systems analysis tool for advanced vehicle modeling," Journal of Power Sources.

[13] Guzzella, L., 2007, "Vehicle propulsion systems: introduction to modeling and optimization," Springer.

[14] Ehsani, M., 2010, "Modern electric, hybrid electric, and fuel cell vehicles: fundamentals, theory, and design," CRC Press.

[15] Wipke, K.B., 1999, "ADVISOR 2.1: a user-friendly advanced powertrain simulation using a combined backward/forward approach," IEEE Transactions on Vehicular Technology.

[16] Corbett, S., 2003, "NASCAR Sponsorship: Putting Your Company in the Driver's Seat," Journal of Integrated Communications.

[17] Larminie, J., 2012, Electric Vehicle Technology Explained 2nd Edition, Whiley and Sons Ltd.

[18] Franke, T., 2011, "Experiencing Range in an Electric Vehicle - Understanding Psychological Barriers." Applied Psychology: An International Review.

[19] Bakker, J., 2011, "Contesting range anxiety: The role of electric vehicle charging infrastructure in the transportation transition." M.S. Thesis, Eindhoven University of Technology.

[20] Nissan Motor Company, "How Conditions Affect Range." Retrieved May 4, 2013, from http://www.nissanusa.com/leaf-electric-car/range

[21] Hayes, J., 2011, "Simplified Electric Vehicle Power Train Models and Range Estimation." Vehicle Power and Propulsion Conference (VPPC) (IEEE).

[22] Karbowski, D., 2012, "Energy Consumption Prediction of a Vehicle along a User-Specified Real-World Trip." Proceedings from the Electric Vehicle Symposium (EVS26).

[23] Minett, C., 2011, "Eco-routing: comparing the fuel consumption of different routes between an origin and destination using field test speed profiles and synthetic speed profiles." IEEE Forum on Integrated and Sustainable Transportation Systems.

[24] Zhang, Y., 2011, "Remaining Driving Range Estimation of Electric Vehicle." Hitachi (China) R&D Corporation.

[25] Ferreira, J., 2012, "Data Mining Approach for Range Prediction of Electric Vehicle." Conference on Future Automotive Technology - Focus Electromobility.

[26] Yu, H., 2012, "Driving Pattern Identification for EV Range Estimation." Electric Vehicle Conference (IEVC).

[27] Oehlerking, A., 2011, "StreetSmart: Modeling Vehicle Fuel Consumption with Mobile Phone Sensor Data through a Participatory Sensing Framework." M.S. Thesis, Massachusetts Institute of Technology.

[28] Rodgers, L., 2012, "Designing an electric motorcycle for the Isle of Man TT Zero race, and how electric vehicle racing could be used to spur innovation." Proceedings for the Electric Vehicle Symposium.

[29] Freund, R., 2006, Regression Analysis, Elsevier Inc.

[30] Guzzella, L., 2007, Vehicle propulsion systems: introduction to modeling and optimization, Springer.

[31] MathWorks Inc., Matlab Documentation, R2012b.

[32] Viet, Q, 1994, "Electronic System and Method for Calculating Distance to Empty for Motorized Vehicles." Ford Motor Company, Patent No. US 5301113.

[33] Cho, I, 2012, "Methods for Estimating Remaining Travel Distance of Electric Vehicle." Kia Motor Corporation, Patent No. US 2012/0143435 A1.

[34] Siy, T., 2012, "Electric Vehicle Range Prediction." General Motors Corp., Patent No. US20120245750 A1.

[35] Google Maps API. Retrieved May 4, 2013, from https://developers.google.com/maps/

[36] Lin, J., 2002, "A Markov Process Approach to Driving Cycle Development," University of California Davis, PhD Thesis.

[37] Gong, Q., 2011, "An Iterative Markov Chain Approach for Generating Vehicle Driving Cycles," SAE International.

[38] Carlson, T., 1997, "Development of Speed Correction Cycles," Sierra Research, Inc.

[39] Dai, Z., 2008, "Driving Cycles: A New Cycle-Building Method that Better Represents Real-World Emissions," University of California Davis.

[40] Nydahl, D., 2009, "Generation of Stochastic Driving Cycles," Chalmers University of Technology, Masters Thesis.

[41] Lin, C., 2004, "A Stochastic Control Strategy for Hybrid Electric Vehicles." Proceedings from the American Control Conference.

[42] Stroock, D., 2005, "An Introduction to Markov Processes," Springer Publication.

[43] Environmental Protection Agenency, 2008, "Kansas City PM Characterization Study Final Report."

[44] Mathworks Inc., K-means Clustering Documentation. Retrieved May 4, 2013, from http://www.mathworks.com/help/stats/kmeans.html

[45] Samadani, S., 2012, "A Review Study of Methods for Lithium-ion Battery Health and Remaining Life Estimation in Hybrid Electric Vehicles." SAE International.

[46] Onorato, J, 2011, "Estimating Remaining Use Time of a Mobile Device." Google Inc., Patent No. US 7,960,945 B1.

[47] Tashiro, E, 2003, "Traffic routing method and apparatus for navigation system to predict travel time and departure time." Patent No. US 2005/0096842 A1.

[48] Mathworks Inc., Kernel Smoothing Function Estimate Documentation. Retrieved May 4, 2013, from http://www.mathworks.com/help/stats/ksdensity.html

[49] Bowman, A. W., 1997, "Applied Smoothing Techniques for Data Analysis," Oxford University Press Inc.

[50] Mathworks Inc., Interactive Analysis of Covariance Documentation. Retrieved May 4, 2013, from http://www.mathworks.com/help/stats/aoctool.html

[51] Wilhelm, E., 2012, "CloudCar: The Vehicular Internet of Things." Verizon's Innovation Center, CloudCar.mobi

[52] Automatic Labs Inc., "Automatic, Your Car and Smartphone, Connected." Retrieved May 4, 2013, from http://www.automatic.com/